Microwave-Assisted Conversion of Sucrose into 5-Hydroxymethylfurfural over Acidic Nanoporous Materials

Nansi Fakhri

A thesis submitted to the
Faculty of Graduate and Postdoctoral Studies
in partial fulfillment of the requirements
for the degree of Master of Science in Chemistry

University of Ottawa
Ottawa, Ontario

Abstract

With increased worries of our Nations' reliance on fossil fuels and their deleterious effects on the environment, researchers are concentrating on developing sustainable alternative sources for energy and chemicals. One potential starting resource that is worldwide distributed and renewable is biomass. Cellulose, the most plentiful source of biomass on earth, can be hydrolyzed into biofuel precursors such as 5-hydroxymethylfurfural (HMF). However, due to the poor solubility of cellulose and its robust crystalline structure, current methods available to degrade cellulose into these biofuel precursors are costly, result in low yields along with a large amount of waste. Generally, fructose is the preferred feedstock for the synthesis of HMF with high efficiency and selectivity. However, the large-scale production of HMF from fructose is limited due to the scarcity and the high cost of fructose. Therefore, it is desirable to use a cheaper renewable starting material for the synthesis of HMF such as sucrose. This study is conducted to develop an efficient one-pot process to synthesize HMF from biomass, particularly sucrose, using various sulfonated heterogeneous catalysts such as ordered mesoporous silica, bridged periodic mesoporous organosilicas (PMO) and carbon materials. The HMF yields in the presence of such acidic nanoporous materials were comparable to those using much less environmentally-friendly metal-based catalysts.

Table of Contents

List of Figures

List of Tables

List of Abbreviations

AC-SO_3H	Sulfonated Amorphous Carbon
BET	Brunauer-Emmett-Teller
BJH	Barrett, Joyner and Halenda
BTEB	1,4-Bis(triethoxysilyl)benzene
BTEBP	4,4′-Bis(triethoxysilyl)-1,1′-biphenyl
[BMIM]Cl	1-Butyl-3-methylimidazolium chloride
[BMIM]BF_4	1-Butyl 3-methyl imidazolium tetrafluoroborate
[BMIM]PF_6	1-Butyl-3-methylimidazolium hexafluorophosphate
2,5-BHF	2,5-Bis(hydroxymethyl)furan
CMC	Critical Micellar Concentration
CMK-3-SO_3H	Sulfonated Mesoporous Carbon
$C_{18}Cl$	Octadecyltrimethylammonium chloride
DFF	2,5-Diformylfuran
DMA	Dimethylacetamide
DMSO	Dimethylsulfoxide
[EMIM]Cl	1-Ethyl-3-methylimidazolium chloride
FDCA	2,5-Furandicarboxylic acid
FTIR	Fourier Transform Infrared
HFCA	5-Hydroxymethyl-2-furancarboxylic acid
HPLC	High Performance Liquid Chromatography
HMF	5-Hydroxymethylfurfural

IUPAC	International Union of Pure and Applied Chemistry
KJS	Kruk-Jaroniec-Sayari
LCTM	Liquid Crystal Template Mechanism
LP-P	Large Pore Phenylene PMO
LP-B	Large Pore Biphenylene PMO
MCM	Mobil Composition of Matter
MIBK	Methylisobutylketone
MI	Microwave Irradiation
MPTMS	3-Mercaptopropyltrimethoxysilane
NMR	Nuclear Magnetic Resonance
OMC	Ordered Mesoporous Carbon
PMO	Periodic Mesoporous Organosilica
PTES	Phenyltriethoxysilane
PVP	Poly(1-vinyl-2-pyrrolidinone)
PMS	Periodic Mesoporous Silica
SEM	Scanning Electron Microscopy
SBA	Santa Barbara Material
SP-P	Small Pore Phenylene PMO
SP-B	Small Pore Biphenylene PMO
TEM	Transmission Electron Microscopy
TEOS	Tetraethylorthosilicate
TGA	Thermogravimetric Analysis
XRD	X-ray Diffraction

Acknowledgements

First and foremost, I would like to thank my supervisor Dr. Abdelhamid Sayari for his constant encouragement and enlightening guidance. From him I have learned the field of nanoporous materials and dedication to science. My greatest gratitude goes to Dr. Andre Beauchemin for allowing me to use the microwave in his laboratory. My utmost appreciation is also extended to Dr. Yong Yang for all his help and guidance regarding the characterization techniques of my samples

I would like to express my sincere gratitude to Dr. Mohamed Abboud for his thoughtful help and generous support. Without his profound knowledge, invaluable ideas and suggestions, I could not have completed all the research in my thesis.

I also thank present and previous members of the Sayari's goup, Asieh Ahmadalinezhad, Ritesh Tailor and Govind Sethia for all the help and support, which gave me the enjoyable study and working environment.

I should also thank Walaa Baslyman who prepared for me a lot of delicious food and more importantly, for the nice and communicative working atmosphere we had during my Master's research program. I am very grateful for the time we spent in fruitful and stimulating discussions, and for all the wise advice.

I owe my deepest gratitude to my family, particularly my mother, Lina, and my father, Joseph for their boundless love and unconditional support over all the past years. I simply wouldn't be where I am today without you. Thank you for sharing with me my worries, and hopefully my ultimate happiness in eventually finishing this thesis.

Chapter I – Introduction and Motivation

Energy is one of the fundamental prerequisite for the development of human civilization. The significance of energy as an essential constituent in technological development, scientific achievement and economic growth as well as in improving the quality of human life is well recognized. Before the discovery of inexpensive fossil fuels, our society was reliant on plant biomass to meet its energy demands [1]. Generally, biomass, mainly in form of wood, was used through direct combustion. The discovery of crude oil in the 19th century gave rise to a cheap liquid fuel source that helped industrialize the world and ameliorated the standards of living. The use of biomass was mostly forsaken due to the extensive availability of cheap fossil fuels. Nowadays, the world is highly dependent on fossil resources such as coal, natural gas and petroleum, which are converted into energy (e.g. electricity, heating, transportation fuels) or utilized as feedstock for a wide variety of chemicals and materials (e.g. plastics, pharmaceuticals, agrochemicals). Coal constitutes approximately 65% of the fossil fuel reserves in the world, the remaining 35% being oil and gas [2]. Unlike oil and gas reserves, coal is the most abundant and widely distributed fossil fuel around the world. The huge dependence of modern civilization on fossil fuels is illustrated in Figure 1.1 which presents the trend of the world consumption of fossil resources from 1965 to 2030. As can be seen, consumption of all three types of fossil fuels will have an increasing trend over the next years. In fact, we recently reached our highest production of petroleum per year at nearly 40 billion metric tons [2].

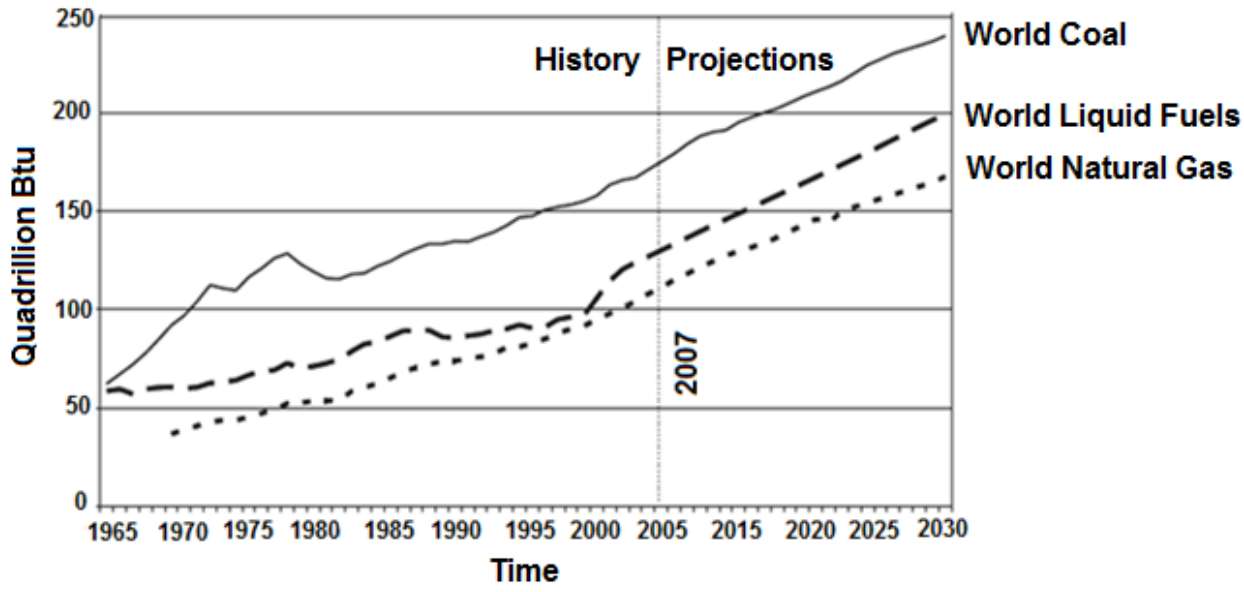

Figure 1.1: Actual and projected consumption of fossil fuel worldwide from 1965 to 2030 [2].

Nowadays, with diminishing petroleum resources, combined with increased demand for petroleum as well as geopolitical and environmental concerns about fossil fuels, it is crucial to develop economical and energy efficient processes for the sustainable production of fuels and chemicals. An attractive renewable resource that is of interest to researchers as a potential raw material for the production of energy, transportation biofuel and chemicals is biomass. It is advantageous to use biofuels over fossil fuels owing to the fact that they generate remarkably less greenhouse gas emissions and are anticipated to be a prospective clean replacement for fossil fuels. The most common examples of biofuels currently available on a global scale are bioethanol and biodiesel. Bioethanol is generally produced from renewable resources such as corn and sugar cane. Unfortunately, ethanol production from edible resources presents a major dilemna. Concerns about its production and use stem from the large area of arable land required for the production of a single crop, which can cause environmental problems such as soil erosion, land clearing and deforestation. On a per volume basis, ethanol has also a lower heat of

combustion than oil, so more volume would be required to travel the same distance as when using oil. Nonetheless, production of ethanol from non-edible biomass such as cellulose would be a major breakthrough. On the contrary, biodiesel can be produced from waste oil and fat. However, the production of biodiesel is not large enough to meet the demand of modern civilization transportation fuels due to the limited quantity of waste oil available. Attention is now focused on the utilization of abundant and renewable lignocellulosic biomass as a source for production of biofuel and fuel additives such as BTX (benzene, toluene and xylene). Lignocellulosic biomass, a name given to all earth living matter, is comprised of mainly three components: cellulose, hemicellulose and lignin (Figure 1.2).

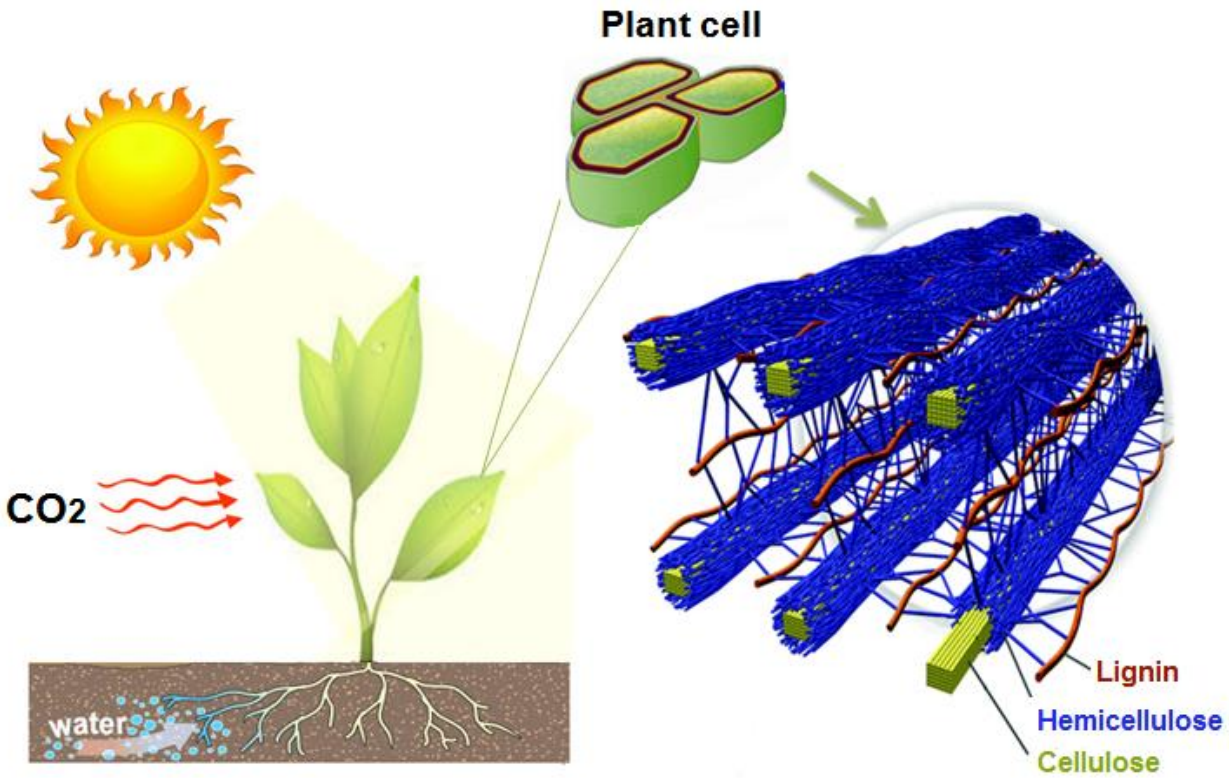

Figure 1.2: Schematic representation of lignocellulosic biomass.

Through photosynthesis, plants use energy from sunlight, carbon dioxide from the atmosphere and water to produce oxygen-rich carbohydrates, the building blocks of biomass [3]. Contrary to the petroleum industry which is based on hydrocarbons, the utilization of carbohydrates in the chemical and fuel industry requires at least the partial removal of oxygen. Acid catalyzed dehydration reactions of sugars is one of the most desired approaches for the removal of oxygen atoms, affording 5-hydroxymethylfurfural (HMF), a key intermediate in the production of biofuel and other chemicals. As shown in Figure 1.3, HMF has two functional groups, hydroxyl group and formyl group. HMF was chosen as the center of interest in this research owing to its possible conversion into a large number of chemicals with applications in diverse industries. Examples of chemicals that can be generated from HMF along with their potential applications are presented in Figure 1.3. In addition to being an intermediate in the synthesis of chemicals, HMF has also some potential uses on its own such as in fuel cells and the treatment of sickle cell diseases [37].

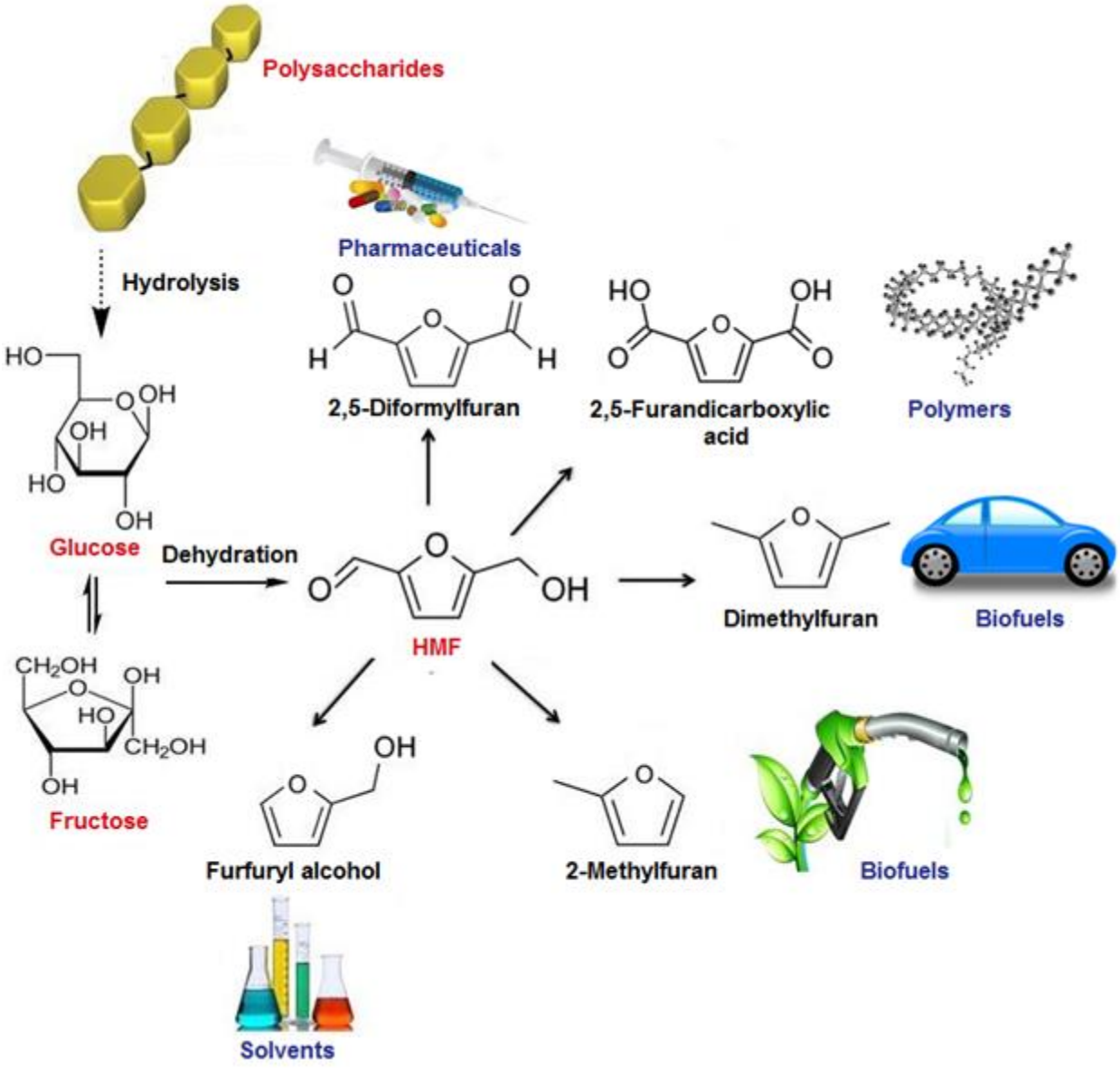

Figure 1.3: Production of HMF as feedstock for chemicals and liquid fuels.

A great number of studies dealt with a range of reaction conditions for laboratory-scale synthesis of HMF from different carbohydrates, such as fructose, glucose, cellulose and sucrose. The polysaccharides in lignocellulosic biomass can be hydrolysed to monosaccharides which can be used as raw materials for the production of HMF. Cellulose, the principle structural component

of biomass, is regarded as a difficult carbohydrate to work with due to its robust crystalline structure, where glucose monomers are highly densely packed together by an extensive network of hydrogen bonds. Much progress has been reported for the conversion of fructose, yet the conversion of other carbohydrates remains very difficult. Commonly, fructose is the more desirable feedstock for the synthesis of HMF with high efficiency and selectivity. However, large-scale production of HMF from fructose is not viable due to the insufficiency and the high cost of fructose. Therefore, it is desirable to use a cheaper and renewable starting material for the synthesis of HMF such as sucrose.

In this study, a microwave-assisted process for the conversion of sucrose to HMF was developed using acidic nanoporous materials in dimethylsulfoxide (DMSO) as catalysts. Most previous and on-going research focuses on improving the production efficiency of HMF from monosaccharides. However, the objective of the current research is to investigate the synthesis of HMF directly from sucrose which offers a great advantage for large-scale production of HMF because this circumvents the step of the synthesis of monosaccharides such as glucose and fructose as well as the corresponding costs. So far, the synthesis of HMF from sucrose has been reported using metallic chlorides and mineral acids as catalysts. Although good results were achieved, the disadvantage of homogenous catalysts is that upon working up the reaction mixture, the catalysts cannot be regenerated and reused. Therefore, they are not desirable either from the environmental or economic point of view. The innovation in our research is the use of heterogeneous solid acid catalysts where the catalyst can be reused for several reaction cycles, which makes their application highly economical. In this work, three catalytic systems were investigated, (i) ordered mesoporous silica (ii) bridged periodic mesoporous organosilicas and

(iii) carbon materials. In all catalysts, Brønsted acid sites were introduced as sulfonic acid groups ($-SO_3H$).

This thesis starts with a brief introduction that outlines the structure of biomass, followed by a discussion of some recent developments in accessing HMF from carbohydrates using mineral acids, Lewis acids and heterogenous catalysts. Thus, Chapter 2 aims at providing the reader with the necessary background information for understanding the work presented in this thesis.

The third chapter is a brief historical overview of nanoporous materials. Hence, the goal of this chapter was to provide an in-depth explanation of the interactions between the surfactant and the inorganic species in order to understand the formation mechanism of this type of materials.

The fourth chapter describes the methodology used in this work, which is mainly experimental, and goes into details about how the acidic nanoporous catalysts were prepared, including details concerning the catalytic reaction as well as the characterization techniques.

The fifth chapter presents the textural and structural characterization of the sulfonated materials and discusses the results obtained in the microwave-assisted conversion of sucrose into HMF using acidic nanoporous materials as catalysts.

Based on the results presented in Chapter 5, conclusions and contributions of this work are summarized in Chapter 6. In addition, recommendations are made for future work.

Chapter II – Literature Review

2.1 Exhaustion of Fossil Fuel Reserves

Faced with the threat of depletion of petroleum reserves, socioeconomic concerns, and the environmental harm associated with CO_2 emissions, alternative resources must be developed to sustain the needs of modern society for energy and chemicals. The development of environmentally sustainable methods for the production of transportation fuels from renewable resources is one of the most important challenges in the 21st century. Biomass provides a potential starting material because of its abundance and renewability. It can be obtained from various sources such as organic wastes (e.g. vegetable waste, crop residues, wood residues, plant-based waste, urban waste, agro-industrial waste, trees, algae, corn, wheat, rye straw, grass, fruits, edible and non-edible crops, etc...). Lignocellulosic biomass is a plant material comprised mainly of cellulose, hemicellulose and lignin. The relative amount of each component in biomass varies according to the type of biomass, tissue type, growth stage and growing conditions of the plant [4]. Cellulose is the major constituent in plant biomass, amounting to 38-50% of the total biomass composition, while hemicellulose corresponds approximately to 23-32% of the plant biomass [5, 52]. Lignin is the largest fraction "non-carbohydrate" component of biomass estimated to 15-25%. Other natural compounds, such as oils, fats, proteins, and other substances, correspond typically to 5% of the biomass.

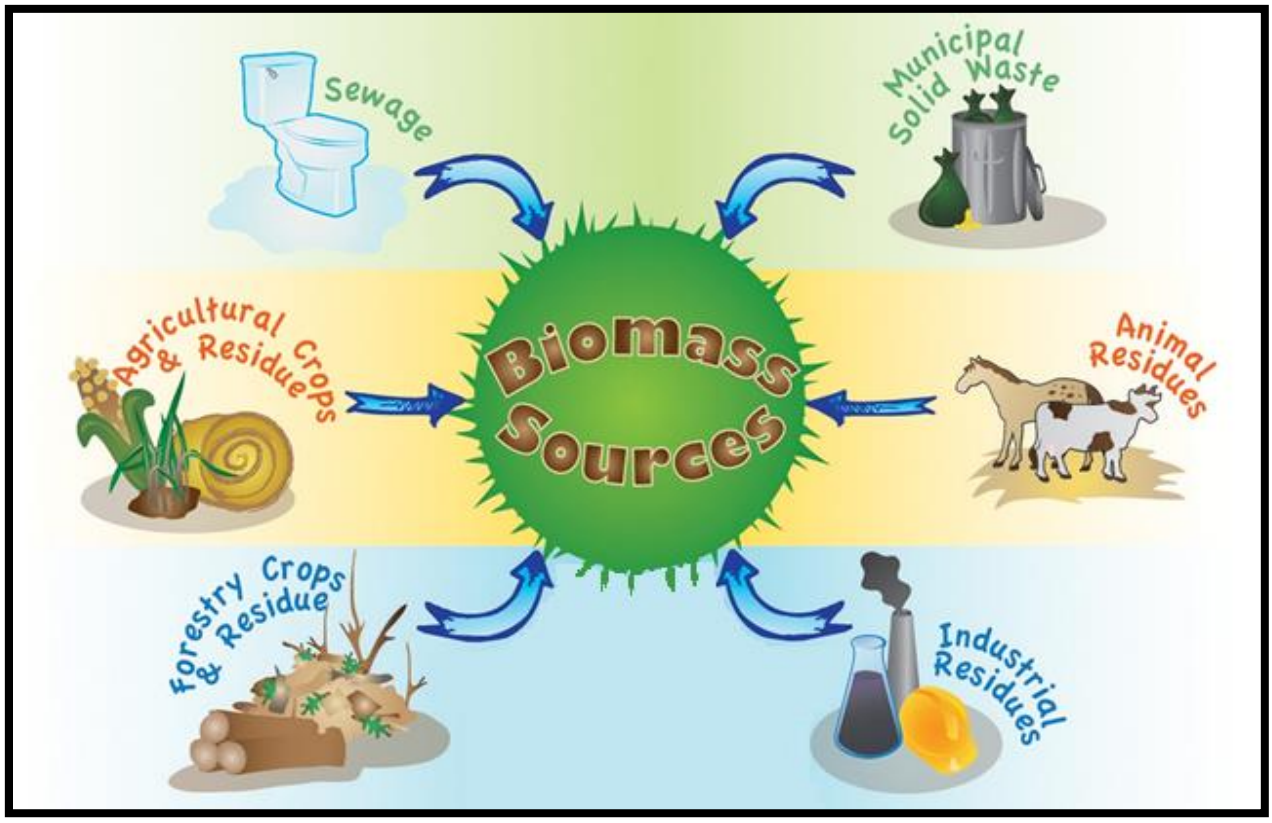

Figure 2.1: Sources of biomass.

2.2 Carbohydrates as Renewable Resource

Cellulose is the principle structural component of plants with an estimated annual worldwide production of 1.5 x 10^{12} tonnes and is considered to be a nearly inexhaustible source of raw biomass material [5]. This polysaccharide consists of a linear chain of several hundred to many thousands D-glucose units connected by β-1,4-glycosidic bonds (Figure 2.2).

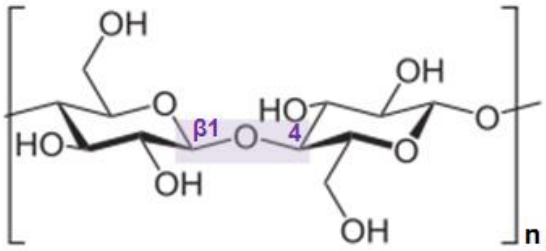

Figure 2.2: Structure of cellulose.

Synthesis of HMF directly from cellulose is advantageous for large-scale production. However, cellulose is regarded as a difficult material to work with due to its densely packed structure (Figure 2.3). The extensive hydrogen bonding and Van der Waals interactions greatly stabilizes cellulose making it particularly resistant to hydrolysis. Due to this robust crystalline structure, the functionalities of cellulose are not easily accessible to solvents, reagents and enzymes.

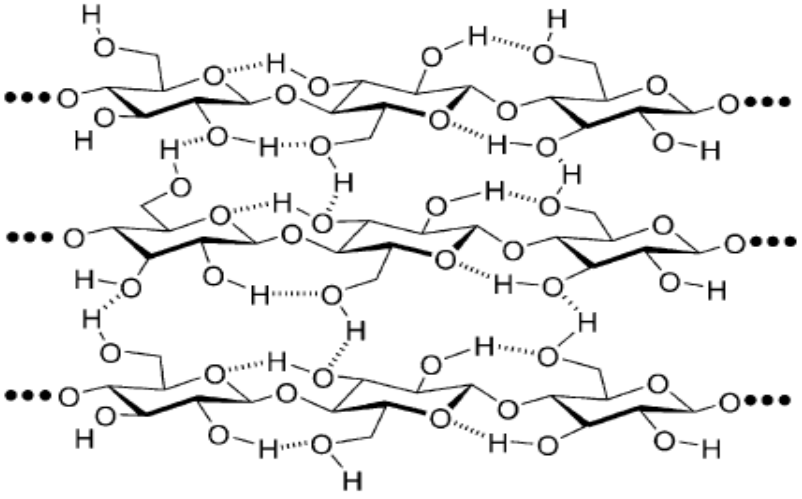

Figure 2.3: Hydrogen bond network of cellulose [4].

On the other hand, hemicellulose is a polymer consisting of five carbon sugars such as xylose, arabinose, and six carbon sugars such as glucose, galactose and mannose. It is the second most abundant polysaccharide in nature after cellulose. The composition of hemicellulose varies depending on the biomass source. Other than arabinose, a five membered-ring sugar in L-configuration, all monosaccharide are in D-configuration and pyranose forms (Figure 2.4). Unlike cellulose, the amorphous structure of hemicellulose degrades more easily to its sugars monomers.

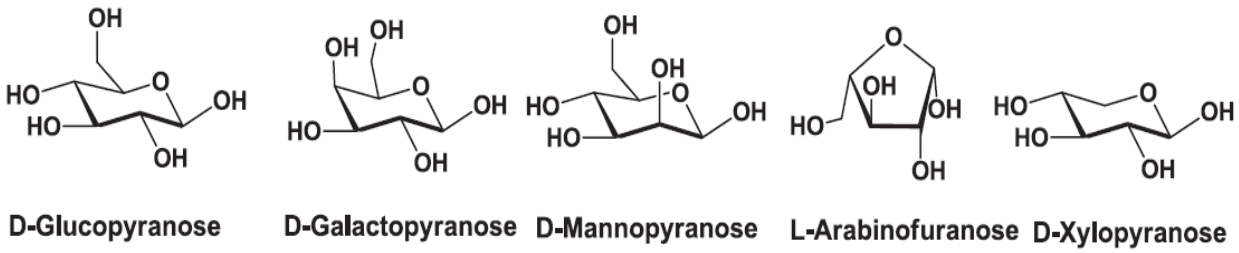

Figure 2.4: Basic constituents of hemicellulose [5].

The hemicellulose and cellulose fractions are surrounded by lignin, which provides plants with structural rigidity as well as a hydrophobic vascular system for the transportation of water and necessary nutrients [13]. Lignin, a non-carbohydrate component of biomass, consists of aromatic compounds in which phenylpropane units, with hydroxyl and methoxy groups are linked primarily through ether bonds [14]. Figure 2.5 shows the structure of a sample fraction of lignin.

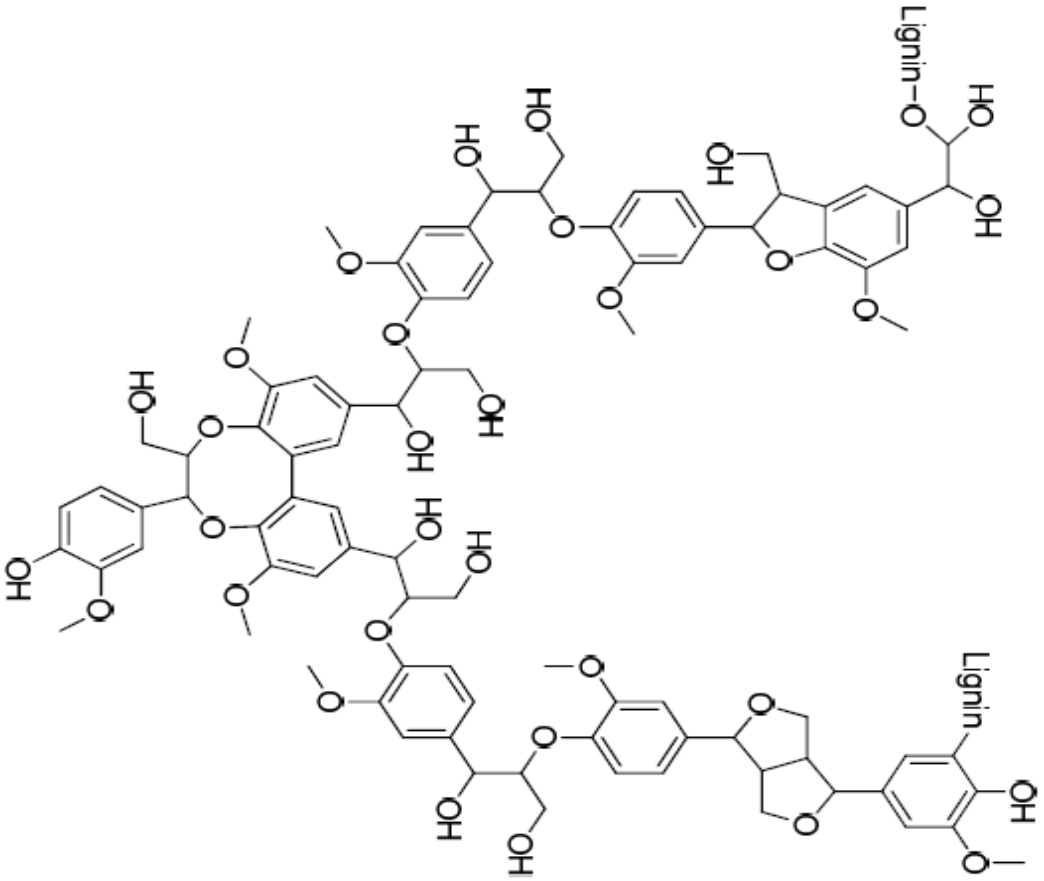

Figure 2.5: Typical structure of lignin [15].

2.3 HMF as a Versatile Building Block

Currently, one of the most promising approaches for the production of biofuel and chemicals from biomass is the conversion of carbohydrates into 5-hydroxymethylfurfural (HMF). HMF molecule consists of a furan ring, with an aldehyde and alcohol functional groups. The true value of this molecule is not in the compound itself, but in its capacity to be transformed into a number of useful compounds for the production of various chemicals and liquid fuels; hence it

has been referred to as a "sleeping giant" [6-7]. As shown in Figure 2.6, the hydroxymethyl group in HMF can for example be oxidized into an aldehyde or carboxyl group and the aldehyde can also be oxidized into a carboxyl group to give 2,5-furandicarboxylic acid (FDCA), 2,5-diformylfuran (DFF) and 5-hydroxymethyl-2-furancarboxylic acid (HFCA). These compounds are excellent raw materials for the synthesis of precursors for pharmaceuticals and the preparation of macrocyclic ligands [9-10]. On the other hand, the reduction of aldehyde group of HMF results in the formation of 2,5-bis(hydroxymethyl)furan (2,5-BHF), a key intermediate for the production of polymers [11]. Moreover, the cleavage of the HMF furan ring takes place under acidic conditions. Consequently, rehydration of HMF allows its decomposition into valuable chemicals such as levulinic acid and formic acid [12].

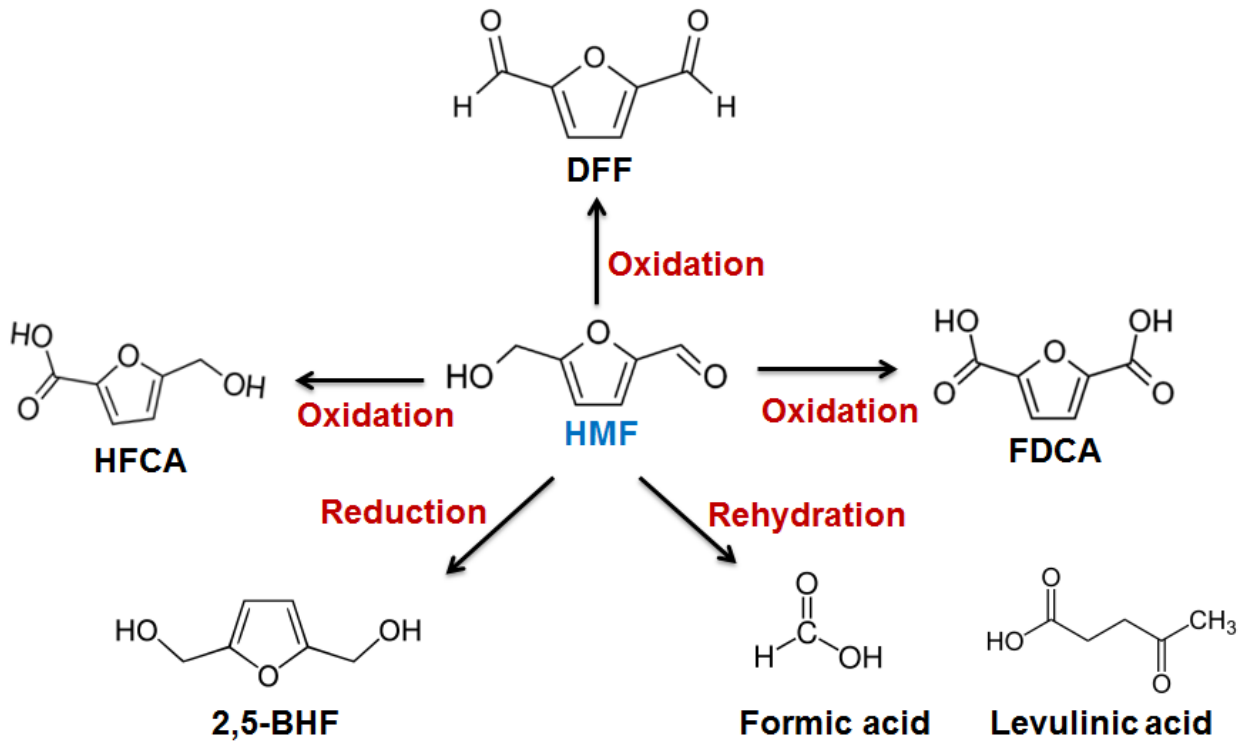

Figure 2.6: Catalytic pathways for the conversion of HMF.

Cellulose, which is made up of D-glucose units connected by β-1,4-glycosidic bonds, is the principal structural component of plants. The selective hydrolysis of cellulose into glucose by the hydrolytic cleavage of β-1,4 glycosidic bonds between anhydroglucose units is a critical step in the conversion of biomass. However, due to the poor solubility of cellulose and its inert structure, current methods to degrade cellulose into biofuel precursors are expensive, result in low yields and produce large amounts of waste [17]. Therefore, it still remains a challenge to effectively convert cellulose into liquid fuels and valuable chemicals.

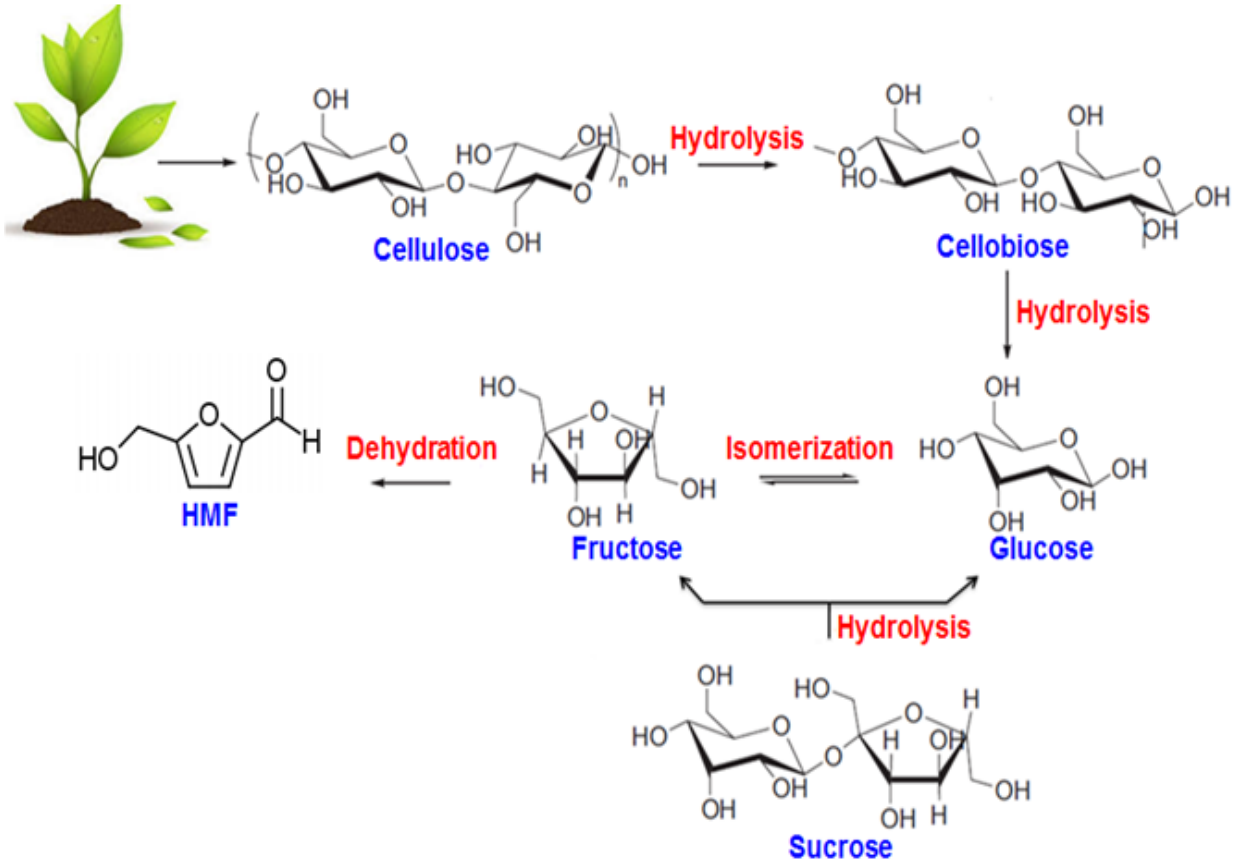

Figure 2.7: Production of HMF from carbohydrates.

Raw biomass containing high amounts of soluble sugars, such as grapes, can be readily converted to HMF without pre-treatment [37]. A large number of researchers have studied a range of reaction conditions for the laboratory-scale production of HMF from monosaccharides such as fructose and glucose. HMF is synthesized mainly by acid-catalyzed dehydration of monosaccharides with the consecutive loss of three water molecules (Figure 2.8) [16].

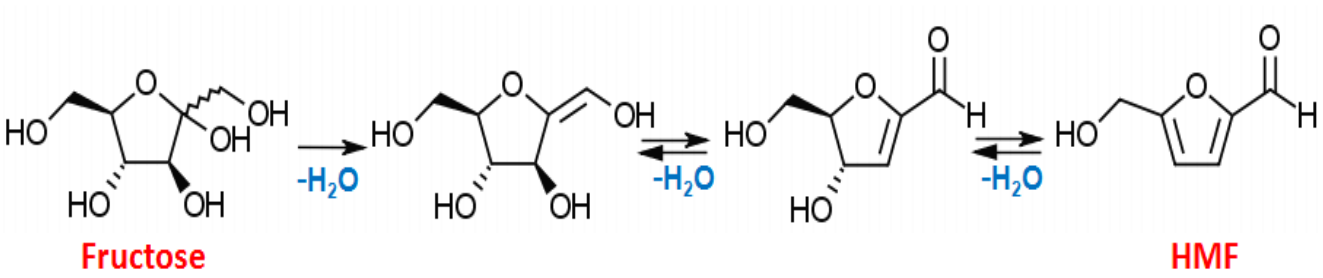

Figure 2.8: Acid-catalyzed dehydration of fructose into HMF.

The mechanism of fructose dehydration to HMF has been studied by numerous groups. The debate concerning the mechanism divided researchers into two groups, those in favor of an open chain mechanism and those promoting a mechanism comprising only cyclic species (Figure 2.9). The open chain mechanism proposes that HMF is synthesized from dehydration of fructose in its furanose form and occurs through a series of cyclic furan pathways [18]. The alternative mechanism suggests that HMF is formed through an open chain enediol pathway [19]. Although acyclic route is favoured by most scientists, Antal et al. [8] reported experimental evidence to prove the existence of cyclic intermediates in the synthesis of HMF from fructose.

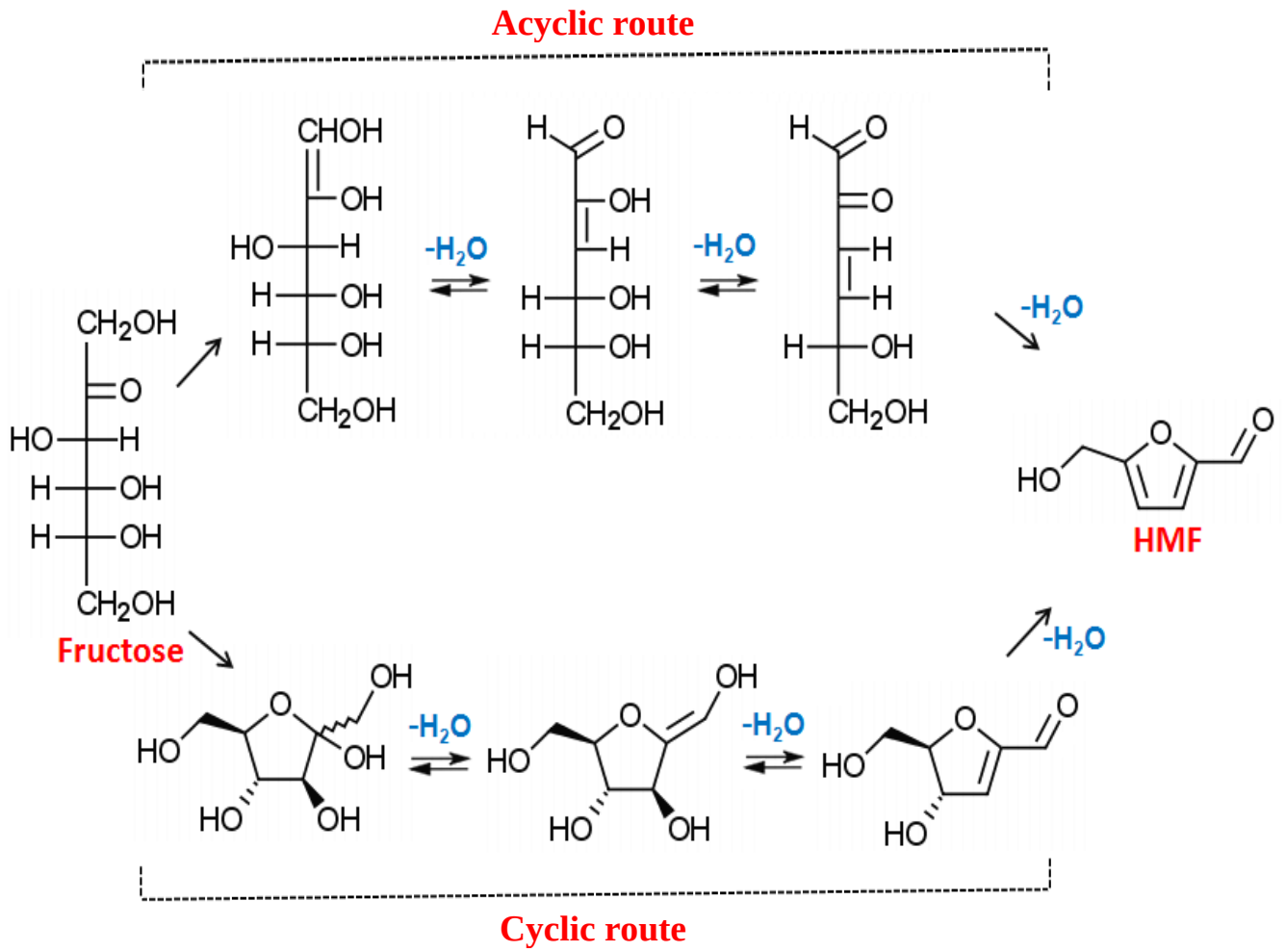

Figure 2.9: Possible mechanism for the dehydration of fructose.

The conversion of glucose is more difficult compared to fructose dehydration due to the higher stability of the pyranoside ring structure of glucose. The 1,2-enediol is an intermediate in the isomerisation of glucose to fructose (Figure 2.10). Thus, glucose has a lower reactivity than fructose, and this fact has been explained by the much lower abundance of acyclic glucose compared to acyclic fructose. Glucose can form a very stable ring structure, so the enolization rate of glucose in solution is lower that fructose, which is the rate determining step for the production of HMF [20]. Therefore, fructose will react much faster than glucose. Although

monosaccharides are easier to convert to HMF, commercial scale production dictates that efforts should focus on the synthesis of HMF from polysaccharides and raw biomass. Disaccharides or polysaccharides, such as sucrose, cellubiose, inulin or cellulose, can be used as raw materials, but hydrolysis is a prerequisite "first-step" for depolymerisation. Sucrose, a disaccharide consisting of glucose and fructose connected by α-1,2-glycosidic bond, is widely present in the plant kingdom. It is classified as the royal carbohydrate with an estimated annual production of 167 million metric tons [21,42]. Compared with the price of fructose and glucose, the price of sucrose is lower. Therefore, synthesis of HMF directly from sucrose shows a great potential for large-scale production of HMF because it circumvents the step of the production of glucose and fructose as well as the corresponding costs.

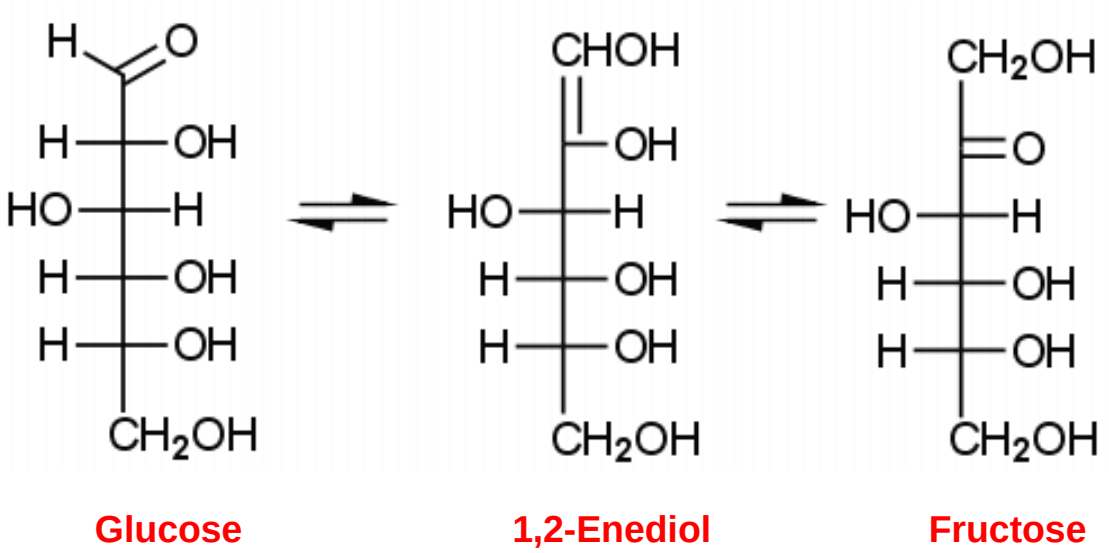

Figure 2.10: Glucose isomerization to fructose.

2.4 Catalysis

Since the beginning of the 19th century, it was found that reaction rates can be increased by the presence of foreign substances, referred to it as catalysts, not involved in the stoichiometric equation. A catalyst is a substance that increases the rate of a chemical reaction without undergoing a net chemical change itself. Thus, a catalyst does not alter the thermodynamic characteristics of a reaction but only its kinetic properties. Moreover, there is no stoichiometric relationship between the catalyst and the reagents.

The catalyst increases the reaction rate by apparently lowering the activation energy. Actually, it does not decrease the activation energy of the reaction, but replaces the reaction pathway by another with the same initial and final state, but a lower activation energy than the non-catalyzed reaction. After the lowering of the energy, there is also an endothermic step in which the product is separated from the catalyst, which can then be reused in a new cycle. In the non-catalytic cycle, a reaction occurs if the interaction between the reactants has enough energy to overcome the activation energy.

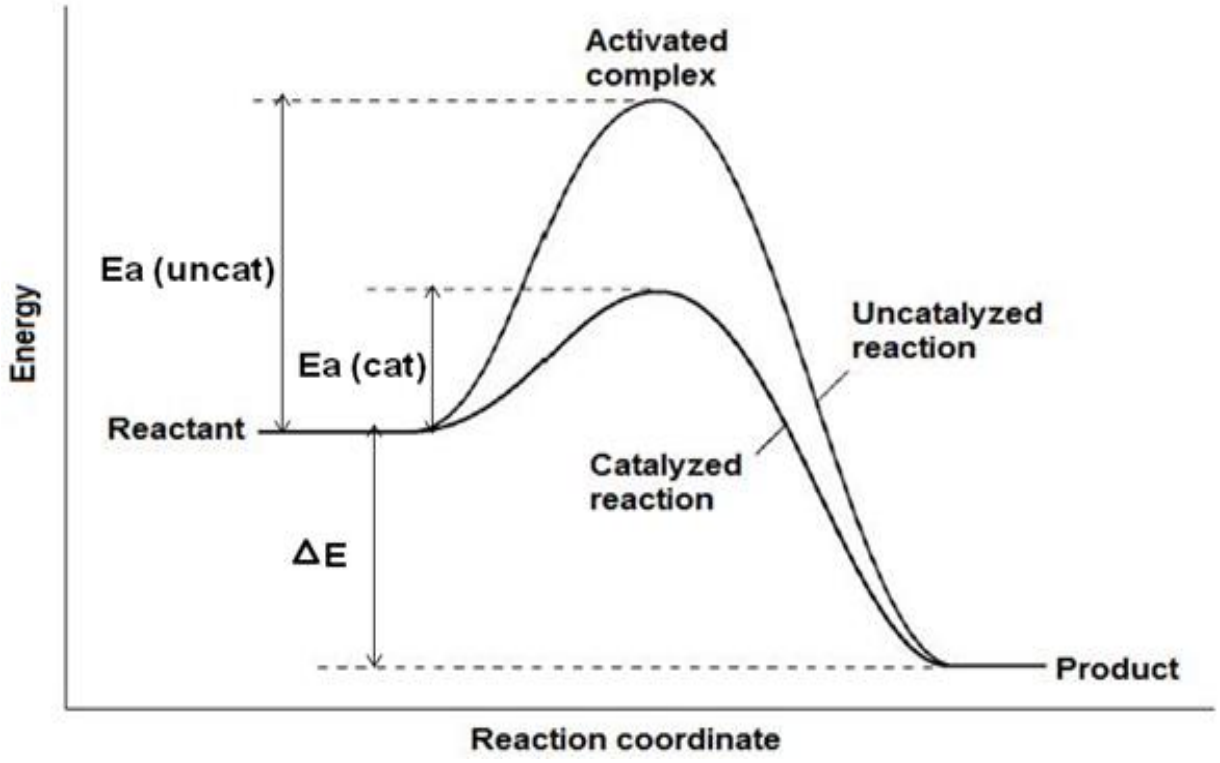

Figure 2.11: Schematic energy diagram for a reaction with and without a catalyst, Ea (uncat) = activation energy for the uncatalyzed reaction; Ea (cat) = activation energy for the catalyzed reaction [22].

Catalysis played a remarkable role in reducing pollution in our environment. With catalysis, reactions can be more efficient and selective, thereby requiring much less energy, and eliminating large amounts of by-products and other waste compounds [23]. To analyze more precisely the role of a catalyst, it is necessary to distinguish between three types of catalysis: enzymatic, homogeneous and heterogeneous. In the enzymatic catalysis, also called bio-catalysis, the reactions can occur in the living environment or on an industrial scale using appropriate enzymes. In homogeneous catalysis, the catalyst and the reactants form a single phase. This can be for example a gas in a gas mixture or, more commonly, a solid, a liquid or even a gas dissolved in a liquid medium (solvent). Finally, in heterogeneous catalysis, the

catalyst forms a separate phase from the reactants. An example of this situation is a solid catalyst in a liquid or gas system. The essential distinction between homogeneous and heterogeneous catalysis is whether or not the catalyst is present in the same phase as the substrate.

2.5 Conversion of Carbohydrates into HMF

Acid catalysis is by far the most important field of catalysis employed by industries in all sectors of chemical manufacturing, especially in the petrochemical industry [13-24]. HMF is the most relevant compound derived from biomass owing to its possible conversion into a large number of chemicals having applications in diverse industries. Hence, biomass is an advantageous replacement of petroleum as a primary energy source. Before this realization can be accomplished, conversion technologies must be developed to enable the efficient and cost effective conversion of biomass to HMF. Nowadays, no such process exists on a commercial scale. Nonetheless, numerous research groups have investigated a range of reaction conditions for the laboratory-scale production of HMF from different carbohydrates such as fructose, glucose, cellulose and sucrose. To enable a better understanding of the development in HMF synthesis in recent years, an overview of synthetic methods to access HMF from carbohydrates will be presented based on the type of catalysts used.

2.5.1 Homogeneous Catalysts

The dehydration of carbohydrates can be catalyzed by Brønsted acids as well as by Lewis acids. As summarized in Tables 2.1 and 2.2, a great number of catalysts such as Lewis acids, organic, and inorganic acidic compounds, have been identified as catalysts for the synthesis of HMF. Mineral acids can be used as homogeneous catalysts for the transformation of carbohydrates (Table 2.1). Hydrochloric, sulfuric and phosphoric acids are most frequently used to catalyze the conversion of carbohydrates due to their readily availability. It was found that HCl is the most successful catalyst in terms of both fructose conversion and yield, followed by H_2SO_4 and H_3PO_3. Antal and coworkers [8] reported the dehydration of fructose with H_2SO_4 as catalyst in subcritical water at 250 °C and obtained HMF with a yield of 53%. Birker et al. [25] also used H_2SO_4 as a catalyst in subcritical water-acetone solvent at 180 °C. The yield of HMF obtained reached 48%. Asghari and Yoshida [27] studied the use of a variety of acids in subcritical water to dehydrate fructose to HMF (Figure 2.12). The highest HMF yield of 39%, was obtained in the presence of H_3PO_4 as catalyst. Hansenet al. [28] used HCl as catalyst for the microwave-assisted dehydration of concentrated aqueous fructose solutions into HMF. The authors compared microwave heating with conventional oil bath heating and found that pure aqueous phase, which normally results in low HMF yields and many by-products when used as a reaction medium, performed substantially better with microwave irradiation to generate HMF rapidly with a selectivity of 63% and fructose conversion of 52%. More recently, Dumesic and coworkers [26] studied the conversion of fructose to HMF in a two-phase reactor system (Figure 2.12). In this biphasic system, fructose was dehydrated in the aqueous phase with HCl as a catalyst and HMF obtained was continuously extracted into an organic methylisobutylketone (MIBK) phase modified with 2-butanol to enhance the partitioning of the HMF in favor of the organic phase.

Dimethylsulfoxide (DMSO) and poly(1-vinyl-2-pyrrolidinone) (PVP) were added to suppress unwanted side reactions. This method afforded high fructose conversion (90 %) with high HMF selectivity (80 %). The authors extended the application of the modified water-organic biphasic reaction system catalyzed with HCl to polysaccharides [29]. Under comparable reaction conditions, a biphasic system containing a water-DMSO mixture as the aqueous phase, combined with an organic extracting phase consisting of a 7:3 (w/w) MIBK: 2-butanol mixture produced a HMF yield of 50, 26, 27 and 75% from sucrose, starch, cellobiose and inulin, respectively at 170 °C.

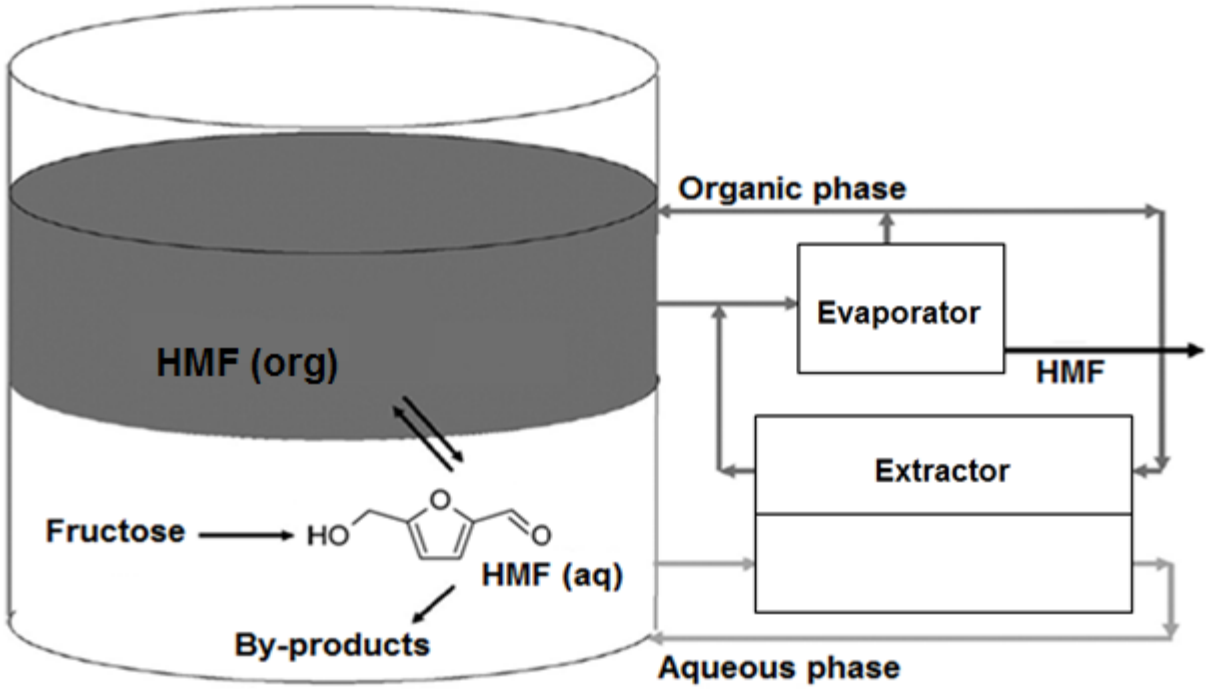

Figure 2.12: Schematic diagram of a biphasic reaction system for HMF production via concurrent extraction and evaporation steps. The aqueous phase contains fructose, DMSO, PVP, and catalyst, and the organic phase contains MIBK and 2-butanol [94].

In parallel, research efforts were also focused on developing sustainable methods for the production of HMF in the presence of Lewis acid catalysts. Some examples of such acid catalysts for HMF synthesis from sugars are summarized in Table 2.2. In 2007, a breakthrough achievement in HMF production from glucose was reported by Zhang and coworkers [43]. They used chromium chloride ($CrCl_2$) as catalyst in ionic liquid [EMIM]Cl, resulting in 70% HMF yield. Moreover, Zhang et al. [44-45] found that cellulose can be depolymerised to HMF with a yield of 61% by microwave heating in [BMIM]Cl with $CrCl_3$. Raines and co-workers [46] also used $CrCl_3$ and $CrCl_2$ in a solvent mixture consisting of N,N-dimethylacetamide (DMA)-LiCl and [EMIM]Cl. However, because of the toxicity and polluting effect of $CrCl_2$ and $CrCl_3$, some other Lewis acids with low toxicity such as zirconium (IV) chloride ($ZrCl_4$) [47] and indium (III) chloride $InCl_3$ [48] were also applied to catalyze the conversion of cellulose into HMF in ionic liquids. Recently, a one-pot process for the conversion of cellulose into valuable HMF in DMSO was reported to be catalyzed by aluminium chloride ($AlCl_3$) [49]. Under mild conditions, $AlCl_3$ effectively promoted cellulose to HMF reaction with a yield of 54.9%.

Table 2.1: *Conversion of carbohydrates using mineral acid catalysts*

Carbohydrate	**Solvent**	**Catalyst**	**Temperature (°C)**	**Time (min)**	**Conversion (%)**	**HMF yield (wt %)**	**Ref.**
Sucrose	9:1 Supercritical acetone/H_2O	H_2SO_4	180	2	90	48	25
Fructose					95	68	
Glucose					92	41	
Inulin					91	68	
Fructose	Subcritical water	HCl	240	2	63	12	27
		H_3PO_4			100	39	
		H_2SO_4			100	20	
		Citric acid			95	35	
		Maleic acid			96	28	
		Oxalic acid			94	13	
Cellubiose	4:6 H_2O/DMSO /7:3 MIBK/ 2-butanol	HCl	170	10	52	27	29
Sucrose				5	65	50	
Starch				11	61	26	
Inulin				5	98	75	
Fructose	Dioxane-water	180	4	84	40	37	180

Table 2.2: *Conversion of carbohydrates using metal chlorides catalysts*

Carbohydrate	Catalyst	Solvent	Temperature (°C)	Time (min)	HMF yield (wt %)	Ref.
Glucose	$CrCl_2$	[EMIM]Cl	100	180	68	43
	$CrCl_3$	DMA-LiCl/ [EMIM]Cl		360	62	46
Glucose	$MgCl_2$	[BMIM]Cl	220 (Microwave)	3.5	26	47
	$AlCl_3$				24	
	$CuCl_2$				30	
	$ZrCl_4$				48	
Fructose	$ZrCl_4$			2	93	44
Cellulose	$CrCl_3$				20	47
Sucrose	$SnCl_4$	$[EMIM]BF_4$	100	180	65	41
Glucose					61	
Fructose					62	

2.5.2 Heterogeneous Catalysts

In recent years, increasingly stringent environmental and economic considerations generated great interest in developing cleaner synthetic methods to achieve a reduction of harmful substances and toxic wastes. In this regard, heterogeneous catalysis can play a key role in the development of environmentally friendly chemical processes, including the oil, petrochemical and pharmaceutical industry. Since homogeneous catalysts are present in the same phase as the

substrate, this causes difficulties in the product separation stage, leading to the generation of large volumes of waste, excessive consumption of energy and loss of expensive catalysts. In contrast to homogeneous catalysts, heterogeneous catalysts can be readily recovered and reused. The use of heterogeneous catalysts to convert carbohydrates to HMF offers several advantages over homogeneous acid catalysts such as easy separation, non toxicity and recyclability. In the dehydration of carbohydrates, a variety of solid acids such as ion-exchange resins, heteropolyacids, metal oxides, zeolites and acid-supported catalysts have been examined for HMF production (Table 2.3). Among solid acid catalysts, studies concerning the application of ion-exchange resins are the most numerous. For example, Smith and co-workers [32] investigated the microwave-assisted dehydration of fructose to HMF using the ion-exchange resin DOWEX 50WX8-100 as catalyst. Although initial work used pure DMSO as solvent, acetone was used as a co-solvent to promote higher HMF selectivity. In only 10 min, a HMF yield of 82% was obtained at 150 ºC in this system, while the catalytic activity of the resin was maintained over multiple runs. The dehydration of fructose to HMF was also carried out using Amberlyst-15 as catalyst in ionic liquids [33]. When the reaction was carried out in [BMIM]BF_4 as solvent and Amberlyst-15 as catalyst, a HMF yield of 50% was obtained after 3 h. The reaction was then performed at 80 °C using two ionic liquids, a hydrophilic ([BMIM]BF_4) and a hydrophobic [BMIM]PF_6 as solvents, Amberlyst-15 as catalyst and DMSO as a co-solvent to assist with sugar solubility. Under these conditions, both ionic liquids allowed the reaction to proceed more rapidly than in DMSO alone, and with HMF yields close to 80% within 24 h. However, a major problem with ion-exchange resin is their limited thermal stability and their deactivation at temperature above 130 °C, which is caused primarily by cleavage of the sulfonic acid groups attached on the resin [50].

Metal oxides are also widely used as catalysts for HMF synthesis. Watanabe and coworkers [34-35] examined the production of HMF from fructose catalyzed by TiO_2 and ZrO_2 under microwave irradiation. In the presence of TiO_2, the yield of HMF reached 38 % with a fructose conversion of 83.6 % at 200 °C after 5 min in microwave. Moreover, a 30.5 % HMF yield and 65% fructose conversion were obtained in the presence of ZrO_2 under otherwise the same conditions. Moreau et al. [30-31] studied the dehydration of fructose in the presence of H-form zeolites as catalysts in a solvent mixture consisting of water and MIBK at 165 °C. A maximum in the rate of conversion of fructose was observed for H-mordenite with a Si/Al ratio of 11. The high selectivity obtained (> 90%) was correlated with the shape selectivity properties of H-mordenites (bidimensional pore structure), and particularly with the absence of cavities within the structure allowing further formation of secondary products. Recent effort was focused on the use of silica and carbon materials functionalized with sulfonic groups for the synthesis of HMF from fructose. Dumesic et al. [143] reported the use of a set of modified SBA-15 silica-supported sulfonic acid groups as catalysts for the dehydration of fructose in a biphasic system, and obtained HMF with a yield of 52-59%. HMF was also successfully produced by the dehydration of fructose using lignin-derived solid acid catalyst in [BMIM]Cl. The yield of HMF obtained reached 57% along with a fructose conversion of 100% [128].

Table 2.3: *Conversion of carbohydrates using heterogeneous catalysts*

Carbohydrate	Catalyst	Solvent	Temperature (°C)	Reaction time	Conversion (%)	Yield (wt%)	Ref.
Fructose	SAPO-44	Water-MIBK	175	1 h	89	55	51
Glucose				4 h	83	47	
Fructose	$Ag_3PW_{12}O_{40}$		120	1 h	83	54	52
	$H_3PW_{12}O_{40}$				86	31	
	SiO_2/H-MOR zeolites		165	5 h	75	33	53
Fructose	$H_3PW_{12}O_{40}$	DMSO	120	2 h	97	68	54
	Amberlyst-70	THF-water	130	10 min	90	54	56
Fructose	α-$Sr(PO_3)_2$	Water	200	5 min	88	55	55
Cellulose			230		N/A	12	
Glucose			200		61	15	
Glucose	Amberlyst-15	DMF	80	9 h	73	30	57
	$Ag_3PW_{12}O_{40}$	Water-MIBK	130	4 h	89	53	144
Fructose	pSO_3H-SBA-15[1]	Water/ MIBK: 2-butanol	130	140 min	79	52	143
	TESAS-SBA-15[2]				84	59	
	SSA-SBA-15[3]				81	52	
	Sulfonated lignin-derived carbon	[BMIM]Cl	110 (Microwave)	10 min	100	59	128
	Sulfonated cellulose-derived carbon		160	15 min	N/A	57	121

[1] Propylsulfonic acid-functionalized SBA-15
[2] 3-(Propylthio)propane-1-sulfonic acid-functionalized SBA-15
[3] 3-(Propylsulfonyl)propane-1-sulfonic acid-functionalized SBA-15

Although considerable work has been undertaken to access HMF from carbohydrate resources, more remains to be done. Much progress has been reported for the conversion of fructose, yet the conversion of other carbohydrates such as glucose, sucrose and cellulose remain difficult. The work at hand is concerned with developing an environmentally benign catalyst system to convert sucrose into HMF. Generally, conversion of sucrose to HMF involves two steps, namely, sucrose hydrolysis to monosaccharide glucose and fructose followed by the dehydration of fructose and glucose to give HMF. Synthesis of HMF directly from sucrose shows a great potential for large-scale production because it circumvents the step of the production of glucose and fructose as well as the corresponding costs. To date, there were some reports on the synthesis of HMF from sucrose using metallic chlorides and mineral acids as catalysts (Table 2.4). Although good results were achieved, these types of catalysts are however harsh or toxic, and with today's emphasis on green chemistry, it is imperative that processes for the transformation of carbohydrates be environmentally benign. Furthermore, they must be amenable to implementation on a large-scale that will be required to meet the demands of the future. This study is conducted to develop an efficient one-pot process to synthesize HMF from biomass, particularly sucrose, using various sulfonated heterogeneous catalysts such as sulfonated bridged periodic mesoporous organosilicas (PMO), porous carbon materials and ordered mesoporous silicas such as SBA-15. Therefore, chapter three focuses on a brief introduction to mesoporous materials.

***Table 2.4**: Conversion of sucrose into HMF*

Solvent	Catalyst	Temperature (°C)	Time (min)	Yield (%)	Ref.
DMSO	$AlCl_3$	120 - Microwave	12	33	36
Dioxane-water (39:7 w/w)	$CrCl_3.6H_2O$; HCl	210 - Microwave	4	36	37
	$AlCl_3.6H_2O$; HCl			31	
Water	H_3PO_4	160	60	12.6	
	Maleic acid			13.2	
	Fumuric acid			11	
	HCl			14.1	
[BMIM]Cl	$CrCl_3$	150 - Microwave	10	76	39
	$GeCl_4$	120	30	55	40
	$ScCl_3$	400W - Microwave	2.5	61	42
$[EMIM]BF_4$	$SnCl_4$	100	180	65	41
Choline chloride	$CrCl_2$		60	48	38

Chapter III – Mesoporous Materials

3.1 Porous Materials

The International Union of Pure and Applied Chemistry (IUPAC) distinguished three classes of porous materials according to their pore diameter [61]:

- Microporous materials, with pore diameters less than 2 nm.
- Mesoporous materials, with pore diameters between 2 and 50 nm.
- Macroporous materials with pore diameters greater than 50 nm.

Some of the best known examples of microporous and macroporous materials are zeolites and silica gel respectively. Zeolites are crystalline aluminosilicates with three-dimensional structure [62]. They exhibit high thermal stability due to their rigid framework consisting of tetrahedrally coordinated aluminosilicates. Some of the most common zeolites are presented in Figure 3.1. In addition, the well defined pore system and charged surfaces of zeolites make them useful for commercial applications such as ion-exchange, water purification and adsorption, while the surface acidity makes them useful in catalysis. The main drawback with zeolites is the limiting pore diameter of less than ~1.5 nm, particularly when dealing with catalytic processes involving larges molecules such as heavy oil cracking.

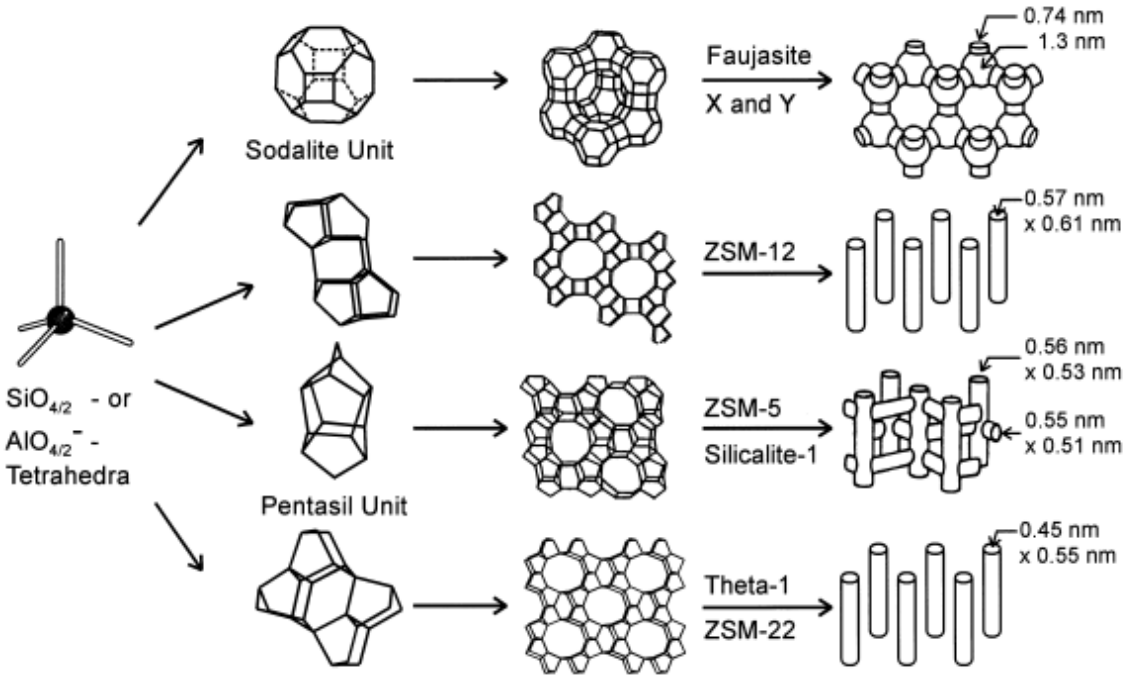

Figure 3.1: Structures of some typical zeolites and their micropore systems [63].

Mesoporous materials may exhibit randomly located pores with broad pore size distributions (PSD), or ordered pore structure with narrow PSD. The following section is devoted to ordered mesoporous materials.

3.2 Ordered Mesoporous Materials

In 1992, a research group at Mobil Oil Corporation discovered a new family of mesoporous silica materials, the so-called M41S, which consists of three mesophases as illustrated in Figure 3.2, namely MCM-41 with a hexagonal pore structure, MCM-48 with a cubic pore structure, and MCM-50 with a lamellar pore structure (MCM: Mobil Composition of Matter).

These materials received intensive attention due to their highly ordered pore structures, tunable pore sizes from 2 to 30 nm and high surface area, typically between 600 and 1300 m^2/g (for silica). Since then, ordered mesoporous materials showed promising behavior in many potential applications such as separation, catalysis, sensing and electronic devices [58-60].

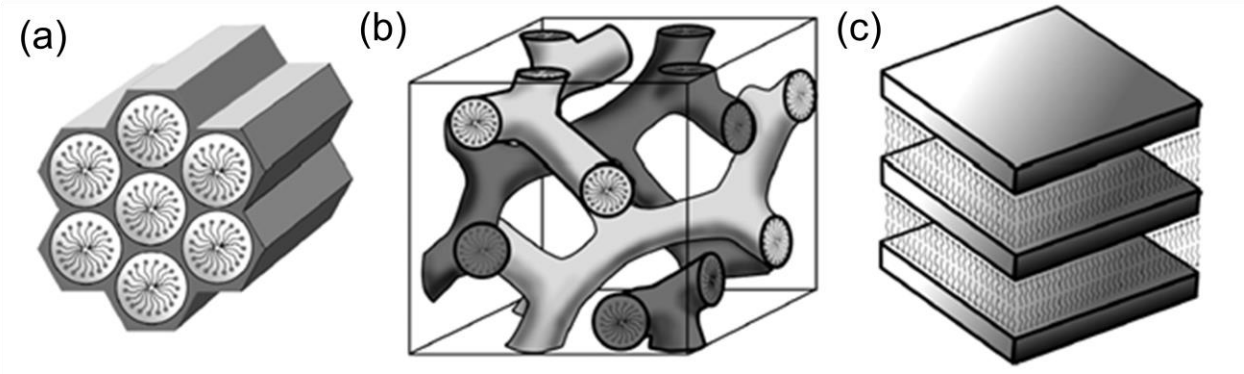

Figure 3.2: Structures of mesoporous M41S materials: (a) MCM-41 (hexagonal, space group *p6mm*), (b) MCM-48 (cubic, space group *Ia3d*), (c) MCM-50 (lamellar, space group *p2*) [73].

An important feature of the silica-based ordered mesoporous materials is the possibility of modifying their internal surface through the covalent attachment of different functional groups. The pore walls are made of an amorphous arrangement of tetrahedral silica, and the presence of silanol groups allows the modification of the surface properties by grafting organic functions (Figure 3.3). As a consequence of the functionalization, organic-inorganic materials are obtained and their hybrid character is based on their architecture consisting of an inorganic framework and organic groups attached onto the pore surface.

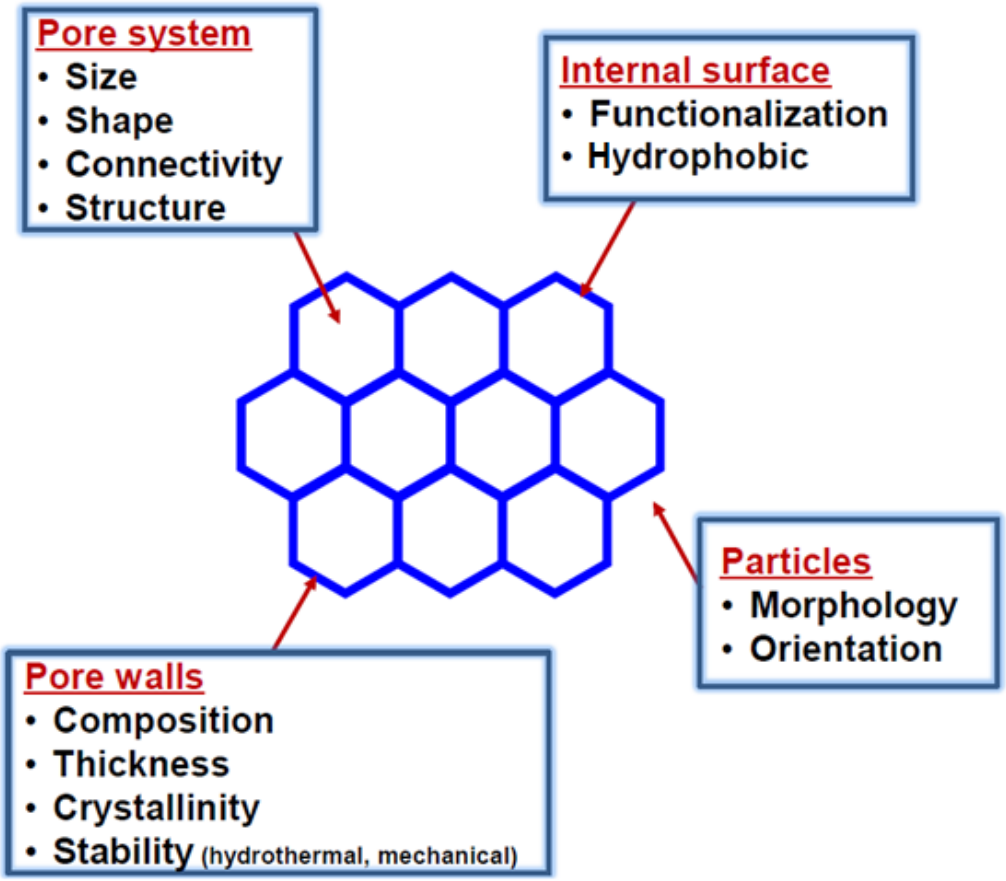

Figure 3.3: Structural parameters for the design of periodic mesoporous materials [64].

Parallel to the discovery of M41S, Yanagisawa et al. [68] from Waseda University and Inagaki et al. [69] from Toyota prepared folded sheets mesoporous material designated as FSM-16. The material was synthesized by an intercalation of quaternary ammonium surfactant as a template in a layered polysilicate kanemite, followed by calcination [70]. The FSM-16 material is structurally similar to MCM-41 (hexagonal, p6mm) and is widely used as an adsorbent and as a host for the inclusion of large molecules.

Mesoporous materials are synthesized according to the liquid-crystal template mechanism (LCTM) whose principle is based on the self-assembly of amphiphile species, leading to a structure akin of liquid crystals, followed by the addition and the condensation of the inorganic precursor (e.g. SiO_4^{4-} or an n-oligomer) thereof. Different families of materials can be obtained (e.g. M41S, SBA-n), depending on the nature of the surfactant (ionic or neutral) used and the reaction medium (acidic or basic) in which the synthesis takes place. Mesoporous materials are basically prepared through silica formation around template micelles assemblies followed by template removal by appropriate methods such as calcination or solvent extraction. The spatial arrangement of the micelles in solution depends on the concentration of surfactant, temperature as well as the presence of other species, and hence, the final pore structure of the material. The well-known and widely used material, MCM-41, is synthesized by self-assembly of a cationic surfactant, typically cetyltrimethylammonium bromide (CTAB) in the presence of a silica source, usually silicon dioxide or tetraethylorthosilicate (TEOS), under basic conditions [65].

After the discovery of M41S materials, extensive effort focused on the development of other types of periodic mesoporous materials and different synthesis routes. In 1998, a research group lead by Stucky at the University of Santa Barbara reported the synthesis of a new family of periodic mesoporous materials, the SBA-n (SBA: Santa Barbara) [66]. SBA-15 has attracted the most attention because of its excellent structural properties, its mechanical and thermal stability, and its high reproducibility. It is synthesized using an amphiphilic triblock copolymer, Pluronic P123 as structure directing agent under acidic conditions and can be easily prepared in a range of temperature between 35 °C and 130 °C [67]. Though both SBA-15 and MCM-41 exhibit two dimensional hexagonal structures (*p*6*mm*), they have some notable differences: SBA-15 has

larger pores and thicker pore walls which give it a higher thermal and hydrothermal stability than MCM-41. Another major difference between these two mesoporous materials is that the parallel channels in MCM-41 do not communicate with each other, while in SBA-15, the parallel channels are connected to each others with microporous or mesoporous bridges, depending on the synthesis temperature (Figure 3.4).

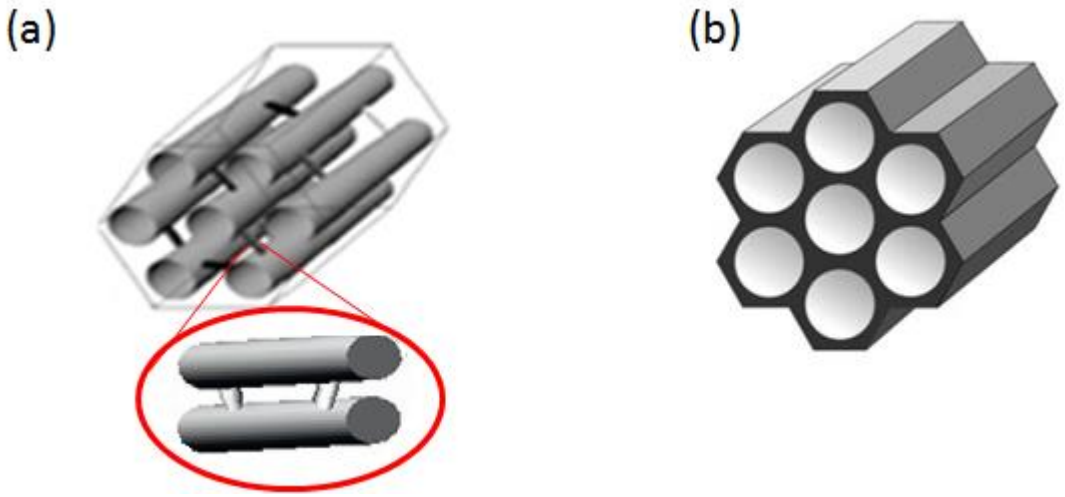

- Non ionic surfactant: Pluronic P123
- Acidic media
- Parallel channels: communicate

- Cationic surfactant: CTAB
- Basic media
- Parallel channels: do not communicate

Figure 3.4: Structures of (a) SBA-15 and (b) MCM-41.

3.3 Synthesis of Periodic Mesoporous Silica

A surfactant is defined as an amphiphilic molecule with a hydrophilic head group and a hydrophobic tail (Figure 3.5)

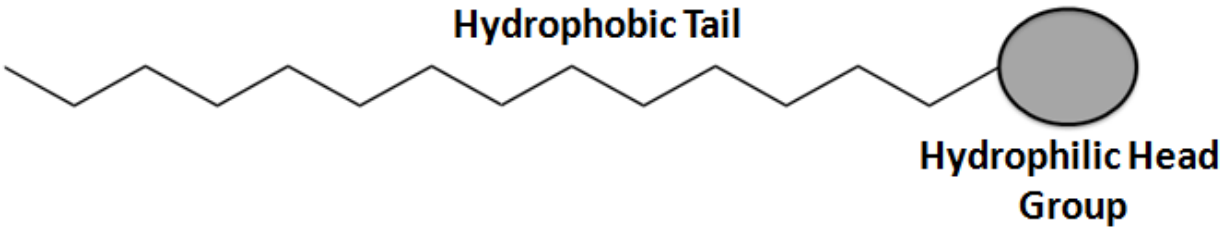

Figure 3.5: Schematic representation of a surfactant.

Surfactant molecules self-organize in water in different structures depending on their concentrations and the temperature. The surfactant molecules are first dissolved in an aqueous solution, and when the concentration reaches the critical micellar concentration (CMC-1), the surfactant molecules aggregate to form spherical micelles (Figure 3.6). In aqueous solution, the micelle exposes its hydrophilic head groups to the water phase and the hydrophobic tails point toward the center. Further increase in the surfactant concentration to CMC-2 leads to coalescence of the spherical micelles to form cylindrical micelles. The CMCs depend on the chemical structure of each amphiphile; for example, a surfactant with greater hydrophobic tail will have a lower CMC. This phenomenon can be explained by the fact that the longer carbon chains tend to come together more easily, which implies a larger decrease in energy. The CMC is then a characteristic of each surfactant and depends on temperature and the solvent. When the concentration increases further, hexagonal close-packed arrays of micelles appear, producing typically a liquid crystal phase with a hexagonal symmetry. Further increase in concentration leads to the coalescence of the adjacent parallel cylinders to produce the lamellar phase or a

cubic phase. All these surfactant mesophases corresponding to supramicellar structures form liquid crystal phases. Once the supramicellar aggregates is formed, the silica precursor, commonly TEOS or fumed silica is added, and condenses to yield a highly condensed silicon oxide around the micelles within the mesostructure. In order to obtain a porous structure, the last step in the synthesis consists in removing the surfactant by calcination or solvent extraction. Calcination consists of heating the material in flowing air at high temperature, typically at 550 °C. Air is flown at a constant rate and the temperature is increased at no more than 2 °C per minute to avoid the collapse of the framework. An alternative to calcination for surfactant removal is solvent extraction. This is a milder approach which involves the usage of an organic solvent such as ethanol with a small amount of acid such as HCl. Other less popular methods involve microwave heating, or extraction with supercritical CO_2.

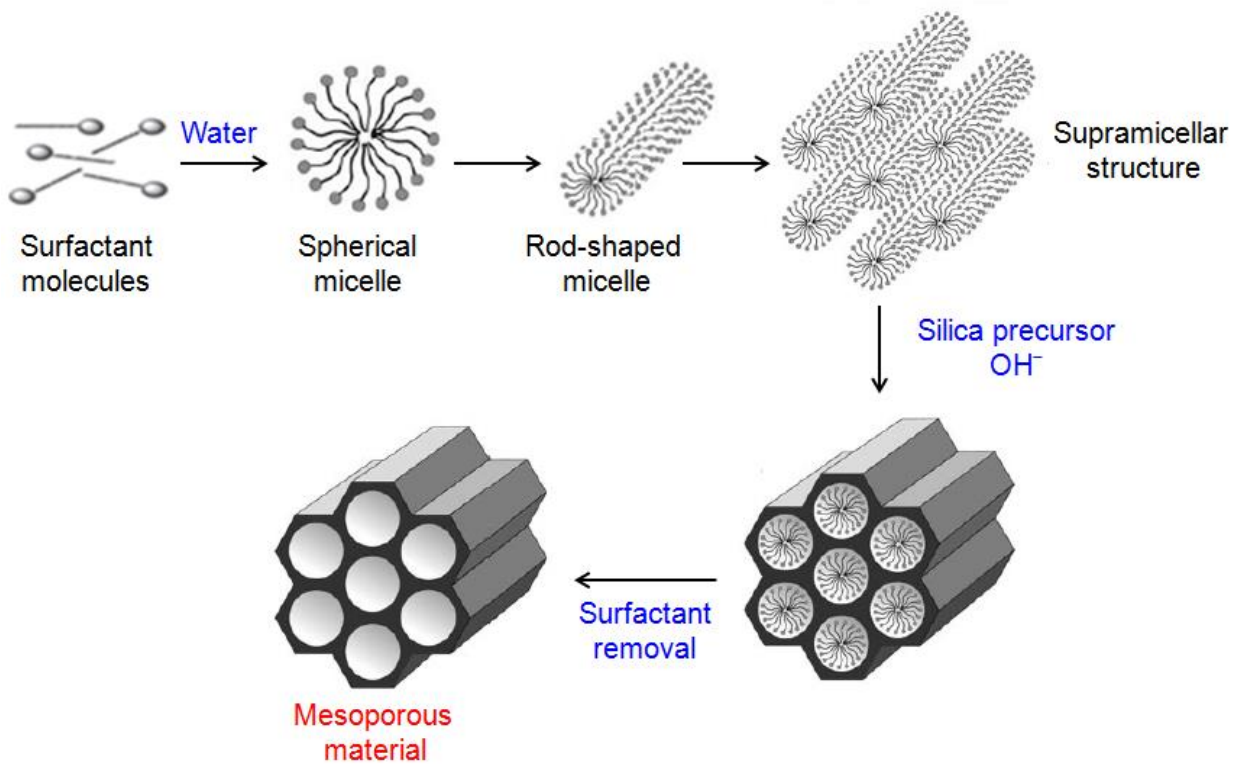

Figure 3.6: Schematic representation of the synthesis of mesoporous material.

Surfactants can be classified into four groups according to the charge of their polar head. Anionic surfactants have a negatively charged polar head group. The hydrophobic portion is a long hydrocarbon chain typically 10 to 18 carbons. The most common polar groups in this type of surfactants are carboxylates, sulphates, sulfonates and phosphates. Cationic surfactants are generally quaternary ammonium salts with a positive charged polar head group and a long alkyl chain as a non-polar group. In comparison with cationic surfactants, anionic surfactants are cheaper and less toxic [75]. Non-ionic surfactants typically have poly (ethylene oxide) as a common polar group and the poly (propylene oxide) as a non-polar group. They can also be long chain alkylamines. Zwitterionic surfactants have two charges of different signs on their head group giving an overall neutral charge. There are also surfactants with multiple head groups.

In this work, we used essentially two surfactants: octadecyltrimethylammonium chloride ($C_{18}Cl$), which is a cationic surfactant, and the triblock copolymer Pluronic P123, which is a nonionic surfactant. The $C_{18}Cl$ surfactant was used in the synthesis of biphenylene bridged periodic mesoporous organosilica (PMO). The amphiphilic triblock copolymer Pluronic P123, used as structure directing agent in the synthesis of SBA-15 and phenylene bridged PMO, presents poly (ethylene oxide) PEO as the hydrophilic portion of the molecule, and poly (propylene oxide) PPO as the hydrophobic part (Figure 3.7).

- **Pluronic P123:**

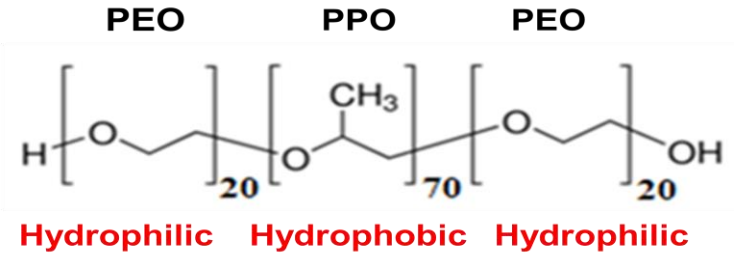

- **$C_{18}Cl$:**

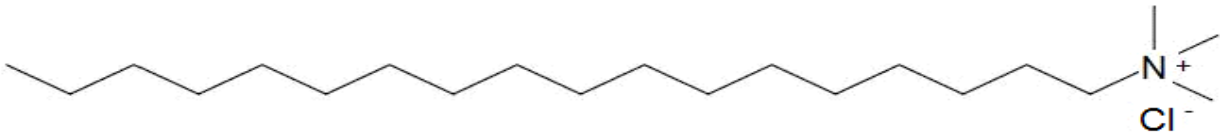

Figure 3.7: Chemical structure of triblock copolymer Pluronic P123 and $C_{18}Cl$.

3.4 Interaction Between Inorganic Species and Surfactant

The synthesis of mesostructured materials is based on the interactions between the polar head group of a surfactant (S) and the inorganic species (I). These interactions may be divided in six groups depending on the charge of S and I, namely $S^+ I^-$, $S^- I^+$, $S^+ X^- I^+$, $S^- M^+ I^-$, $S^0(IX)^0$ and S^0I^0 (Figure 3.8).

The synthesis of mesoporous materials can take place in an acidic medium wherein the surfactant and the inorganic species are both positively charged. The association between S^+ and I^+ occurs through the intercalation of a counter ion (X^-) via an indirect electrostatic interaction ($S^+ X^- I^+$) leading to the formation of materials such as SBA-1, SBA-2 and SBA-3 [71-72].

Conversely, the preparation of mesoporous materials can also occur in a basic medium in which the negatively charged silicate (I^-) cannot directly interact with the negatively charged surfactant (S^-). In order to balance the charges, a mediator ion positively charged (M^+) must be added which gives rise to the $S^- M^+ I^-$ pathway.

A direct self-assembly pathway occurs when oppositely charged inorganic precursor and surfactant molecules are introduced into the reaction mixture ($S^+ I^-$, $S^- I^+$). For example, MCM-41 which is prepared under basic conditions and in the presence of cationic surfactant (S^+) undergo a direct electrostatic interaction $S^+ I^-$.

In the case of nonionic surfactants (S^0 for a long-chained amine; N^0: polyethylene oxide), the formation of the hybrid mesophase is governed by interactions involving hydrogen bonding between the polar head of surfactant and the silica source at acidic $S^0(IX)^0$ or neutral pH (S^0I^0). Under acidic conditions, the silica source is positively charged after its hydrolysis in the presence of H^+ ions and the interaction ($S^0 H^+ X^- I^+$) takes place through a combination of electrostatic interactions and hydrogen bonding, leading to the synthesis of materials such as SBA-15 and SBA-16 [66,73].

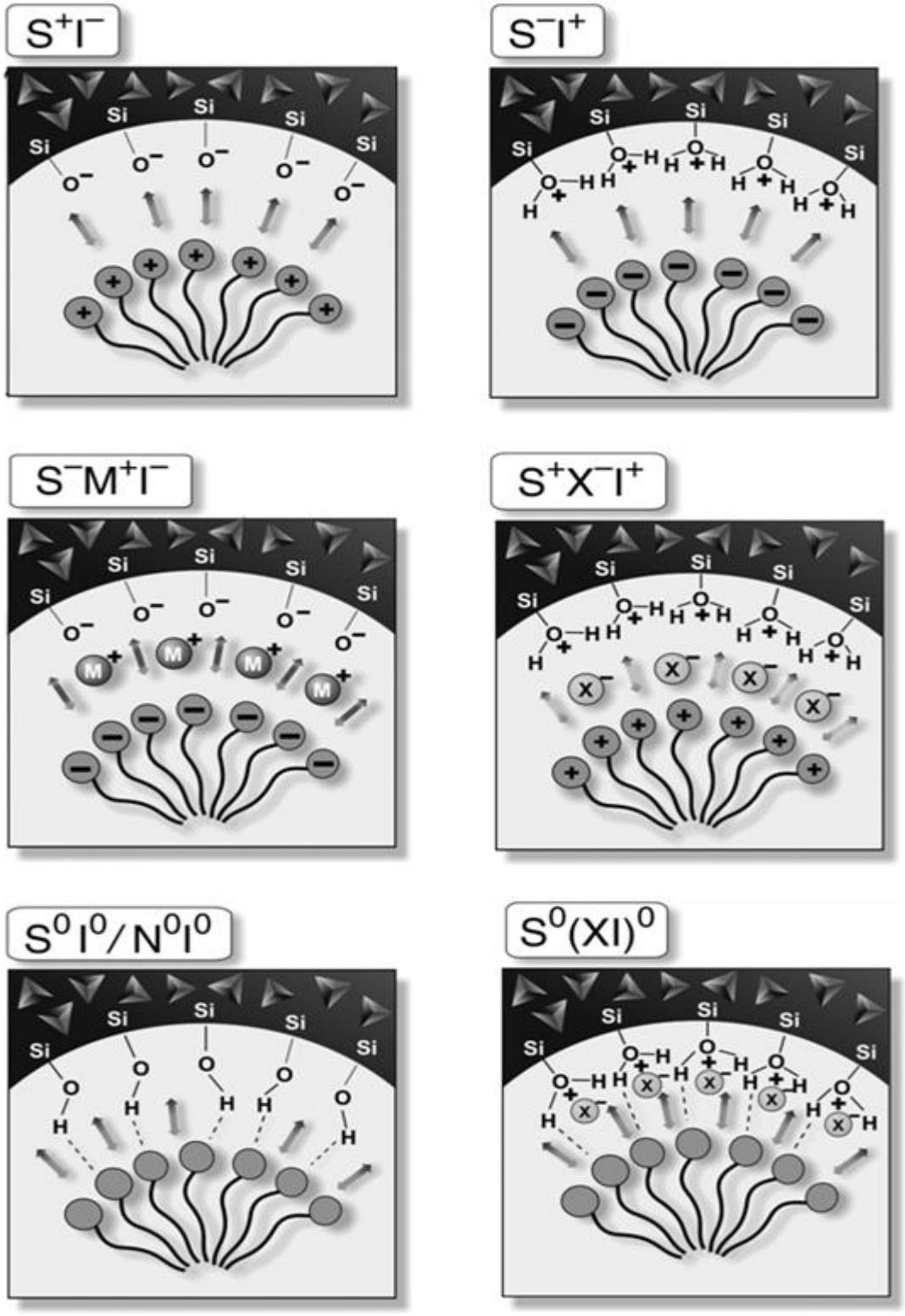

Figure 3.8: Schematic representation of the six different types of surfactant interactions with inorganic species [73].

3.5 Surfactant Packing

The interactions between the surfactant and the precursor lead to the formation of hybrid mesophase. In aqueous solution, the molecules of amphiphilic surfactants, depending on their concentration, give different periodic structures known as mesophases. To predict which three-dimensional structure could be obtained, a model based on geometrical considerations was developed by Israelachvili et al. [74]. Table 3.1 shows the expected mesophase as a function of the packing parameter (*g*), which is a dimensionless number used to predict the geometry of the resulting mesophase, and is calculated using the following equation:

$$g = \frac{V}{a_0 \, l}$$

where V is the volume of the hydrocarbon chain, a_0 is the effective surface area of the head group and l is the length of the hydrocarbon chain. Thus, the parameter g is dependent on the molecular geometry of the surfactant. The value of g increases when a_0 or l decreases or when V increases. As indicated in Table 3.1, if the packing parameter is less than 1/3, the micelles will self-organize in the solution into a hexagonal mesophase. The parameter g equal to 1/3 creates aggregates having a cubic structure.

***Table 3.1**: Packing parameter of different mesophases* [72,75]

Packing parameter « g »	Mesophase	Space group	Example
< 1/3	3D Hexagonal	$P6_3/mmc$	SBA-2
1/3	Cubic	Pm3n	SBA-1
1/2	2D Hexagonal	P6mm	MCM-41
1/2-1/3	Cubic	Ia3d	MCM-48
1	Lamellar	P2	MCM-50

3.6 Functionalization of Periodic Mesoporous Silica

The pore wall surfaces of PMS are susceptible of undergoing chemical modifications via reaction of existing silanol groups and organic species through a functionalization process. The modified silica becomes an organic-inorganic material that combines the properties of the siliceous skeleton such as mechanical stability and mesoporosity as well as the chemical reactivity of the introduced organic groups. Depending on the nature of the grafted groups, these modified materials can be used in a variety of applications such as catalysis, separation and controlled release of drugs [58-60]. Two pathways are available for surface functionalization: post-synthesis grafting and co-condensation. The post-synthesis grafting consists of preparing a siliceous support and subsequently modifying its surface with an organic group (Figure 3.9a). This process is carried out by reaction of organosilane molecules of the type [$RSi(OR')_3$] with the free silanol groups of the pore surfaces. In the process of post-synthesis functionalization, the accessibility of silanol groups at the surface of the silica affects the efficiency of the grafting process. If the organosilane molecules react preferentially at the pore openings during the initial stage of the process, the diffusion of organic species deeper into the pores can be impeded, leading to a non-homogeneous distribution of the functional groups within the pores and a loss of efficiency. In extreme cases (e.g., with very bulky grafting species), this can lead to complete pore blocking. Compared to surface grafting of mesoporous materials, co-condensation is a direct synthesis method where the organic group is added during the synthesis of the mesoporous material (Figure 3.9b). Modification of the surface by the one-pot method offers several advantages such as short preparation time, avoidance of pore blocking and homogeneously distributed organic groups within the mesoporous structure.

a) Post-synthesis (grafting)

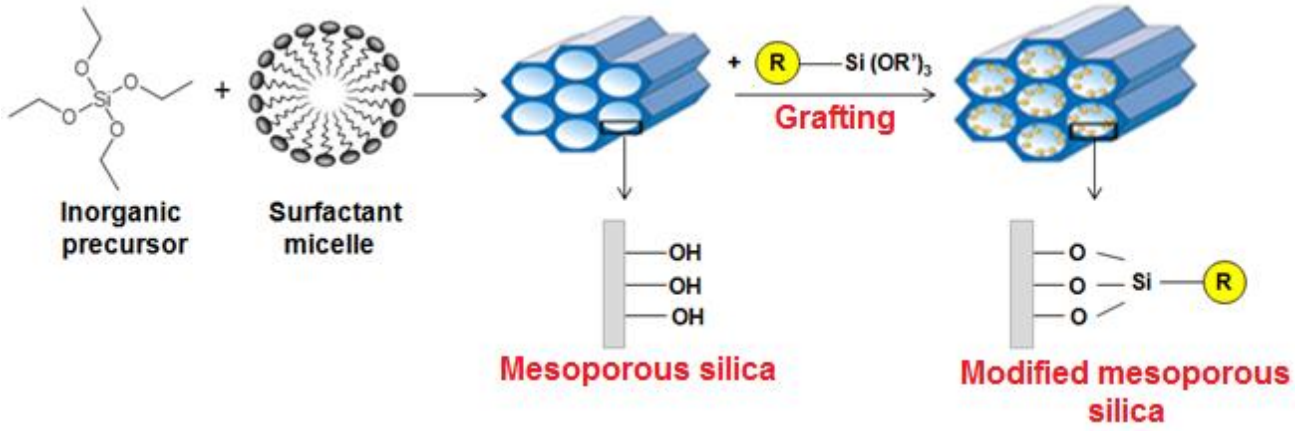

b) One-pot synthesis (co-condensation)

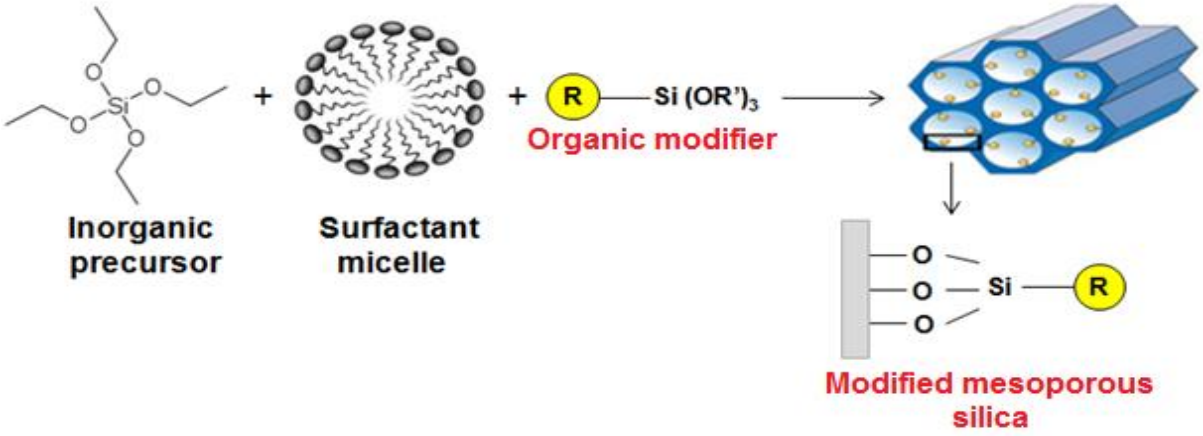

Figure 3.9: Schematic representation of organic modification of mesoporous materials.

3.7 Periodic Mesoporous Organosilicas

In 1999, three independent research groups, namely Inagaki et al. [76] , Ozin et al. [77] and Stein et al. [78] reported the synthesis of a new family of materials, known as periodic mesoporous organosilica (PMO) using organic bridged alkoxysilane precursors. The precursor is represented by $(OR')_3Si\text{-}R\text{-}Si(OR')_3$ with R as the organic linker and OR' as the alkoxy moieties, usually methoxy or ethoxy groups. Inagaki et al. [76] synthesized a highly ordered ethane-bridged PMO

using 1,2-bis(trimethoxysilyl)ethane in the presence of octadecyltrimethylammonium chloride as template. The resulting material exhibited a hexagonal symmetry with a pore diameter of 3.1 nm. Ozin's group [77] used 1,2-bis(triethoxysilyl)ethene to synthesize a similar material in the presence of cetyltrimethylammonium bromide (CTAB) as structure directing agent under basic conditions. The ethene-bridged PMO obtained showed a hexagonal symmetry with a specific surface area of 637 m^2/g, a pore diameter of 3.9 nm and a pore volume of 0.6 cm^3/g. At nearly the same time, Stein and coworkers [78] also synthesized ethylene and ethane-bridged PMO using CTAB as template in the presence of ethane and ethylene bridged siloxane precursors. The two bridged PMO materials obtained had MCM-41 comparable structures, with high surface areas (ca. 1200 m^2/g) and narrow pore size distributions. In 2000, Sayari et al. [117] extended the synthesis of such materials by preparing periodic mesoporous organosilicas with two-dimensional and three-dimensional hexagonal as well as cubic symmetry using bridged silsesquioxane species $(RO)_3Si\text{-}CH_2\text{-}CH_2\text{-}Si(RO)_3$ with R= CH_3 or C_2H_5 as precursors and cetyl- or octadecyltrimethylammonium chloride (C_{16}TMACl or C_{18}TMACl) as structure-directing agents. Initially, research on PMO was focused on the synthesis of materials using small aliphatic bridging groups such as ethane, methane and ethylene due to the commercial availability of the precursors. The first phenylene bridged PMO was reported by Inagaki and coworkers [79]. The distinctive feature of this PMO was not only the incorporation of a new aromatic bridging group, but more importantly, the introduction of molecular scale periodicity within the pore walls. The appearance of crystallinity in the framework was evidenced by powder X-ray diffraction that showed a series of sharp, intense and equidistant peaks with lattice spacing of 7.6 Å [80]. This was a breakthrough in organosilica materials where amorphous walls were normally observed (Figure 3.10).

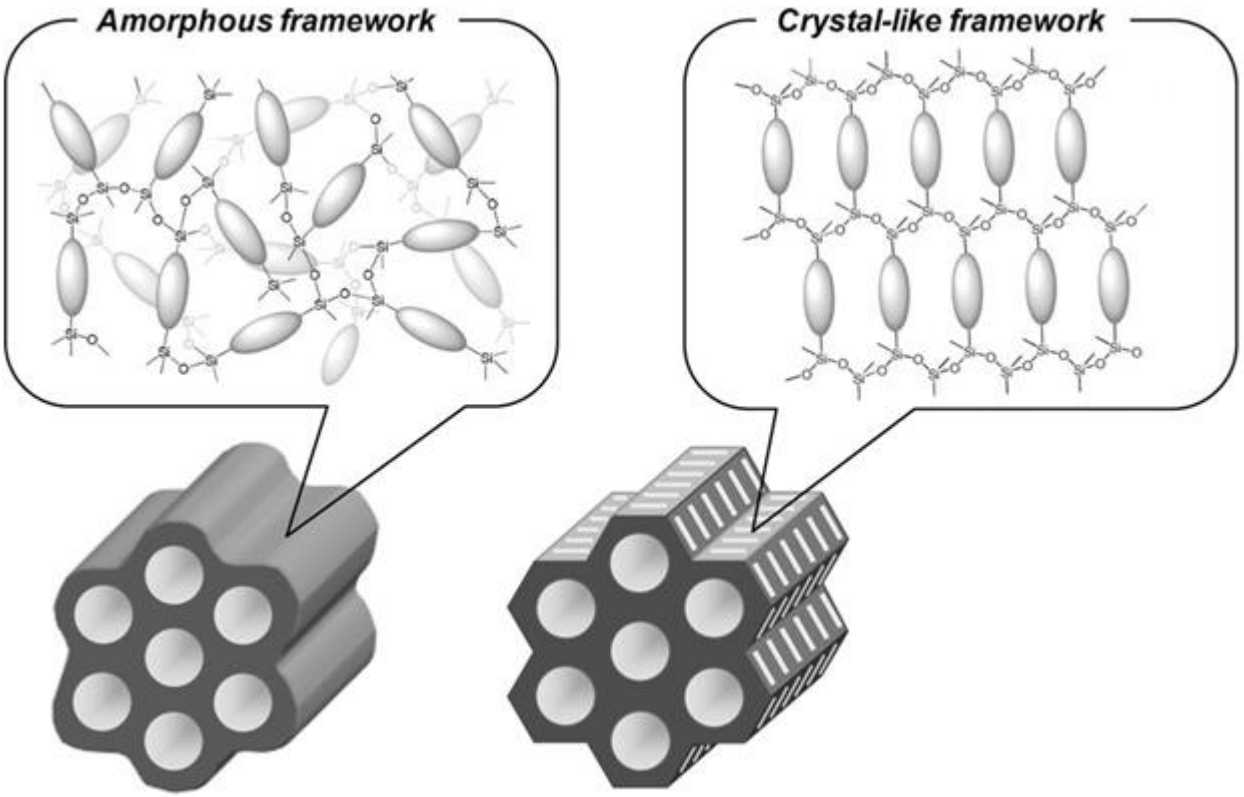

Figure 3.10: Schematic illustration of amorphous and crystal-like frameworks of PMO [80].

PMOs are prepared using hydrothermal procedures similar to the synthesis of ordered mesoporous inorganic materials. Nevertheless, a few major and important differences between PMS and PMO exist. The pore walls of PMS are composed entirely of silica which limits their use in applications where hydrophobicity is desired or when the interaction between the porous material and guest species needs to be tuned. To overcome this limitation, researchers proposed two approaches to organically modify the pore wall surfaces: post-synthesis and co-condensation. PMOs exhibit higher loadings and uniform distribution of organic groups compared with surface modified periodic mesoporous silicas. In addition, the organic groups in PMO are distributed not only on the surface of the material, but throughout the framework. The functional groups inside the pore walls are not reachable; therefore not susceptible of undergoing

chemical modifications. However, these organic groups add more rigidity or flexibility to the overall structure of PMO material. In contrast, the organic groups on the surface of PMO materials are accessible and can be chemically modified. Different organic bridges can be used starting from very simple aliphatic and aromatic groups such as methane, ethane, benzene and thiophene to more complex moieties [80]. PMO materials have found many potential applications in catalysis, separation, optical devices and luminescence to name a few [80-84].

3.8 Ordered Mesoporous Carbons

In 1999, Ryoo and coworkers opened the field of highly ordered mesoporous carbon (OMC) materials with the synthesis of CMK-1, a carbon with ordered mesoporous structure, using MCM-48 as a hard template [85]. The term CMK stands for Carbon Mesostructured by KAIST (Korea Advanced Institute of Science and Technology). Their method is based on the idea of nano-casting, in which a mesoporous silica material is used as a hard template to produce an inverse carbon replica of the original material. In the synthesis developed by Ryoo's group, sucrose was used to fill the mesoporous channels of MCM-48, then converted to carbon by a carbonization process with sulfuric acid as a catalyst. The mesoporous carbon material was obtained by removing the silica framework with an aqueous solution containing NaOH and ethanol. This synthetic process resulted in a cubic structured mesoporous carbon, CMK-1, with an average pore size of 3 nm. After the discovery of CMK-1, various types of ordered mesoporous carbons with different mesostructures were synthesized using different silica templates. The mesoporous carbons belonging to the CMK-family and the corresponding silica templates employed for their synthesis are summarized in Table 3.2.

Table 3.2: *Different types of ordered mesoporous carbons and their silica templates*

Ordered mesoporous carbons	Name and structure of silica template	Carbon morphology Rods vs. Tubes	Reference
CMK-1 CMK-2	MCM-48, *Ia3d* SBA-1, *Pm3n*	Rods	85 86
CMK-3 CMK-5	SBA-15, *P6mm*	Rods Tubes	87
CMK-6 CMK-7	SBA-16, *Im3m*	Rods Tubes	88
CMK-8 CMK-9	KIT-6, *Ia3d*	Rods Tubes	89

As shown in Table 3.2, the carbon structure formed within the mesopores of silica can be tuned to be either rod-type or tube-type structure, depending on the amount of carbon precursor. The rod-type carbons are obtained if the carbon precursors such as sucrose are carbonized after the template pores are completely filled. On the other hand, the tube-type carbons are obtained if the carbon precursors are coated on the pore walls of the template before carbonization. Nevertheless, the tube-type carbons are much more difficult to synthesize than the rod-type due to the capillary condensation or the pore filling of the carbon precursor. For example, the SBA-15 replication permits to obtain exact inverse replica, CMK-3, with a hexagonal structure composed of ordered carbon rods interconnected by irregular carbon threads. It is even possible to go back to SBA-15 using silica condensation in CMK-3 and removing the carbon by combustion. CMK-5, an analogous structure to CMK-3, which consists of ordered carbon pipes

instead of carbon rods, is formed when an incomplete filling of the ordered mesopores of SBA-15 with carbon precursor is achieved. All ordered mesoporous carbons presented in Table 3.2 maintain the same structural symmetry of the corresponding silica template, except the CMK-1 carbon. If the CMK-1 carbon maintains its structure after the template removal, the resulting carbon material should have the same structural symmetry as the MCM-48 template (cubic structure of *Ia3d*). However, the resultant CMK-1 has a cubic structure of $I4_1/a$, indicating that CMK-1 is not a true inverse replica of the MCM-48 ordered silica. This structural change was explained in terms of the displacement model, or the change in the relative position of the two non-interconnecting mesopore systems filled with carbon in MCM-48 after the silica template was removed [90]. Porous carbon materials have attracted much attention because of their high surface areas, large pore volumes and high mechanical stability making them attractive for a lot of applications such as adsorption, catalysis and electrode materials [91].

Chapter IV - Experimental & Instrumentation

➢ *Materials*

The two precursors, 1,4-bis(triethoxysilyl)benzene (BTEB) and 4,4′-bis(triethoxysilyl)-1,1′-biphenyl (BTEBP), as well as the structure directing agents, octadecyltrimethylammonium chloride ($C_{18}Cl$) and the triblock poly(ethylene oxide)-poly(propylene oxide)-poly-(ethylene oxide) copolymer Pluronic P123 (MW = 5800) were purchased from Sigma-Aldrich. The tetraethylorthosilicate (TEOS) used as a silica source for the synthesis of SBA-15, as well as 3-mercaptopropyltrimethoxysilane (MPTMS) and phenyltriethoxysilane (PTES) were supplied by Aldrich. Sucrose and glucose were purchased from Sigma-Aldrich while dimethylsulfoxide (DMSO), used as a solvent for the reaction, and acetonitrile (99.99% HPLC grade), employed as a mobile phase, were purchased from Fisher Scientific. HMF (98%) and vinyl sulfonic acid sodium salt were obtained from Alfa Aesar. All chemicals were reagent grade and were used without further purification.

➢ *Synthesis of Acidic Nanoporous Materials*

4.1 Functionalization of SBA-15 with Sulfonic Acid Groups

4.1.1 Synthesis of Mercaptopropyl-Functionalized SBA-15 by Co-condensation and Sulfonation Thereof (Propyl-SBA-15)

The propylamine-modified SBA-15 (propyl-SBA-15) was synthesized using MPTMS in the presence of TEOS under acidic conditions. The preparation procedure was as follows: 4.0 g of

Pluronic P123 and 8 g of KCl were added to a mixture of 30 mL of water and 120 mL of 2 M HCl aqueous solution in a Teflon-lined container, which was stirred at 40 °C, usually overnight. Then, 8.5 g (40.8 mmol) of TEOS was added and prehydrolyzed for 2 h before adding 1.18 g (6.0 mmol) of MPTMS, which corresponds to MPTMS/TEOS molar ratio of 0.15. The mixture was stirred at the same temperature for 20 h, then heated at 100 °C for 24 h in static conditions. The surfactant was removed by refluxing 1.5 g of as-made material in 400 mL of ethanol for 24 h. The product was filtered and dried in vacuum at 100 °C for 3 h. Following solvent extraction, the thiol group was oxidized to sulfonic acid by adding 1.0 g of thiol functionalized material in 2.4 mL of 30 % H_2O_2 in the presence of 7.0 mL of methanol at room temperature. The oxidized material was resuspended in 25 mL of 1 wt% H_2SO_4 for 4 h, washed with water, and dried in vacuum for 3 h at 120 °C.

4.1.2 Synthesis of Phenyl-Functionalized SBA-15 by Co-condensation and Sulfonation Thereof (Phenyl-SBA-15)

The phenyl-SBA-15 was synthesized following the same procedure as for propyl-SBA-15, except that PTES (1.44 g, 6.0 mmol) was used instead of MPTMS. Following solvent extraction, 1.5 g of phenyl-functionalized material was added to a solution of 0.3 mL of chlorosulfonic acid in 75 mL of dichloromethane and the suspension was stirred at room temperature overnight. The sulfonated solid was filtered, washed with dichloromethane (30 mL) and dried in vacuum for 24 h at 70 °C.

4.2 Synthesis of Periodic Mesoporous Organosilica (PMO)

4.2.1 Synthesis of Biphenylene Bridged PMO (Biph-PMO)

The biphenylene PMO was synthesized using BTEBP in the presence of $C_{18}Cl$ as structure-directing agent under basic conditions (Figure 4.1). The material was prepared by co-condensation following a procedure described elsewhere [92]. Typically, 0.835 g (2.4 mmol) of $C_{18}Cl$ was dissolved in a mixture of 25.2 g of distilled water and 0.40 g (10 mmol) of NaOH at 35 °C. BTEBP (1.20 g, 2.5 mmol) was added to the $C_{18}Cl$ solution under vigorous stirring. The stirring was maintained overnight, then the mixture was transferred into a Teflon-lined autoclave and heated at 100 °C for 20 h. The resulting white precipitate was recovered by filtration and dried to yield as-made PMO material. The surfactant was removed by stirring 1.0 g of as-made material in 150 mL of ethanol and 5 g of concentrated HCl aqueous solution at room temperature for 5 h. The material obtained was denoted as Biph-PMO (yield = 81 %).

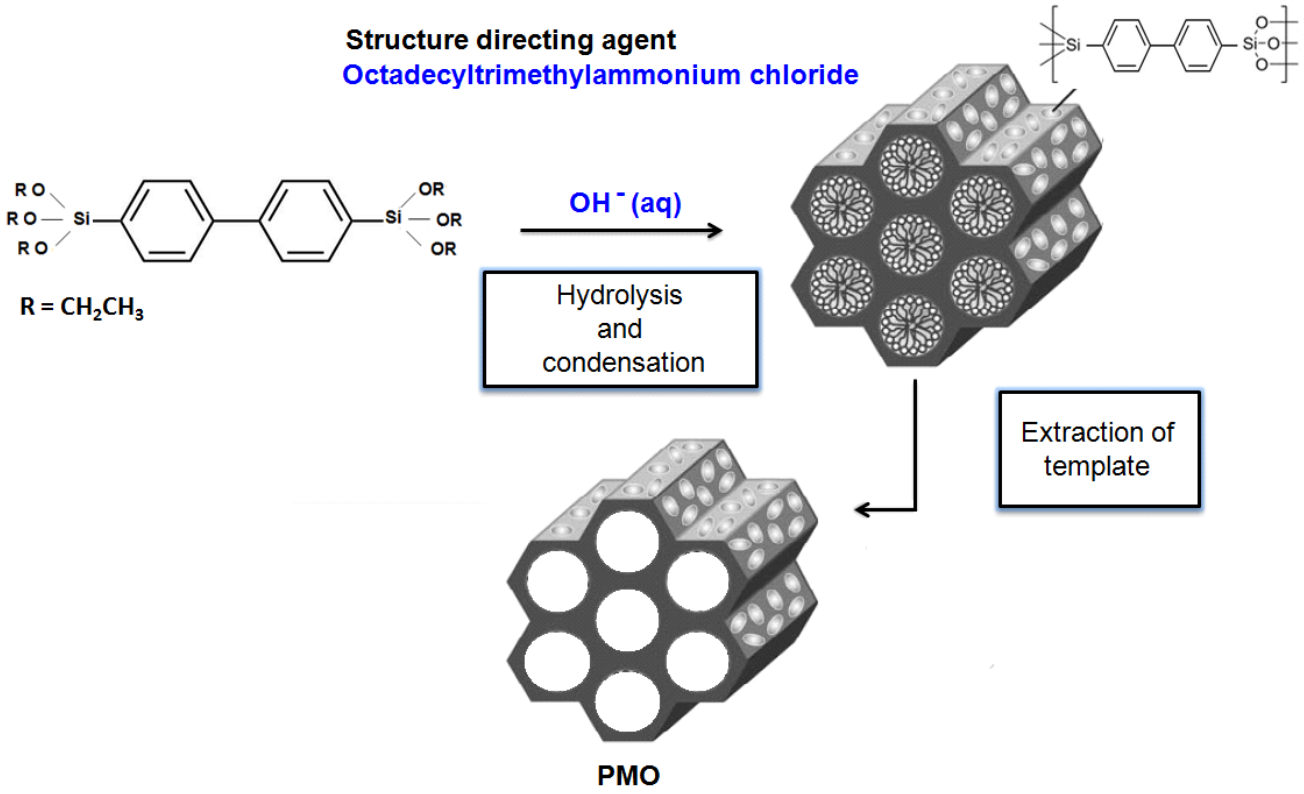

Figure 4.1: Schematic illustration for the synthesis of biphenylene bridged PMO.

4.2.2 Synthesis of Phenylene Bridged PMO (Ph-PMO)

Phenylene bridged mesoporous organosilica was prepared using BTEB precursor in the presence of Pluronic P123 under acidic conditions (Figure 4.2). In a typical synthesis, 0.99 g of Pluronic P123 was dissolved in 36 mL of distilled water and added to 200 µL of HCl (36 wt%). BTEB (1.0 g, 2.5 mmol) was added to the solution and then stirred for 1 h at 0 °C. Then, the mixture was stirred at 40 °C for 20 h, followed by aging in a closed vessel at 100 °C for 24 h. The white precipitate was recovered by filtration and washed repeatedly with water. The surfactant was removed by solvent extraction with ethanol followed by calcination at 250 °C in

air. This temperature was found to be high enough to remove the template without material decomposition. The material obtained was labelled as Ph-PMO.

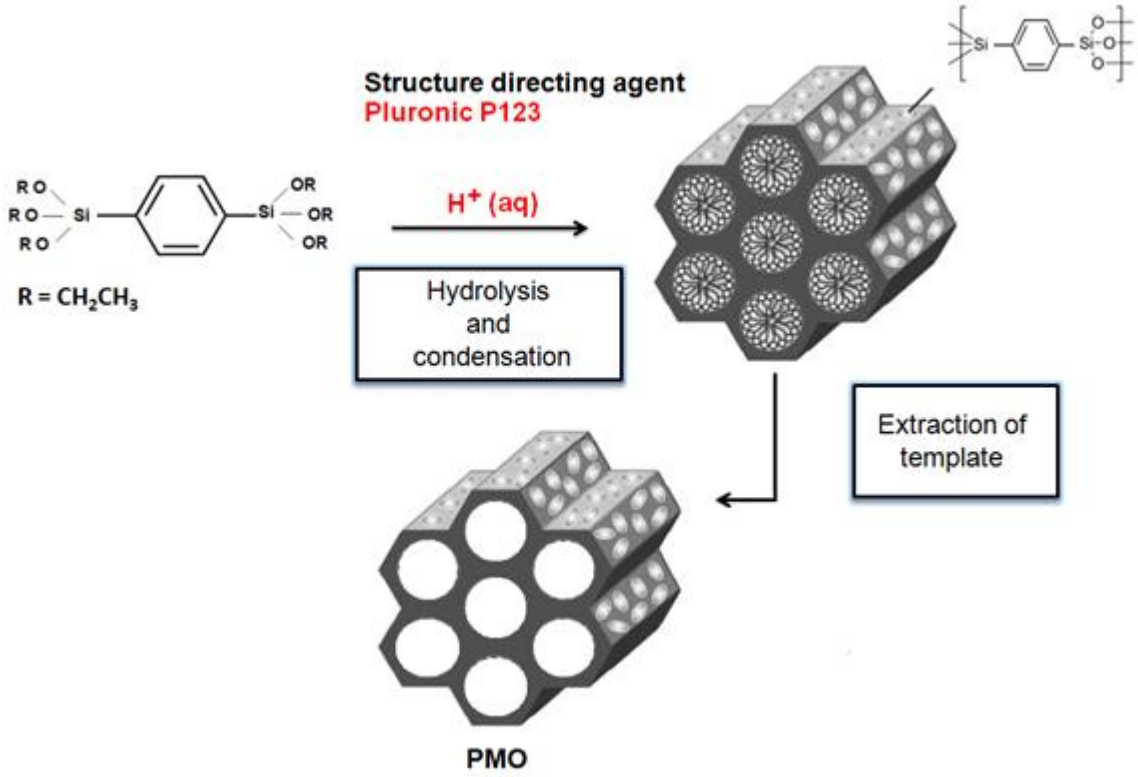

Figure 4.2: Schematic illustration for the synthesis of phenylene bridged PMO.

4.3 Sulfonation of PMO

The sulfonation of bridged PMO was carried out as follows [126]: PMO (1.5 g) was added to a solution of chlorosulfonic acid (0.3 mL) in dichloromethane (75.0 mL), and the suspension was stirred at room temperature overnight. The solid was filtered and washed with dichloromethane (30 mL) and dried at 70 °C for 24 h.

4.4 Synthesis of Carbon Materials

4.4.1 Synthesis of Sulfonated Mesoporous Carbon CMK-3-SO_3H by the Hard Templating Procedure

4.4.1.1 Synthesis of SBA-15

SBA-15 was synthesized according to the procedure reported by Sayari et al. [67]. The preparation was as follows: 4.0 g of Pluronic P123 was added to a mixture of 30 g of water and 120 g of 2 M HCl aqueous solution in a Teflon-lined container, which was stirred at 35 °C overnight. Then, 8.50 g of TEOS was added to this solution under vigorous stirring. After 5 min, the mixture was kept under static conditions at 35 °C for 20 h, followed by 24 h at 100 °C. The solid product was collected by filtration, washed with water, dried, and calcined at 550 °C in flowing air.

4.4.1.2 Synthesis of CMK-3-SO_3H

Ordered mesoporous carbon CMK-3 was prepared following the procedure suggested by Ryoo et al. [95]. The synthesis procedure was as follows: 2.1 g of calcined SBA-15 was impregnated with 2.6 g of sucrose which has been dissolved in 4.2 g of deionized water containing 0.25 g of 98% H_2SO_4, and the resultant mixture was heated at 100 ºC for 6 h. Subsequently, the oven temperature was raised to 160 ºC and maintained there for 6 h to allow a partial carbonization. The obtained sample was impregnated again with 1.7 g of sucrose, 0.2 g of 98% H_2SO_4 and 3.2 g of deionized water, and then carbonized at 160 ºC. The SBA-15 silica/carbon composite was pyrolyzed under a stream of nitrogen at 550 ºC for 6 h to induce a deep carbonization.

The CMK-3 mesoporous carbon replica was obtained after removing the silica framework in a 5 wt.% HF solution followed by filtration, washing with deionized water and drying at 100 ºC. The sulfonation of the carbon material was carried out in a Teflon-lined autoclave where 0.3 g of CMK-3 was contacted with the vapor from 5 mL H_2SO_4 (98%) at 60 ºC for 48 h. The sulfonated sample, denoted as CMK-3-SO_3H, was washed with hot deionized water, filtered and dried at 100 ºC.

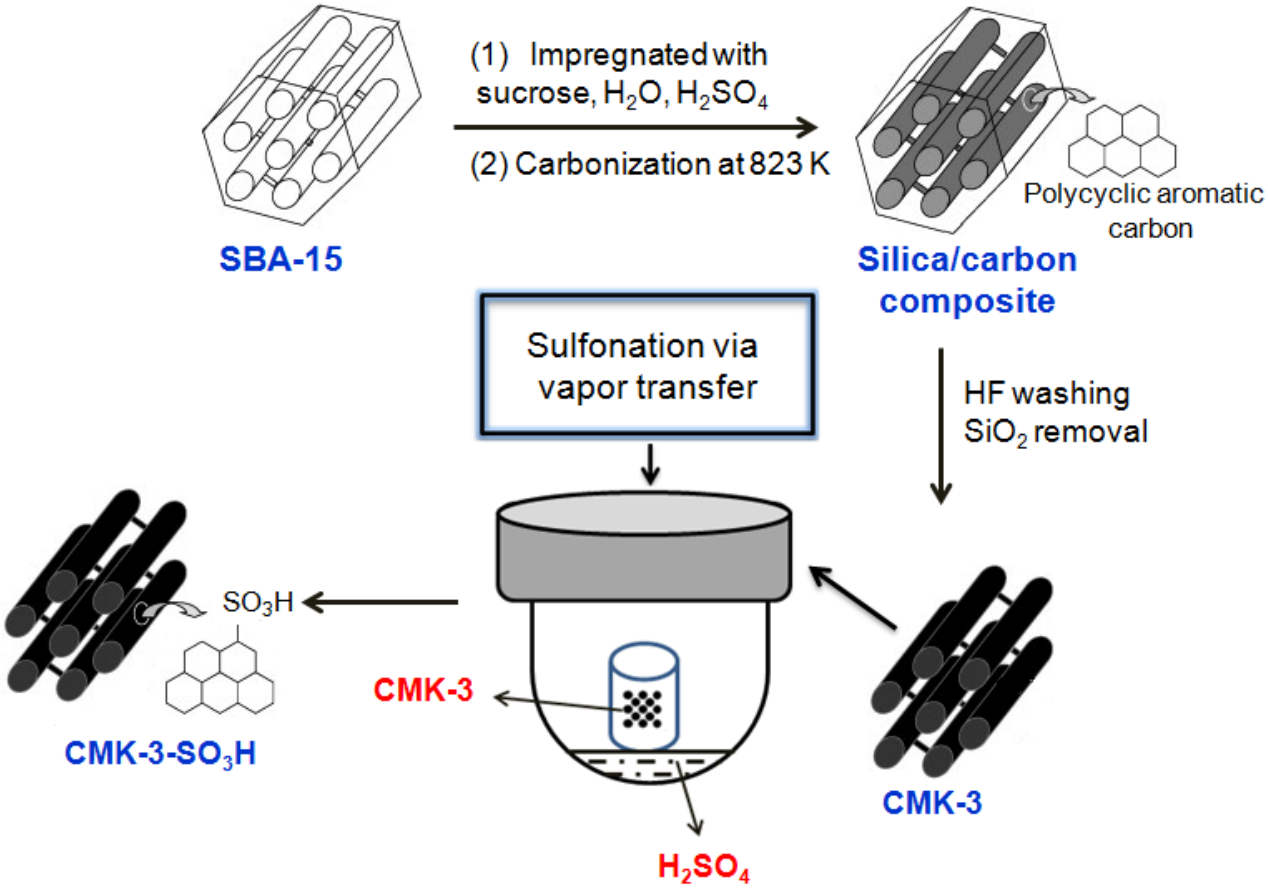

Figure 4.3: Schematic representation for the preparation of sulfonated mesoporous carbon CMK-3-SO_3H.

4.4.2 Synthesis of Sulfonated Amorphous Carbon AC-SO_3H

A mixture of vinylsulfonic acid sodium salt (21.5 g), glucose (6.0 g) and water (42.5 mL) was placed in a Teflon-lined autoclave, and hydrothermally treated at 190 ºC for 16 hours. The material obtained was filtered and washed several times with water. The resulting product was stirred in 100 mL of aqueous 0.1 M HCl for 3 h, washed several times with water to remove all excess acid and dried under vacuum at 80 ºC overnight. The material was identified as AC-SO_3H.

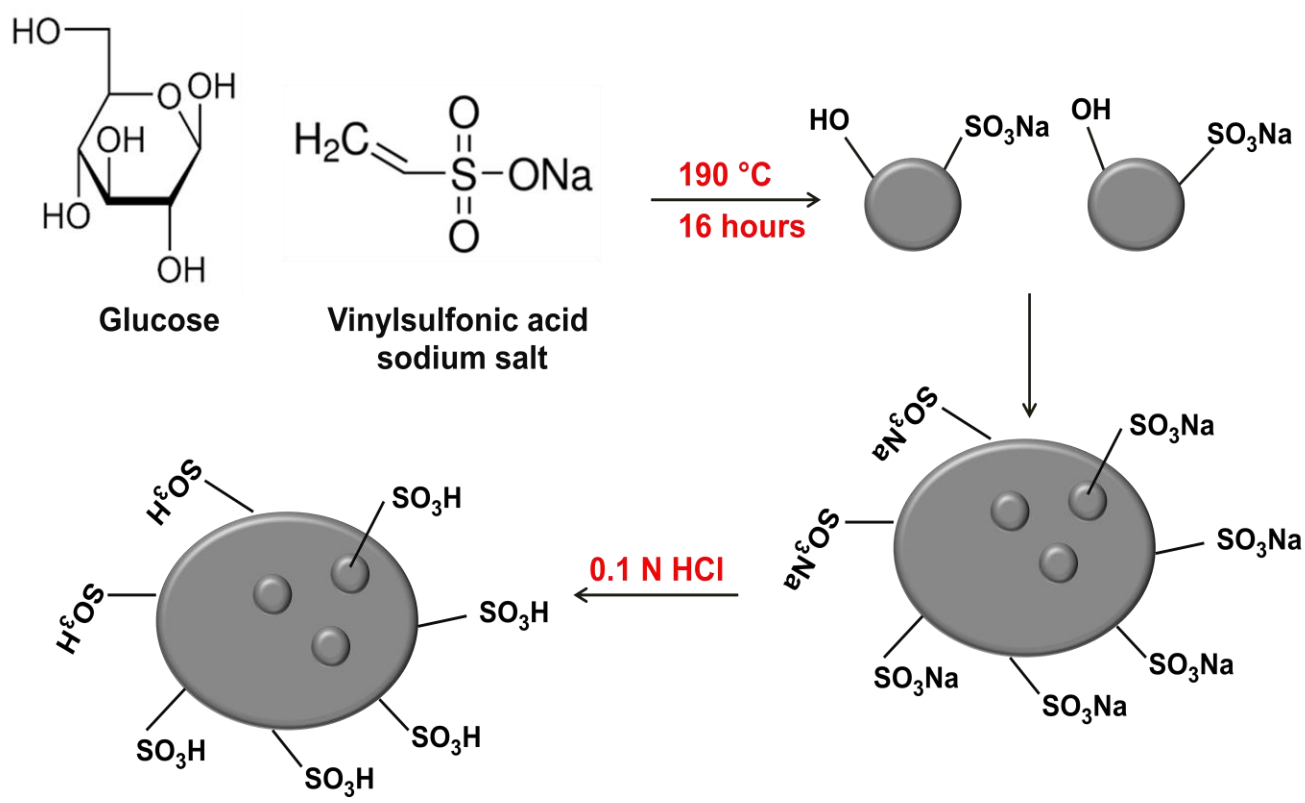

Figure 4.4: Schematic representation for the synthesis of sulfonated amorphous carbon AC-SO_3H.

4.5 Analytical Methods

4.5.1 Catalytic Conversion of Sucrose into HMF

A typical experiment was performed using a microwave reactor vessel charged with 2 mL DMSO, 0.1 g sucrose, 0.05 g of catalyst and a magnetic stirrer. After being sealed with a cap, the vessel containing the mixture was mounted in a microwave apparatus (Biotage Initiator) and a pre-stirring of 15 s was set to ensure a homogeneous mixture. Irradiation began and the microwave power was automatically adjusted to reach the selected temperature (180 ºC). When the preset temperature was reached, the experiment time (10 min) countdown started. The vessel was then purged externally with air to allow rapid cooling to 40 ºC before being removed from the chamber.

4.5.2 Quantification Procedure for HMF Yield

After reaction, samples were withdrawn from the reaction mixture (M_1), diluted with deionized water and then filtered through 0.45 μm filter membrane. The concentration of HMF in samples was calculated based on an external standard calibration curve with a regression coefficient of 0.999 (see Appendix I). The quantitative analysis of HMF was achieved by high-performance liquid chromatography (HPLC) method, using a reversed phase C18 column and an ultraviolet detector at 280 nm. The column oven temperature was maintained at 30 ºC, and the mobile phase was acetonitrile-deionized water (85:15) at a flow rate of 0.5 mL/min. The yield of HMF was calculated according to the following equations:

- Weight of HMF in the reaction mixture = HMF concentration (mg/mL) x V x (W_0/W_1)
- HMF yield (%) = $\frac{\text{Weight of HMF in mixture}}{\text{Theoretical weight of HMF (mg)}}$ x 100

where HMF concentration (mg/mL) was calculated based on the standard calibration curve, W_0 is the weight of the reaction mixture, W_1 is the weight of sample withdrawn from the reaction mixture and V is the volume of the sample after dilution with water.

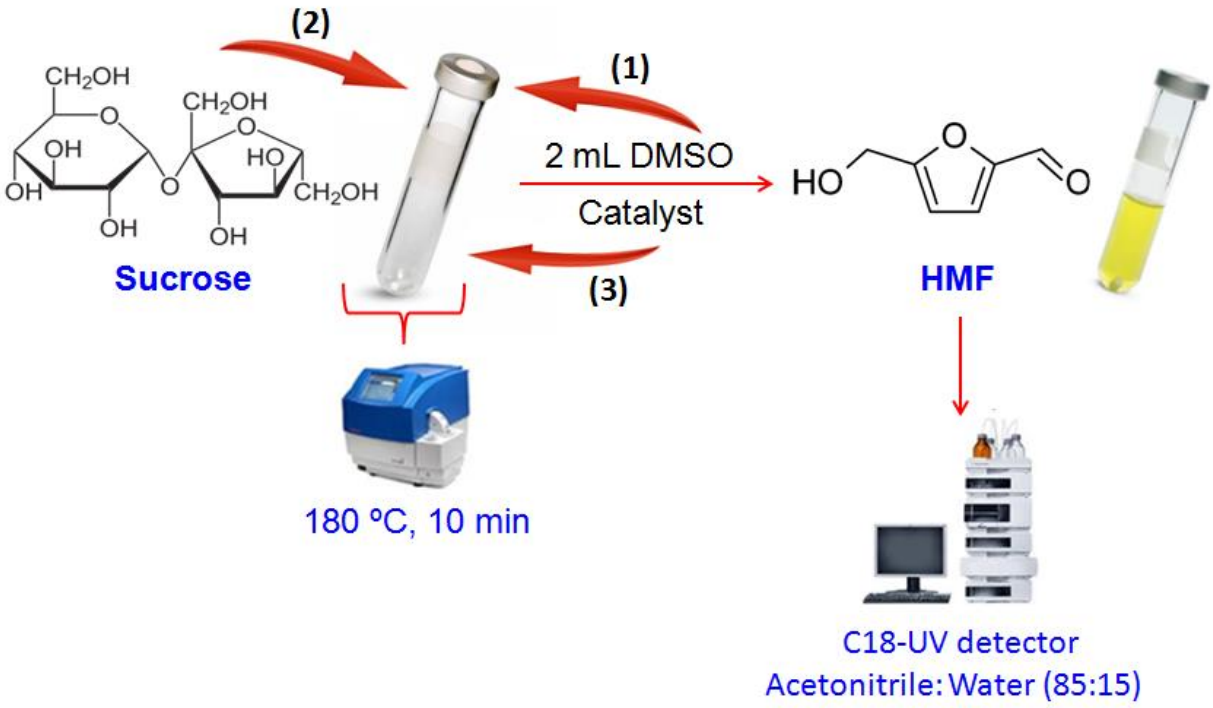

Figure 4.5: Schematic representation for the microwave-assisted conversion of sucrose and product analysis.

4.5.3 Recyclability of Sulfonated Porous Materials

After the first run, the catalyst was filtered, washed with water and dried in air. Subsequently, the recovered catalyst was used in the next run by adding fresh sucrose sample and DMSO under the same reaction conditions.

4.6 Characterization Techniques

4.6.1 Nitrogen Adsorption/Desorption Isotherm

The structural properties of the samples were determined by nitrogen adsorption at 77 K using a Micromeritics ASAP 2020 volumetric apparatus. Prior to each analysis, the samples were degassed under vacuum at 60 °C for 3-5 h to remove any pre-adsorbed species. The surface area was determined by the BET method, whereas the pore size distribution was calculated using the Kruk–Jaroniec–Sayari (KJS) approach. The pore volume was determined from the amount of liquid nitrogen adsorbed at a relative pressure about 0.99.

4.6.2 Thermal Gravimetric Analysis (TGA)

The thermal decomposition of the materials was performed using a thermogravimetric analyzer (Q500 TGA, TA Instruments). Briefly, the sample was first treated in a flow of ultra-high purity N_2 at 150 °C for 2 h to remove pre-adsorbed moisture. Subsequently, the organic layer was decomposed by heating at 10 °C/min to 800 °C under flowing nitrogen, then at 10 °C/min to 1000 °C under air.

4.6.3 Nuclear Magnetic Resonance Spectroscopy (NMR)

Solid state ^{13}C CP MAS NMR and ^{29}Si MAS NMR measurements were collected at room temperature on a Bruker Avance 200 III instrument in a magnetic field of 4.7 T using 7 mm zirconia rotors as sample holders spinning at a MAS rate of 5000 Hz. The resonance frequencies were 50.3 and 39.7 MHz for ^{13}C and ^{29}Si MAS NMR, respectively. The chemical shift reference sample for C was the glycine C=O at 176.5 ppm, while for Si tetrakis(trimethylsilyl)silane Si ($Si(CH_3)_3)_4$ at 10.02 ppm was used as a reference. Recycle delay for all CP MAS experiments was about 2 s.

4.6.4 Elemental Analysis (CHNS)

The sulfur, nitrogen, hydrogen and carbon contents were determined by elemental analysis using a Micro Cube elemental analyser made by Elementar, Germany. Weighed samples placed into tin capsules were flash combusted with oxygen at about 1800 ºC and the gases were carried by helium through a reduction/oxidation column to yield N_2, CO_2, SO_2 and H_2O. The gases are trapped within a single "trap and purge" adsorption column, separated and quantified as they pass through a gas chromatograph thermal conductivity detector (TCD).

4.6.5 X-Ray Diffraction (XRD)

X-ray diffraction patterns of all samples were recorded using a Philips PW 3020 X'pert instrument equipped with solid-state detector using Cu Kα radiation with 0.15418 nm wavelength, a step size of 0.02º 2θ, and a counting time per step of 4.0 s over a $2\theta < 10°$ range. The lowest angle was limited to ca. $2\theta = 2°$.

4.6.6 Fourier Transform Infrared Spectroscopy (FTIR)

Attenuated total reflectance (ATR) spectra were obtained using a Thermo Scientific Nicolet 6700 FTIR instrument. Samples were placed on a Zinc-Selenium plate and the absorption spectra were measured in the region between 400 and 4000 cm^{-1}. Each spectrum corresponds to 64 scans with a resolution of 4 cm^{-1}.

4.6.7 Scanning Electron Microscopy (SEM)

The morphology of the mesoporous materials was observed by scanning electron microscopy. This technique involves scanning the surface of a sample with an electron beam of high energy which leads to the emission of backscattered and secondary electrons. These electrons are directed to a detector which transmits the signal. The electrons allow then the reconstruction of a magnified image of the surface. SEM was performed using a JSM-7500F FESEM (JEOL) microscope where the sample was placed on an aluminum support coated with a thin layer of graphite.

4.6.8 Transmission Electron Microscopy (TEM)

The pore structure of the mesoporous materials was examined by transmission electron microscopy. Transmission electron micrographs were obtained using a JEOL 2100F operated at 200 kV. Before examination, the materials were dispersed in anhydrous ethanol and deposited on a holey carbon film on a copper grid.

Chapter V – Results and Discussion

This project deals with a comparative investigation of different acidic nanoporous materials as catalysts in the one-step synthesis of HMF directly from sucrose under microwave irradiation. Since biomass is highly rich in oxygen, some or complete removal of oxygen is necessary. Acid-catalyzed dehydration of sugars was chosen to convert carbohydrates into HMF. As mentioned in chapter II, a vast number of pioneering researchers have investigated the HMF production from different substrates, such as raw biomass, monosaccharides and polysaccharides. Biomass with a high content of sugars, such as grapes, can be easily converted into HMF without pre-treatment. However, the use of edible crop-derived biomass is not favorable for large-scale production because it competes with food supply.

Sucrose, the most plentiful source of biomass on earth, is an interesting feedstock consisting of glucose and fructose connected by α-1,2-glycosidic bond (Figure 5.1). The conversion of sucrose to HMF involves the following three steps: **(1)** hydrolysis breaks the glycosidic bond, thus converting sucrose into glucose and fructose; **(2)** glucose is isomerized into fructose; **(3)** fructose is dehydrated to HMF. Synthesis of HMF directly from sucrose shows a great potential for large-scale production of HMF because it circumvents the step of the production of glucose and fructose as well as the corresponding costs.

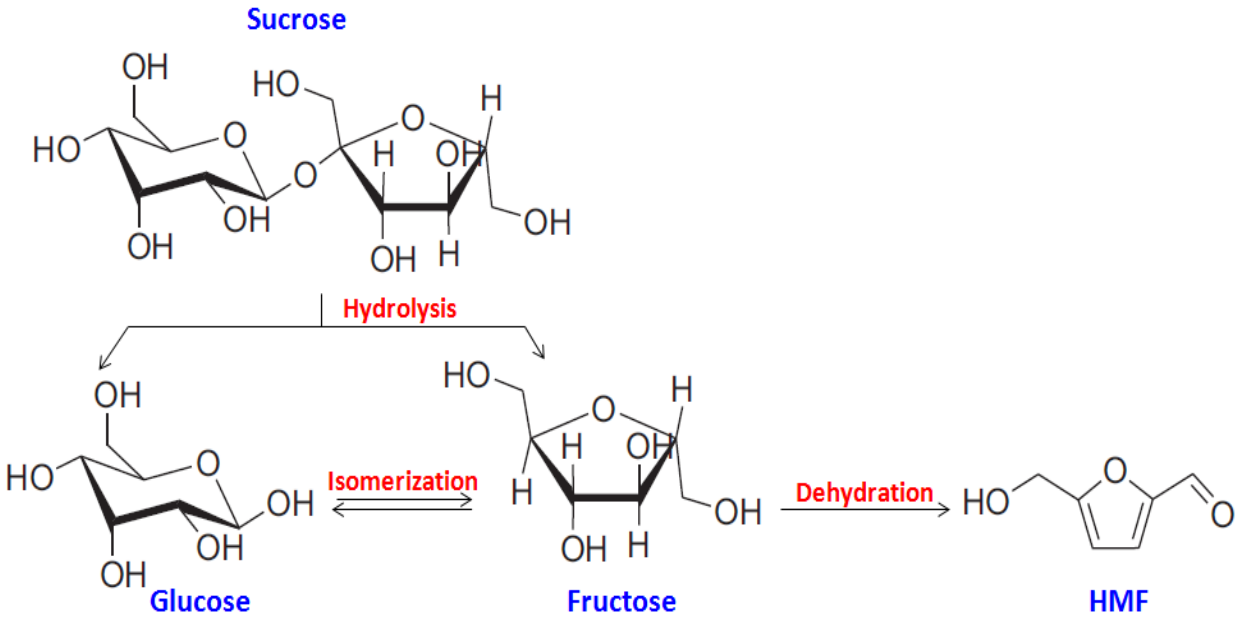

Figure 5.1: Conversion of sucrose into HMF.

In this work, we report the synthesis of organosulfonic-functionalized mesostructured materials as mesoporous supports and discuss their performance as novel solid acid catalysts in the synthesis of HMF. Mesoporous materials are promising catalyst support and exhibit interesting structural properties namely a highly ordered structure, tunable pore size, high surface area as well as their ease of chemically modifying their surfaces by introducing suitable chemical groups. The functionalization of mesoporous materials with sulfonic acid groups allows for the preparation of solid acid catalysts and has been shown to be active acid catalysts in various reactions [96-100]. However, they have not been used in the catalytic conversion of sucrose. Therefore, the aim of this study is to prepare and characterize periodic mesoporous silica materials anchored with propyl and phenyl-sulfonic acid groups through a co-condensation synthetic route, as well as two carbon-based materials bearing sulfonic acid groups, mesoporous carbon (labelled as CMK-3-SO_3H) and amorphous activated carbon (denoted as AC-SO_3H) and

test their performance in the microwave-assisted conversion of sucrose to HMF. In addition, periodic mesoporous organosilica are attractive catalyst supports due to their versatility as their structural and chemical properties can be altered. A proper selection of the organic bridge introduces tailor-made functionalities and modifies the physical properties of the material, such as stability, hydrophobicity, etc. Phenylene and biphenylene-bridged PMO materials were prepared and sulfonation was performed using chlorosulfonic acid to introduce strong Brønsted acid site ($-SO_3H$).

In this work, we aimed to present a comparative study on both the catalytic activity and reutilization capability of mesostructured materials functionalized with sulfonic acid goups. In this regard, the sulfonic acid groups were bonded to a phenyl ring that was the functional organic group of the periodic silica materials (SBA-15 and PMO) and the building block of the two carbon materials. The presence of a phenyl ring in our catalytic reaction presents several advantages. Firstly, phenyl ring is suitable for post synthesis modifications, which allows easy introduction of sulfonic acid groups into the support structure. Secondly, the dehydration of fructose into HMF occurs via sequential steps leading to abstraction of three molecules of water in the presence of acidic catalysts. The presence of phenyl ring in the acidic nanoporous materials creates a hydrophobic environment on the surface of the support. Thus, the catalysts are stable in the reaction. Thirdly, the phenylsulfonic acid groups present more electron withdrawing capability than the aliphatic sulfonic acid groups which increases the acidic strength of the protons, thus promoting the catalytic performance of the reaction [122].

5.1 - Surface Characterization of Solid Materials

Adsorption is the binding of species in the gas or liquid phase called adsorbate on the surface of a solid adsorbent. Depending on the nature of the interactions between the adsorbate molecules and the adsorbent surface, adsorption can be classified into two types: chemisorption and physisorption.

Chemisorption or chemical adsorption occurs when the adsorbate molecules are chemically bonded to the adsorbent surface. Since chemisorption requires the formation of a bond between the adsorbate and the adsorbent, the adsorption sites at which adsorption can occur are specific and their number is limited. It is also often irreversible. On the other hand, the physisorption or physical adsorption occurs when a molecule is adsorbed on a surface without the formation of a chemical bond. The attractive forces are of Van der Waal's type (electrostatic interactions). Since the interactions are weak, physisorption is a reversible process and allow the formation of multiple layers on the surface.

Nitrogen physisorption at low temperature, typically 77 K, is the most commonly used technique to characterize the textural properties of solid materials, allowing the determination of the surface area, the pore volume and the pore size distribution using different models.

Because of its chemical inertia, nitrogen is often used as a universal adsorbate for surface characterization and the measurements are performed at 77 K, normal boiling temperature of nitrogen. Before adsorption measurements, the sample is pretreated under vacuum for few hours at a desired temperature to remove any pre-adsorbed species in order to better access the whole pore system. After that, the measurement cell containing the sample of known mass is immersed

in liquid nitrogen. Then, nitrogen gas is introduced into the cell at a known initial pressure. This pressure gradually decreases due to the physical adsorption of some nitrogen molecules on the solid surface and then reaches an equilibrium value. The amount of N_2 adsorbed is calculated at this equilibrium pressure, often expressed in terms of relative pressure p/p_0 where p_0 is the saturation pressure of the adsorbate at the temperature of adsorption; in this case p_0 = 1 atm. The gradual addition of nitrogen gas in the measurement cell allows the determination of the amounts of adsorbed gas as a function of p/p_0. The plot of the amount of nitrogen adsorbed vs. the relative pressure represents the adsorption isotherm. As the physical adsorption is reversible, we can measure a desorption isotherm by gradually decreasing the pressure of the nitrogen in the measurement cell. Depending on the nature of the material, the adsorption and desorption isotherms can be superimposed or not. In the latter case, a hysteresis loop is formed between the two isotherms in a certain pressure range. The shape of the adsorption/desorption isotherm and the hysteresis allow to determine qualitatively the textural properties of mesoporous materials.

According to UIPAC classification, physisorption isotherms are classified into six types as shown in Figure 5.2 [101]:

- Type I is characteristic for microporous materials.

- Types II and III are typical for non-porous and macroporous solids.

- Types IV and V are characteristic for mesoporous solids.

- Type VI (not very common) is a multistep adsorption on a nonporous or macroporous substrate.

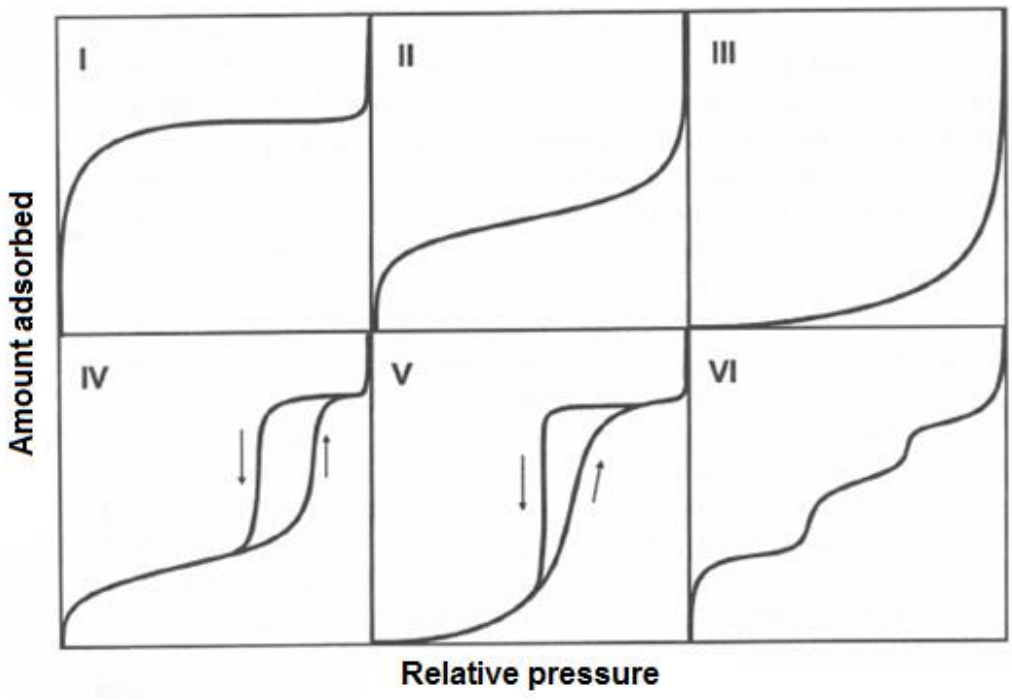

Figure 5.2: The six types of adsorption isotherms as classified by IUPAC [102].

The adsorption isotherm represents the amount of adsorbed species per gram of material vs. pressure at a given temperature. Type IV is the typical isotherm for mesoporous materials. A hysteresis loop is observed in the isotherm of type IV because the capillary evaporation of nitrogen in the mesopores does not occur at the same relative pressure as the capillary condensation, and hence, the process is not reversible. The appearance of a hysteresis loop in N_2 adsorption isotherm indicates the occurrence of mesopores larger than 4 nm [139].

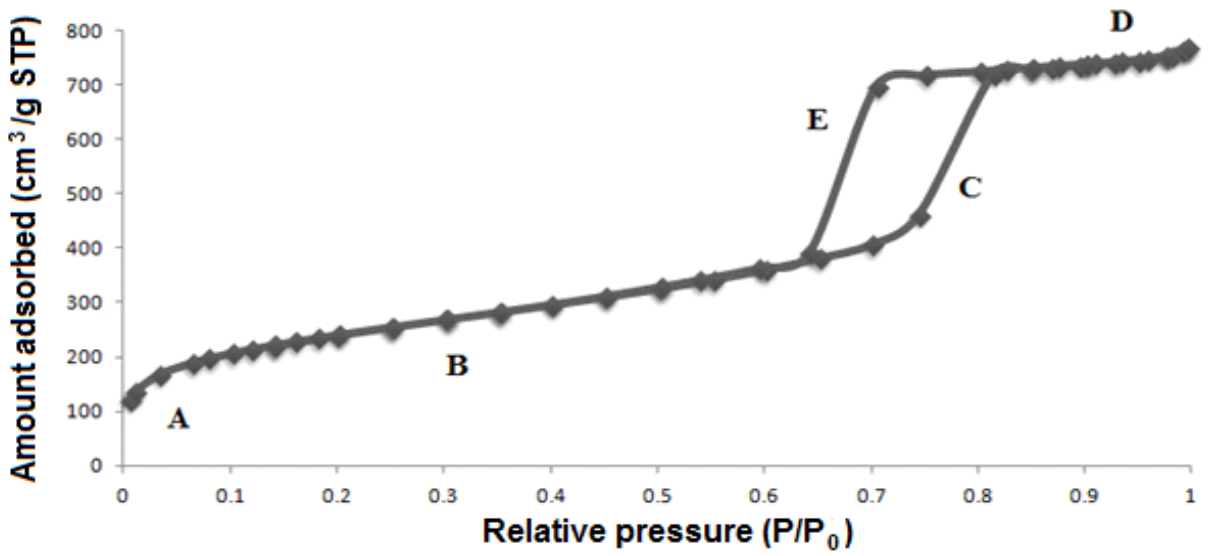

Figure 5.3: N_2 adsorption-desorption isotherm of SBA-15.

The physisorption isotherm shows several stages corresponding to different adsorption mechanisms (Figure 5.3). At low relative pressures, stage **(A)** corresponds to the adsorption of a monolayer film to form the so-called Langmuir monolayer **(B)**. If the material contains micropores, these are also filled at very low pressure. At higher relative pressure, the gradual increase of the adsorbed volume corresponds to a multilayer adsorption where the adsorbed layer gradually thickens, but not layer by layer. Starting at a certain pressure, the rapid increase in the volume adsorbed **(C)** is associated with the capillary condensation in the mesopores followed by the appearance of a saturation level **(D)**. The relative pressure corresponding to capillary condensation increases with the size of mesopores. Moreover, the steeper the capillary condensation, the narrower the pore size distribution. As the physical adsorption is reversible, nitrogen desorption is achieved by progressively reducing the pressure of nitrogen in the measuring cell. Generally, the adsorption and desorption isotherms are superimposed. However, in the case of mesoporous materials with pores larger than ca. 4 nm within a certain pressure

range, the amount adsorbed by increasing the pressure is less than the amount which remains adsorbed by decreasing the pressure [144]. This creates a loop, known as hysteresis **(C-E)**. Thus, the appearance of a hysteresis loop corresponds to the presence of mesopores larger than 4 nm.

The adsorption-desorption isotherm consists of three distinctive areas where different theoretical models are used to calculate different properties such as the surface area, the pore volume, pore size and pore size distribution (Figure 5.4). The most frequently used procedure to determine the surface area of a porous material is the Brunauer- Emmett –Teller (BET) method. Originally, the concept of adsorption on surfaces was developed by Langmuir. He suggested that the adsorption corresponds to a dynamic equilibrium between a gas and a solid surface resulting in a monolayer molecular adsorption [103]. The BET theory is an extension of Langmuir theory that uses a similar kinetic approach, but allows for multilayer adsorption. Using the BET equation (shown below), the specific surface area can be calculated based on the low pressure section of the adsorption isotherm shown as region **(A)** in Figure 5.4:

$$\frac{p/p_0}{V_a(\,1-\frac{p}{p_0})} = \frac{1}{V_m C} + \frac{(p/p_0\,)(C-1)}{V_m C}$$

where V_a is the volume of nitrogen adsorbed, p/p_0 is the relative pressure, V_m is the volume required to form a monolayer and C is the BET constant [102]. A plot of $\frac{p/p_0}{V_a(\,1-p/p_0\,)}$ versus (p/p_0) yields a straight line with slope and y-intercept equal to $\frac{C-1}{V_m C}$ and $\frac{1}{V_m C}$, respectively. From these quantities, V_m and C can be determined. The linear relationship of this equation is maintained in the low pressure range, typically at p/p_0 = 0.05-0.3. In addition, multilayer adsorption does not occur if the material contains micropores, which makes the BET model not

valid for microporous materials. Analysis of the adsorption isotherm by the BET model is only valid for non-porous, mesoporous and macroporous materials, although it is often applied to microporous materials.

The second important section of the adsorption isotherm type IV is the capillary condensation step (region **B,** Figure 5.4). The adsorption data from this area can be used to determine the pore size distribution using the Barret-Joyner-Halenda (BJH) method. This method uses the Kelvin equation that relates the pore diameter with the pressure at which the capillary condensation occurs

$$\ln \frac{p}{p_0} = - \frac{2 \gamma V}{R T r_m}$$

where p/p_0 is the relative pressure of the adsorbate in equilibrium with the meniscus whose radius is r_m, γ is the surface tension, V is the molar volume of the liquid nitrogen, R is the universal gas constant and T is the absolute temperature in Kelvin. It has been shown that the BJH method underestimate the pore size by ca. 1.0 nm. Kruk, Jaroniec and Sayari (KJS) introduced a correction factor that takes into account the thickness of the film formed at p/p_0 which gives better results [104].

The third region of interest in the isotherm designated as region **C** in Figure 5.4 is the area where pore saturation occurs. This region can be used to determine the pore volume of the material which is the volume of the amount of adsorbate, considered in liquid state, adsorbed at a relative pressure as close as possible to 1.

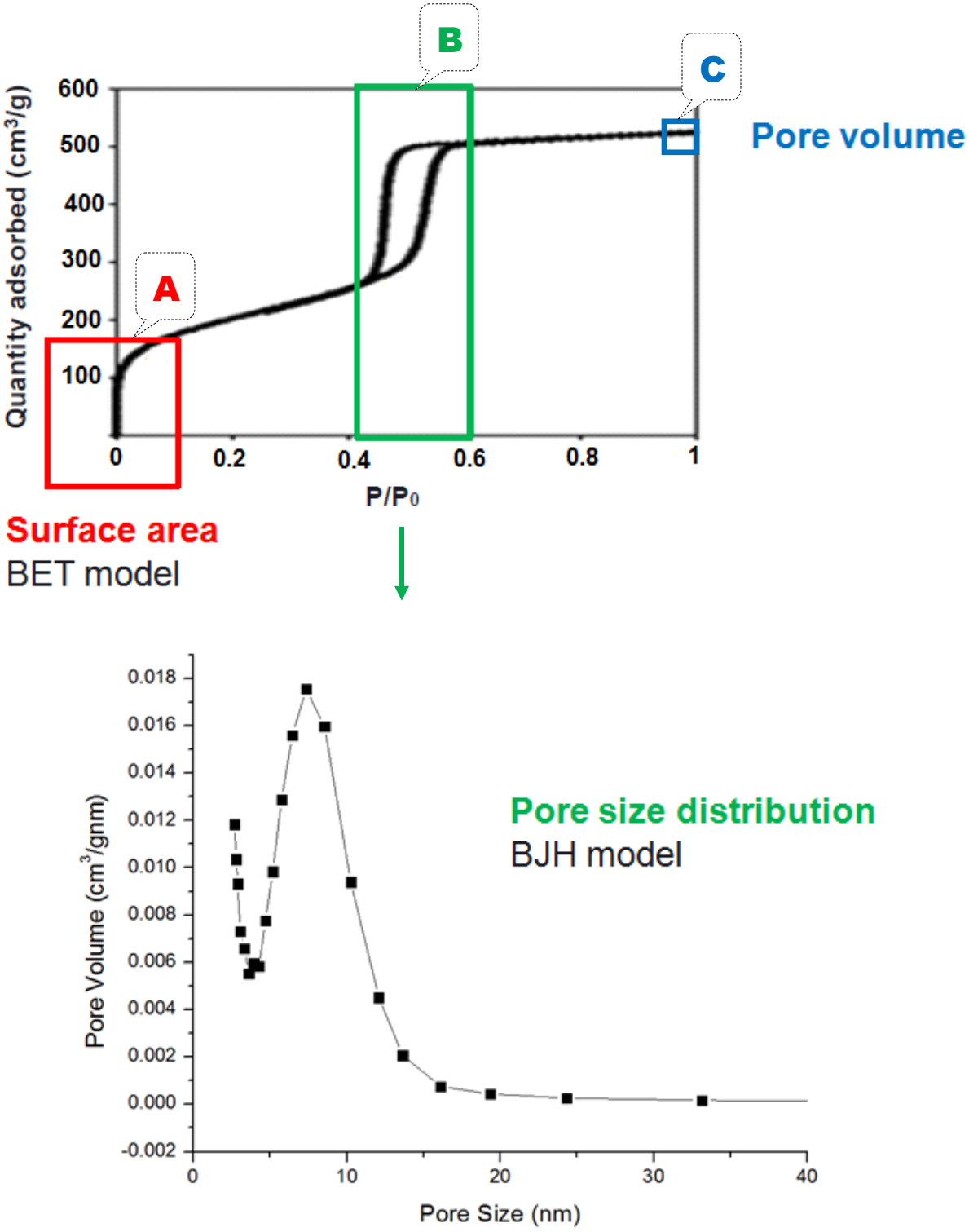

Figure 5.4: The areas of N_2 adsorption-desorption isotherm used for the calculations of different properties.

5.2 - Characterization of Periodic Mesoporous Silica

Mesoporous silicas functionalized with sulfonic acid (propyl-SBA-15 and phenyl-SBA-15) were synthesized through a one-pot procedure involving the co-condensation of a silica source, TEOS, and organosiloxane precursors MPTMS and PTES respectively, in the presence of Pluronic P123 as template (Figure 5.5). The introduction of sulfonic acid groups in the mercaptopropyl-functionalized SBA-15 (-C_3H_6SH) was achieved by post-oxidative transformation of the thiol (-SH) into sulfonic (-SO_3H) groups. Sulfonated phenyl-SBA-15 was achieved by post-synthesis sulfonation upon using chlorosulfonic acid. The textural and structural characterization of the synthesized sulfonic acid-modified mesostructured silicas were carried out through XRD, N_2 adsorption-desorption isotherms and SEM.

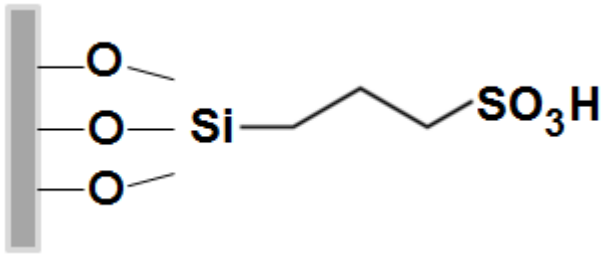

a) Propyl-SBA-15

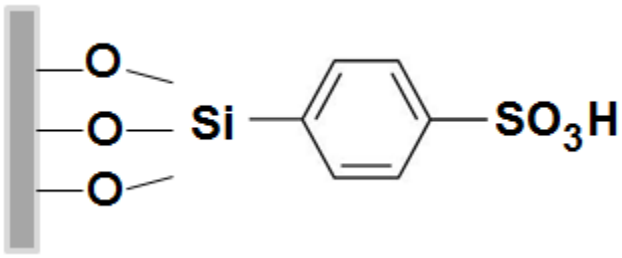

b) Phenyl-SBA-15

Figure 5.5: Schematic illustration of the sulfonic acid incorporated on SBA-15 silicas.

The XRD patterns show three reflections associated with p6mm symmetry: a single intense peak corresponding to $d_{(100)}$ and two low intensity signals assigned to $d_{(110)}$ and $d_{(200)}$ spacing. Thus, Figure 5.6 confirms that both samples exhibit a well ordered hexagonal structure. Notice that the (100) peak is not well resolved due to limitations of XRD instrument at very low angles.

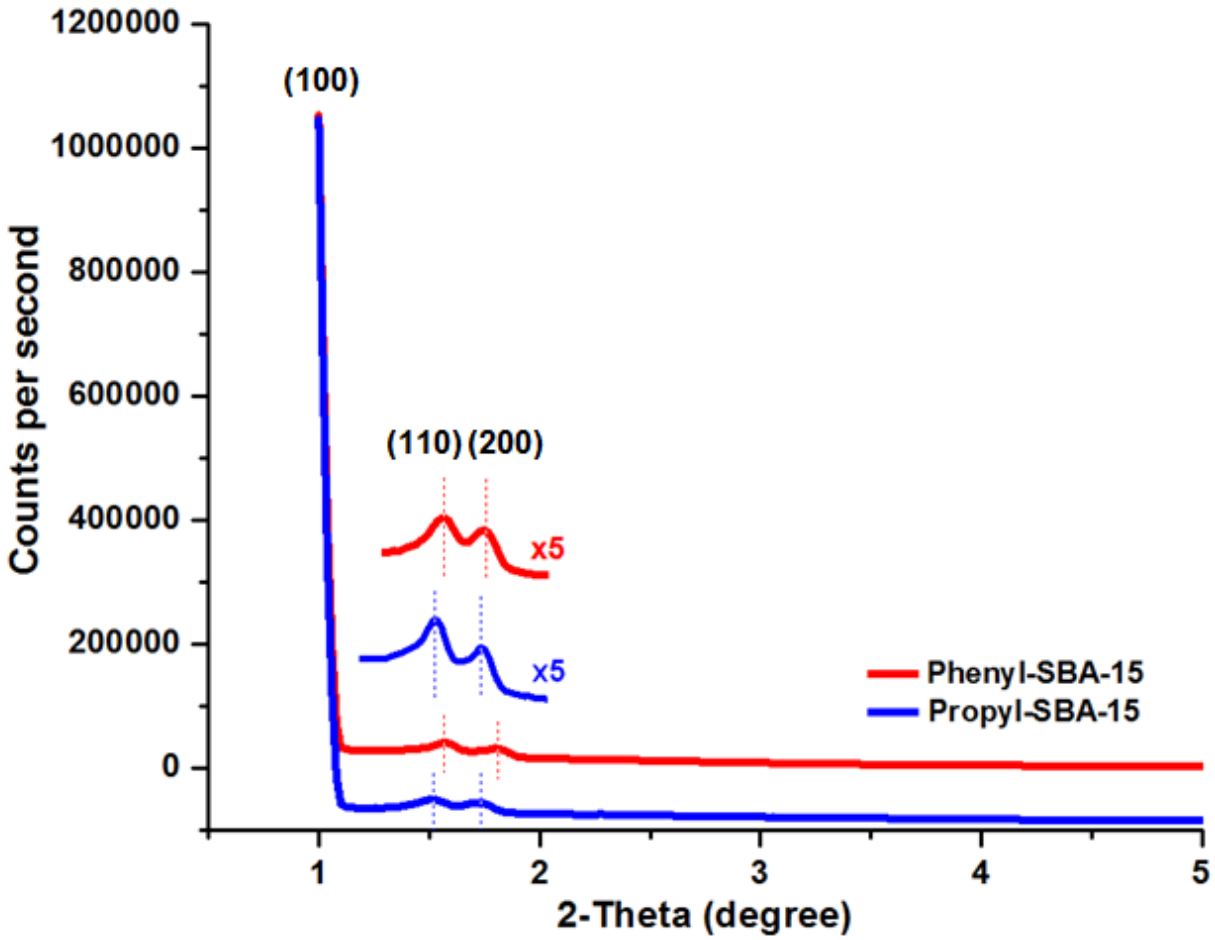

Figure 5.6: X-Ray diffraction patterns of sulfonic acid modified SBA-15 silicas.

The morphology of the SBA-15 materials was observed by scanning electron microscopy. The images (Figure 5.7) show that the samples consist of rod-like particles with ca. 0.5 μm average diameter and 1-1.5 μm length.

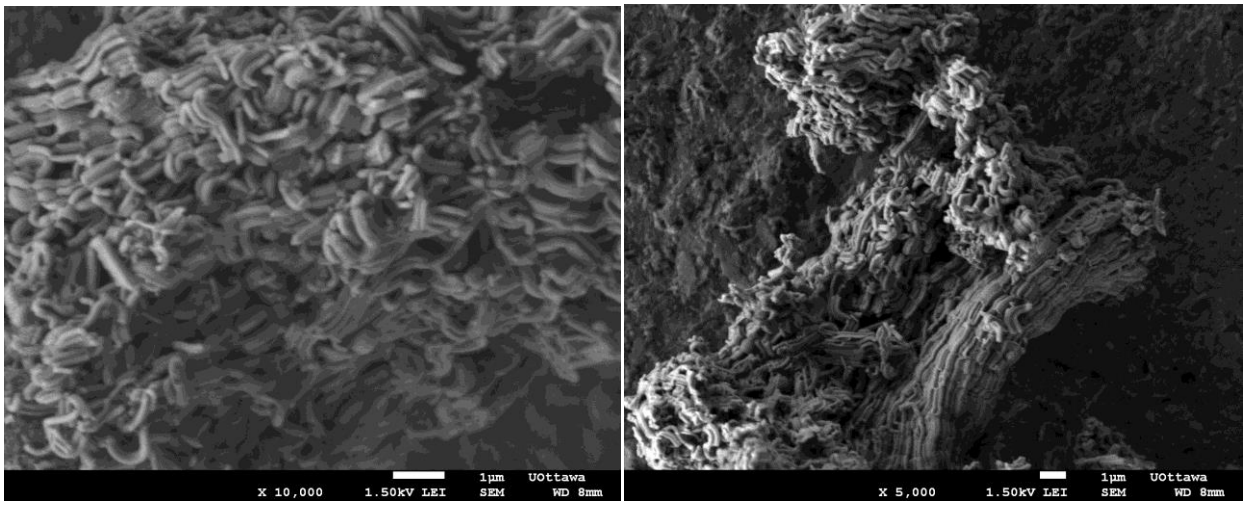

a) Propyl-SBA-15 **b) Phenyl-SBA-15**

Figure 5.7: SEM images of sulfonic acid modified SBA-15.

The nitrogen adsorption-desorption isotherms at -196 °C for the SO_3H-functionalized SBA-15 displayed a type IV isotherm, according to the IUPAC classification, with a hysteresis loop associated with capillary condensation and evaporation of nitrogen into the mesopores (Figure 5.8).

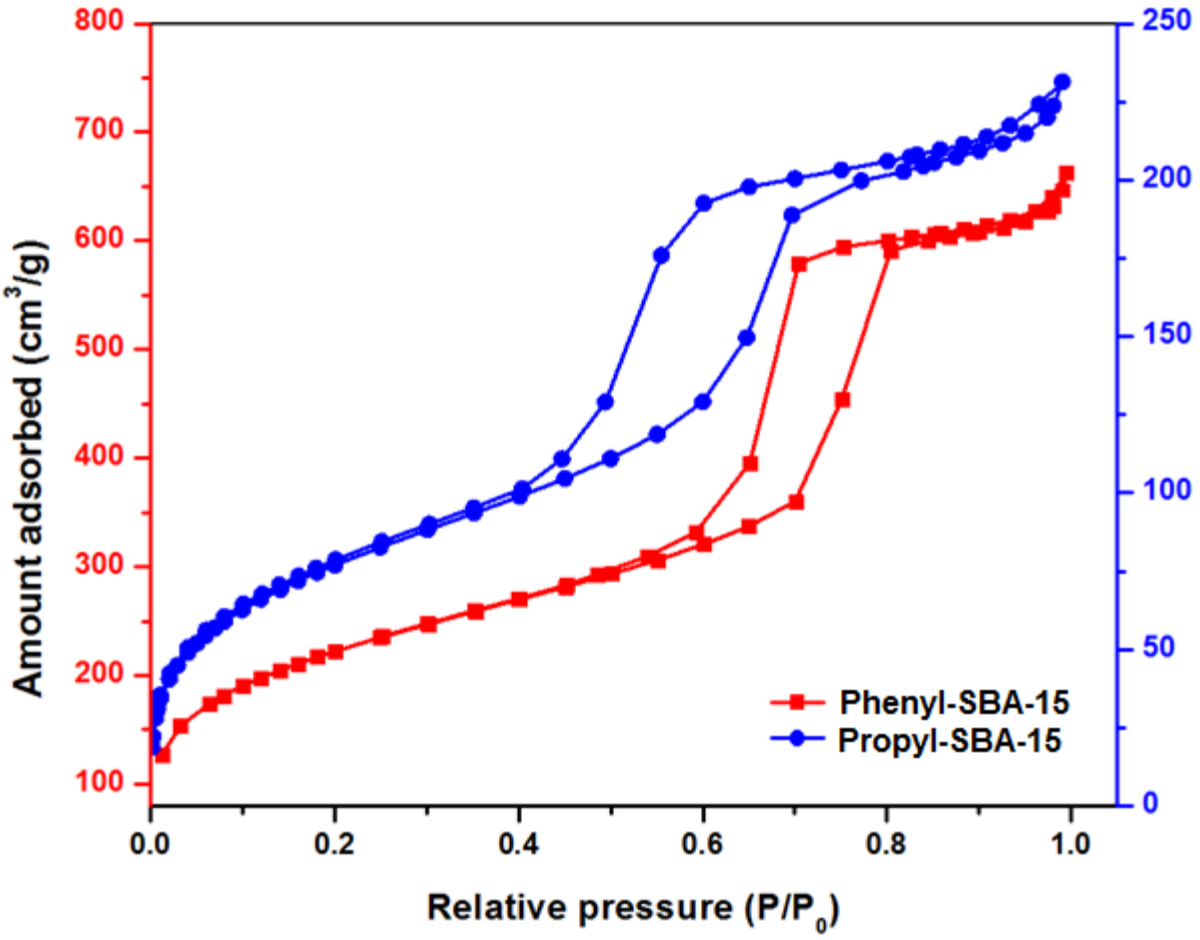

Figure 5.8: N_2 adsorption-desorption isotherms of sulfonic acid functionalized SBA-15.

The resulting specific surface area was 653 m^2/g for propyl-SBA-15 and 774 m^2/g for phenyl-SBA-15. Figure 5.9 displays the pore size distributions calculated by the adsorption branch of N_2-isotherm using the Barret-Joyner-Halenda (BJH) method. The average pore size was 8.6 nm for phenyl-SBA-15 and 7.2 nm for propyl-SBA-15. The structural and physicochemical properties for the synthesized sulfonic acid functionalized SBA-15 are summarized in Table 5.1.

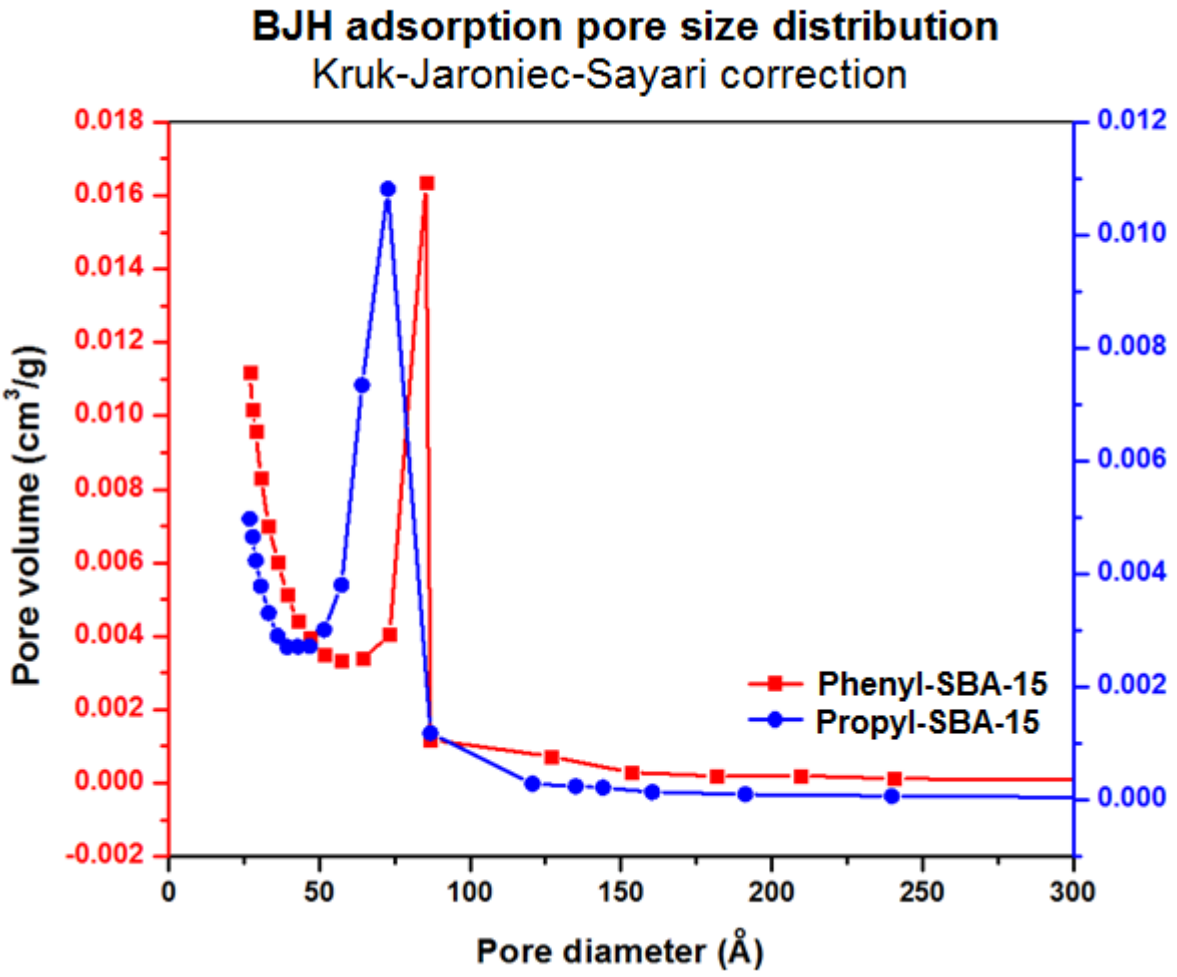

Figure 5.9: BJH pore diameter distribution of sulfonic acid functionalized SBA-15.

Table 5.1: *Physicochemical and textural properties of sulfonic acid modified mesostructured silicas*

Sample	Surface area (m^2/g)	Pore volume (cm^3/g)	Pore size (nm)	Elemental analysis %C	%S
Propyl-SBA-15	653	0.77	7.2	10.4	4.2
Phenyl-SBA-15	774	0.97	8.6	5.1	0.8

The effective incorporation of the organic functional groups covalently attached to the SBA-15 silica frameworks was proved by FTIR, ^{13}C NMR and elemental analysis. Figure 5.10 shows the FTIR spectra of the propyl-SBA-15 and phenyl-SBA-15 in comparison with a non-functionalized SBA-15 sample. All samples show the characteristic bands around 1060 and 804 cm^{-1} assigned to the Si-O-Si stretching and bending vibrations of the condensed silica network and the peak around 960 cm^{-1} corresponds to non-condensed Si-OH groups [105-106]. The broad band around 3370 cm^{-1} and the peak at 1630 cm^{-1} are due to the stretching and bending vibrations of adsorbed water [105]. The peaks corresponding to the S=O stretching vibrations are normally observed in the range 1000-1400 cm^{-1}. These peaks cannot be clearly resolved due to their overlap with the strong and wide band associated to Si-O-Si at 1060 cm^{-1}. The incorporation of phenyl and propyl sulfonic acid groups into the silica materials could be confirmed by spectra manipulation that consist of subtracting the FTIR spectra of functionalized samples from that of non-functionalized SBA-15. The resulting spectra in Figures 5.11 and 5.12 reveal a peak at around 947 cm^{-1} attributed to S-O symmetric stretch and two peaks at 1040 and 1103 cm^{-1} assigned to the symmetric and asymmetric stretching of S=O, respectively [107]. In addition, there is a peak of medium intensity at 790 cm^{-1} assigned to the stretching of S-O. Both functionalized SBA-15 samples have small bands in the range 2940-3000 cm^{-1} and at around 1350-1470 cm^{-1} attributed to the C-H stretching and bending vibrations of the propyl and phenyl groups. Elemental analyses studies also establish the incorporation of organic species within the silica framework (Table 5.1).

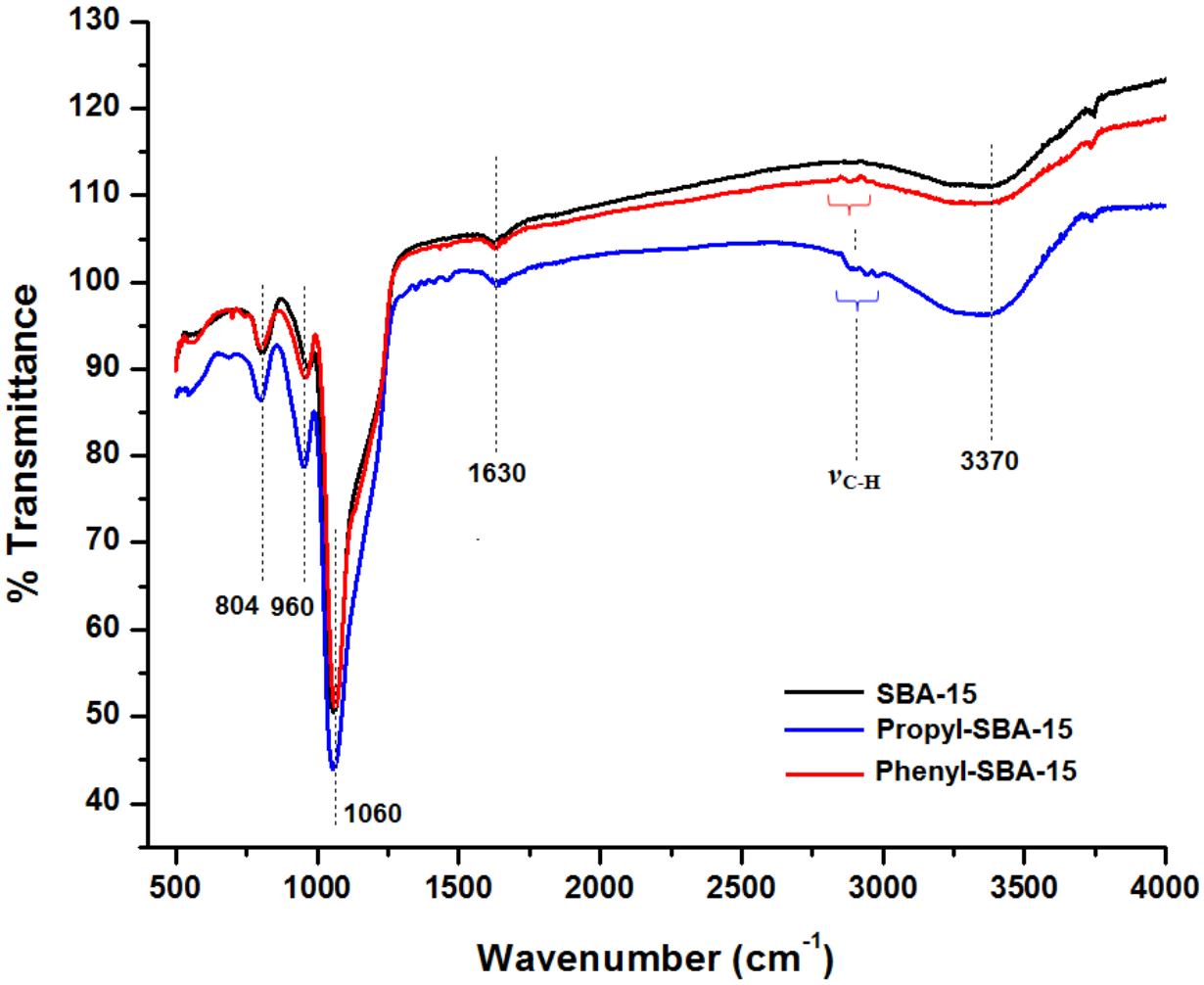

Figure 5.10: FTIR spectra of mesoporous silica samples.

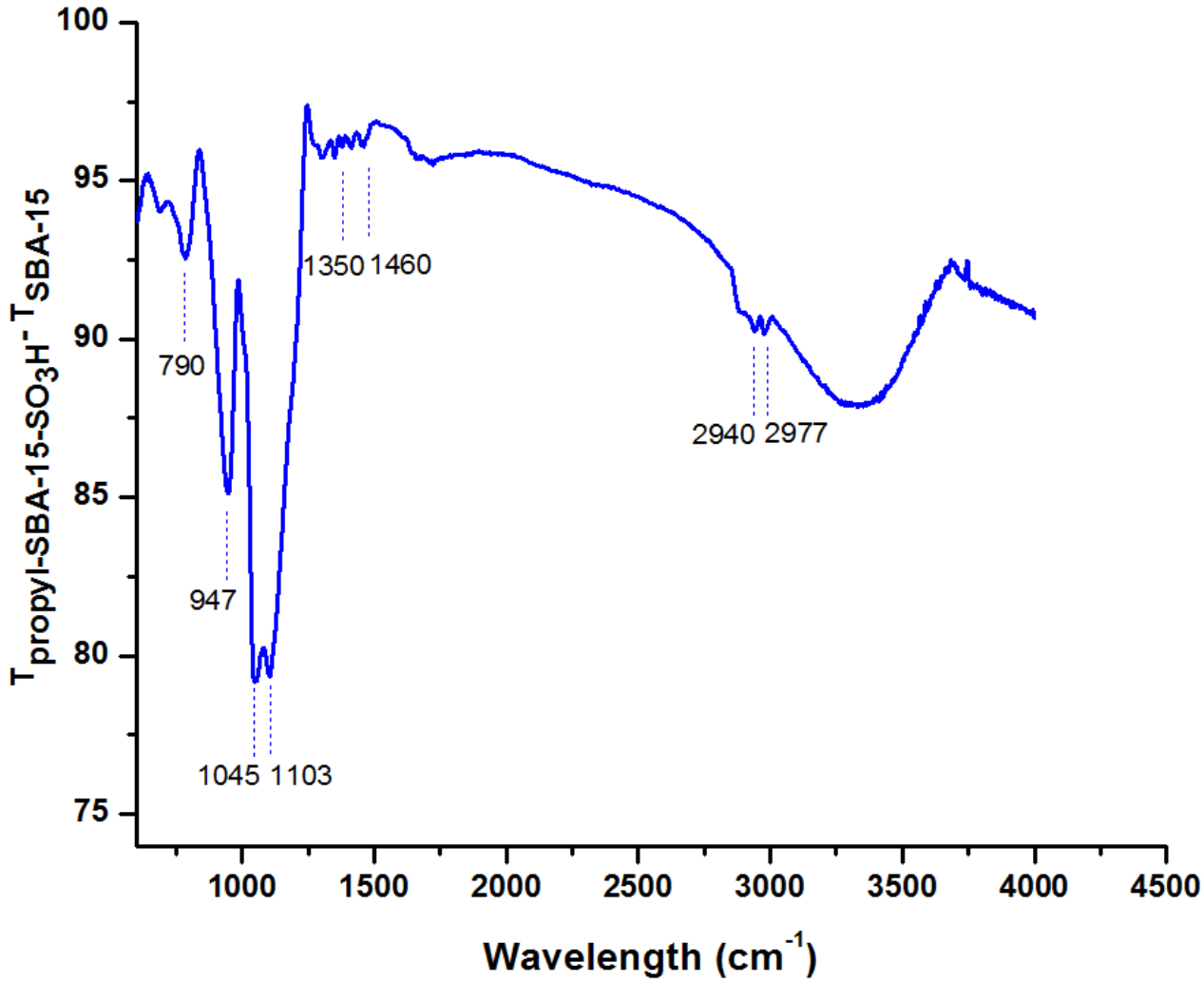

Figure 5.11: Difference spectrum between propyl-functionalized and non-functionalized SBA-15 samples.

Table 5.2: *FTIR absorption bands for periodic sulfonated mesoporous silicas*

Absorption bands (cm^{-1})	Assignment
~ 1060, ~ 800	Si-O-Si bending
~ 960	Si-OH
~ 1040	S=O symmetric stretching
~ 947	S-O symmetric stretching
~ 1103	S=O asymmetric stretching
~ 790	S-O stretching
~ 2940-3000	C-H stretching
~ 1350-1470	C-H bending
~ 1630	C=C stretch in aromatic ring

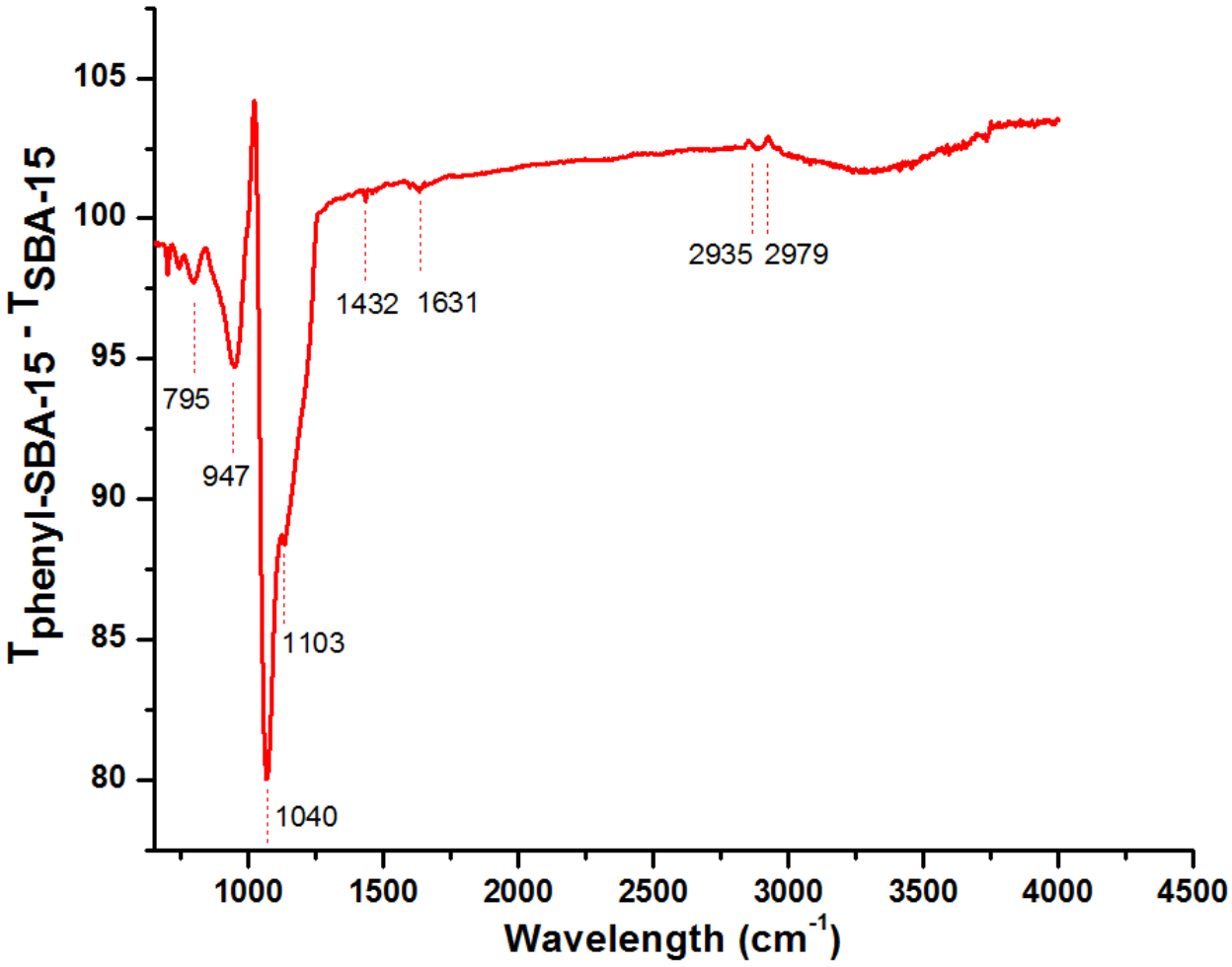

Figure 5.12: Difference spectrum between phenyl-functionalized and non-functionalized SBA-15 samples.

The solid state ^{13}C MAS NMR spectrum of SBA-15 with propylsulfonic acid groups on the surface showed three intense signals which can be assigned to the three carbon atoms of the propyl group (Figure 5.13). The resonances appearing at 12.5 and 17.7 ppm belong to C_1 attached to silicon and C_2, respectively [108]. The signal at 53.6 ppm is assigned to C_3 bearing sulfonic acid function [109, 130].

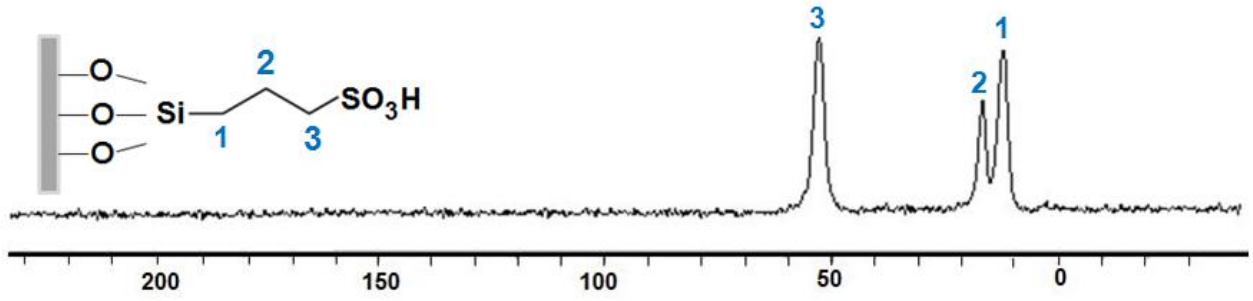

Figure 5.13: ^{13}C CP MAS spectrum of propyl-SBA-15.

The ^{13}C MAS NMR spectrum of phenyl-SBA-15, in turn, has three resonances belonging to the three types of carbon atoms of the aromatic ring (Figure 5.14). The signal 2 appearing at 136.5 ppm correspond to the carbon bonded to silica framework and the resonance at 141 ppm (signal 3) assigned to the carbon bearing the sulfonic acid group. The remaining peak at 128.6 ppm is assigned to non-substituted carbon of the aromatic ring bonded to hydrogen. The two very small peaks at 17.6 and 59.2 ppm are due to residual ethoxy groups [110].

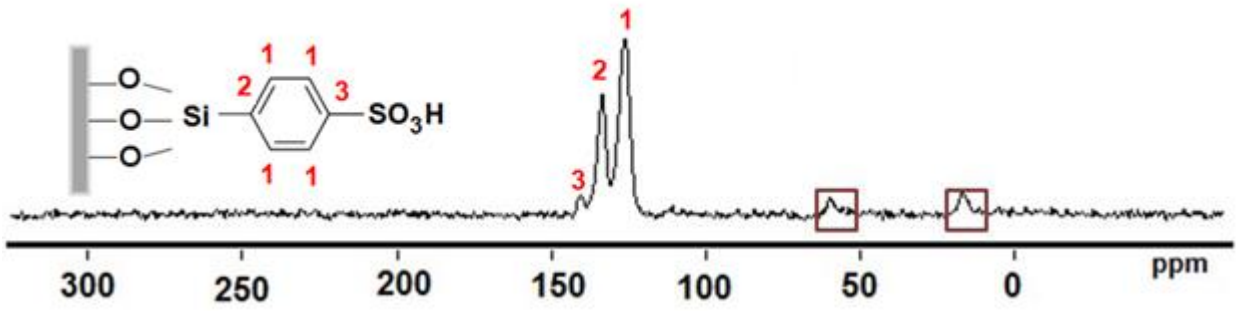

Figure 5.14: ^{13}C CP MAS spectrum of phenyl-SBA-15.

The two samples were then characterized by means of thermogravimetric analysis to determine the amounts of organic groups anchored on SBA-15 materials. Thermogravimetric analyses corresponding to propyl and phenyl-sulfonic acid functionalized mesoporous catalysts typically showed weight loss profiles that can be divided in two regions (Figure 5.15). Conceptually, the modification procedure of a surface with an organic group can be reasoned as an elimination reaction between the surface hydroxyl groups and the alkoxy ligands of the silane, with loss of alcohol. However, one or two alkoxy groups per silane may not react [111]. For this reason, the SBA-15 samples were first treated in a flow of N_2 at 120 °C for 2 h to remove pre-adsorbed moisture and any ethanol stemming from the hydrolysis of unreacted ethoxy groups (Region I). Subsequently, the organic layer was decomposed by heating at 10 °C/min to 800 °C under flowing N_2, then at 10 °C/min to 1000 °C in flowing air. The weight loss of propyl-SBA-15 and phenyl-SBA-15 in the temperature range between 200 °C and 1000 °C indicated that the amount of organic group was respectively 1.0 and 0.8 mmol/g (Region II). Overall, the results obtained are in good agreement with what previously reported [112-113].

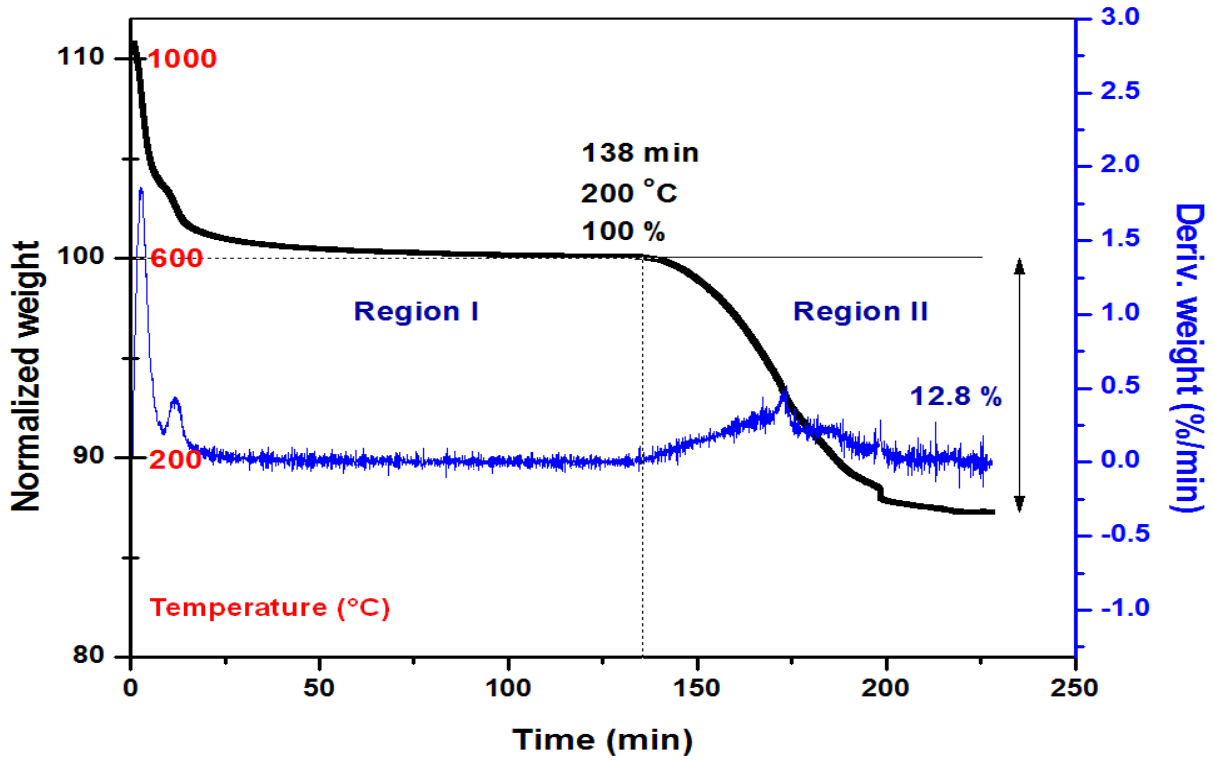

(A) Propyl-SBA-15

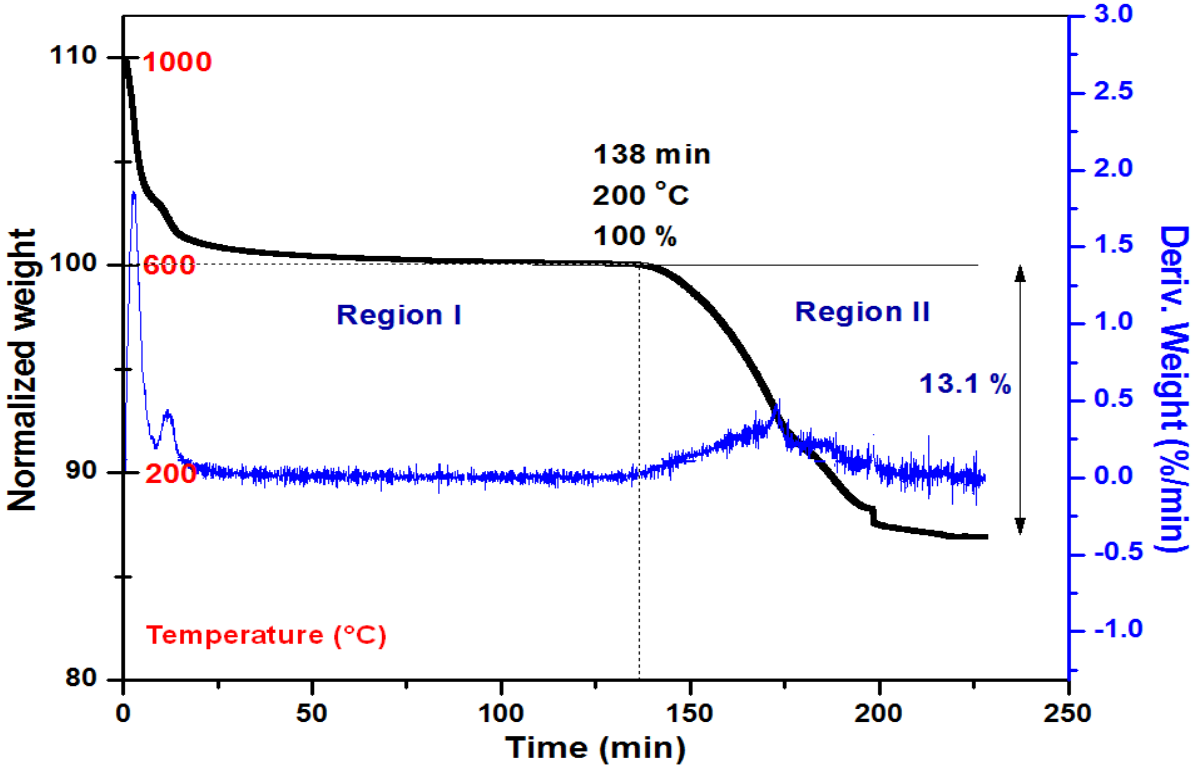

(B) Phenyl-SBA-15

Figure 5.15: Weight loss curves for sulfonic acid modified SBA-15.

5.3 - Characterization of Periodic Mesoporous Organosilica

Our goal was to prepare phenylene and biphenylene-bridged mesoporous materials that have the great advantage of molecular-scale periodicity in the pore walls [92-93,114]. These functionalities are suitable for further chemical modification to introduce Brønsted acid sites ($-SO_3H$) and have the potential to be used as a solid acid catalyst in a catalytic reaction. Biphenylene-bridged PMO was synthesized using BTEBP as a precursor, in the presence of $C_{18}Cl$ as structure directing template under basic conditions. On the other hand, phenylene-bridged PMO was prepared using Pluronic P123 as structure-directing agent under acidic conditions.

The powder XRD profile of the phenylene-PMO, illustrated in Figure 5.16 , revealed three peaks in the low-angle diffraction regime ($2\theta < 5$), which are assigned to (100), (110) and (200) with two-dimensional hexagonal symmetry [108]. In addition, the molecular-scale ordering of the organic spacer within the pore walls as a result of organization of phenylene-silica moieties was proved by an additional peak ($2\theta = 12°$) with a d-spacing of 0.8 nm as reported in previous work [93].

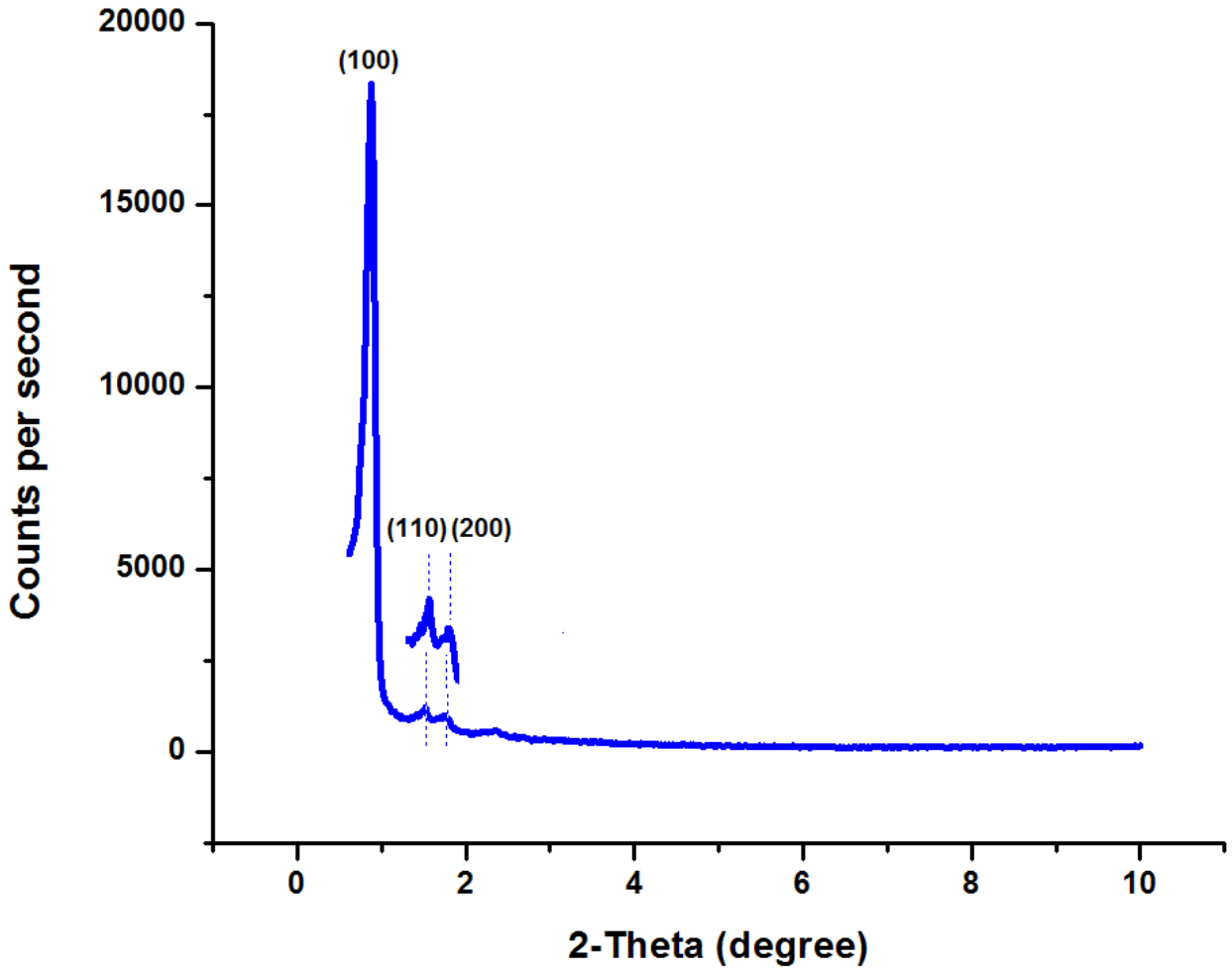

Figure 5.16: Powder X-Ray diffraction profile of phenylene-bridged PMO.

Similarly, biphenylene-bridged PMO exhibited a main peak at 2° 2θ indicating the occurrence of a mesophase (Figure 5.17). No additional peaks attributable to the mesophase structure were detected. However, additional diffraction peak appeared at 2θ = 7.5° assigned to the lamellar structure within the pore walls with a d-spacing of 1.1 nm, as reported by Sayari et al. [92]. This was proved by a series of regularly spaced diffraction peaks appeared at d-spacing of 11.6, 5.9, 3.9, 2.9 and 2.4 Å.

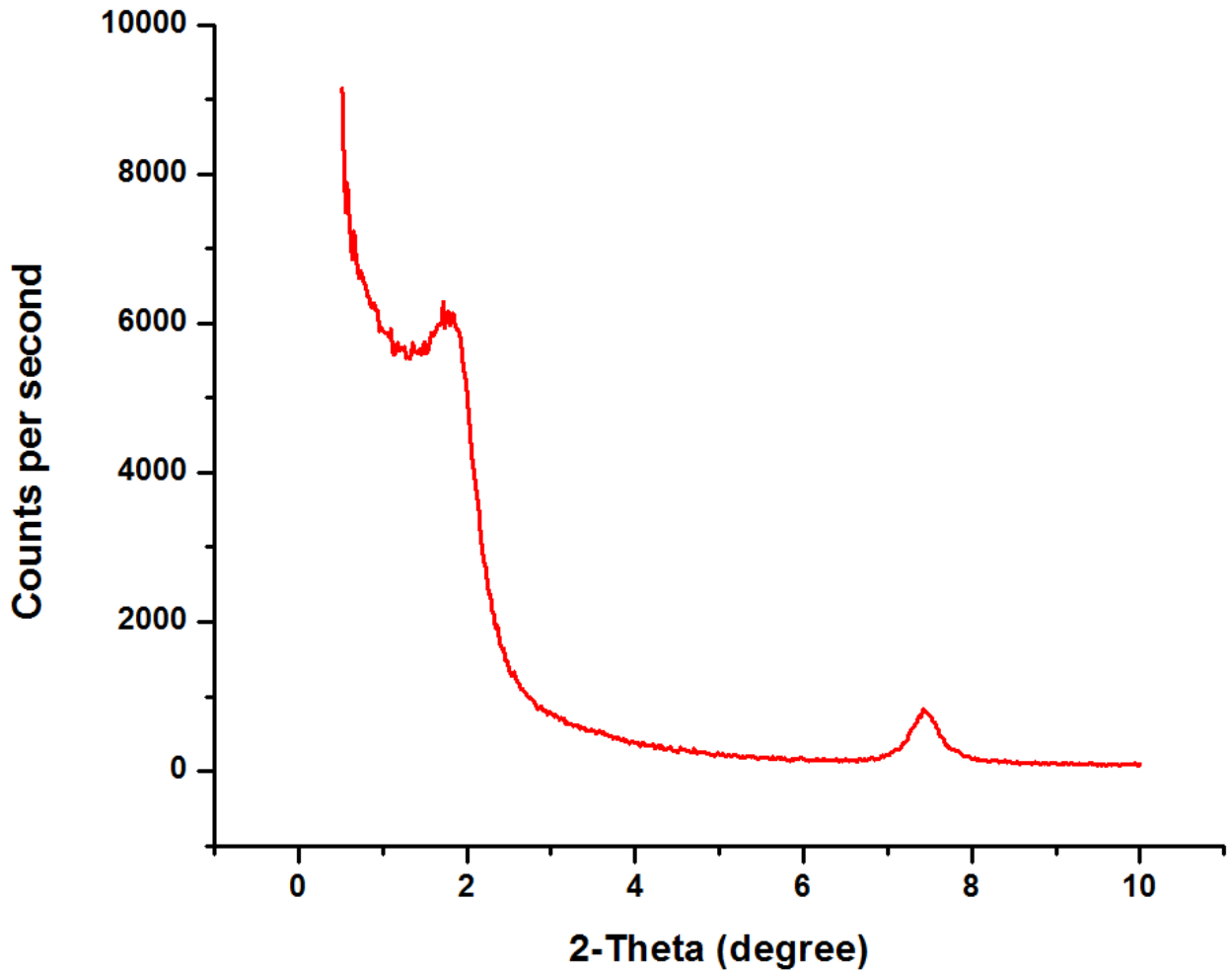

Figure 5.17: Powder X-Ray diffraction profile of biphenylene-bridged PMO.

The nitrogen adsorption-desorption isotherms for the phenylene and biphenylene-bridged PMO are presented in Figure 5.18. Both isotherms displayed a hysteresis loop in the relative pressure range of 0.4-0.8 associated with capillary condensation and evaporation of nitrogen into the mesopores.

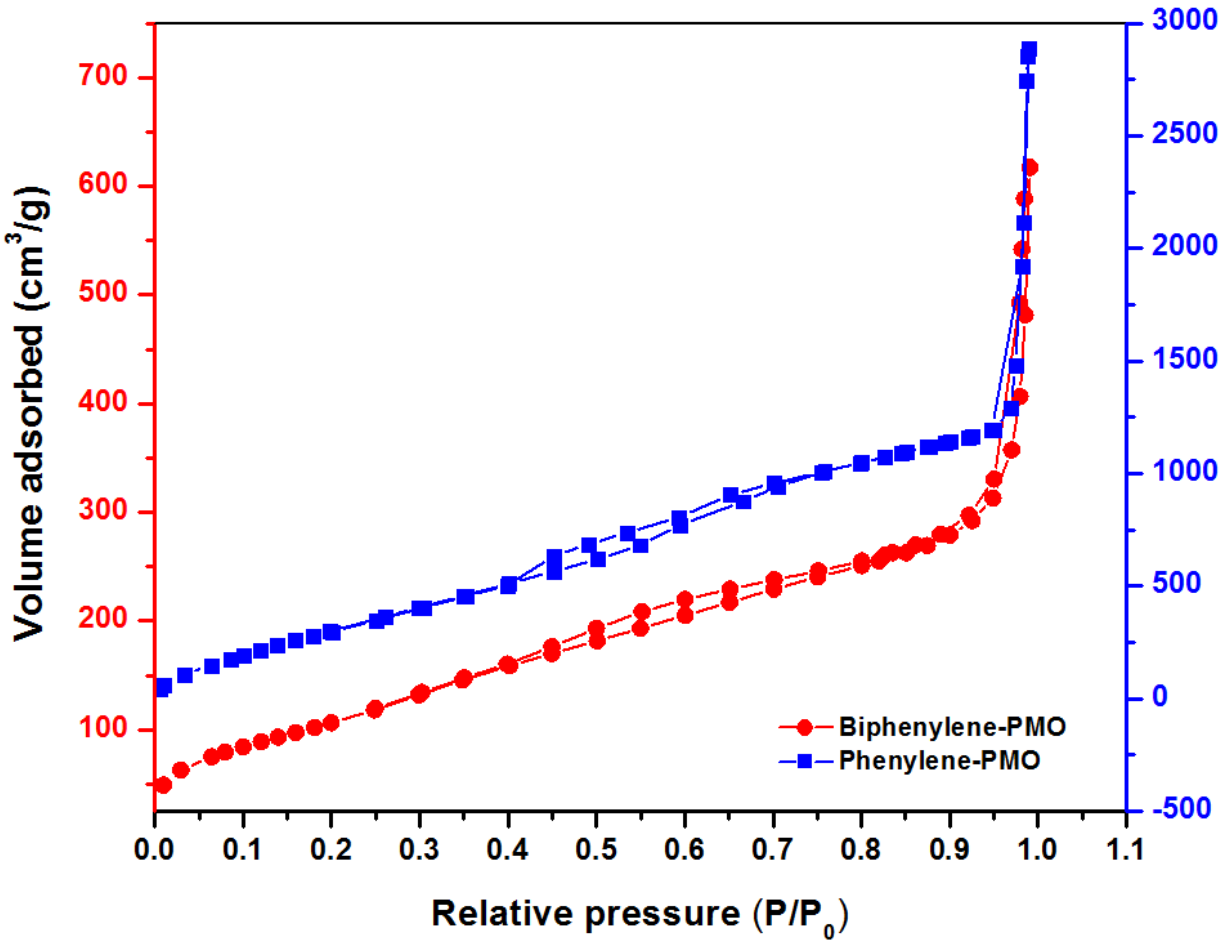

Figure 5.18: N_2 adsorption-desorption isotherms of biphenylene and phenylene-bridged PMOs.

The BJH pore diameter, BET surface area, and pore volume as derived from the nitrogen adsorption isotherms are summarized in Table 5.3. As it can be seen, the resultant textural properties and pore characteristics of the PMOs are highly dependent on the surfactant and conditions used. Phenylene-bridged PMO has high surface area of 1265m^2/g, large pore diameter of 7.9 nm, and high pore volume of 1.5 cm^3/g, as is commonly observed in PMO synthesized under these conditions [93]. In contrast, biphenylene-PMO with lower surface area of 462 m^2/g and smaller pore diameter of 3.4 nm resulted from the $C_{18}Cl$ structure-directing agent under

basic conditions. Pore sizes for the alkyl ammonium cationic surfactant are generally smaller than for the non-ionic surfactant Pluronic P123 due to a smaller micelle size, thus, the difference in the textural properties between Ph-PMO and Biph-PMO can be ascribed to the nature of the surfactant (ionic or neutral) used and the reaction medium (acidic or basic) in which the synthesis takes place.

Table 5.3: *Physicochemical properties of mesoporous organosilicas*

Sample	Surface area (m^2/g)	Pore volume (cm^3/g)	Pore size (nm)
Phenylene-PMO	1265	1.51	7.9
Biphenylene-PMO	462	0.55	3.4

The pore structure of the mesoporous organosilica materials was examined by transmission electron microscopy. TEM images, presented in Figure 5.19, revealed the formation of an ordered mesostructure with a hexagonal arrangement of mesoporous channels. The morphology of the mesoporous organosilica materials was observed by scanning electron microscopy. Phenylene and biphenylene-bridged silica exhibited different morphologies. The biphenylene PMO consisted of uniform particle less than 1 μm in length, whereas the phenylene PMO consisted of rod-like elements with ca. 0.5 μm average diameter.

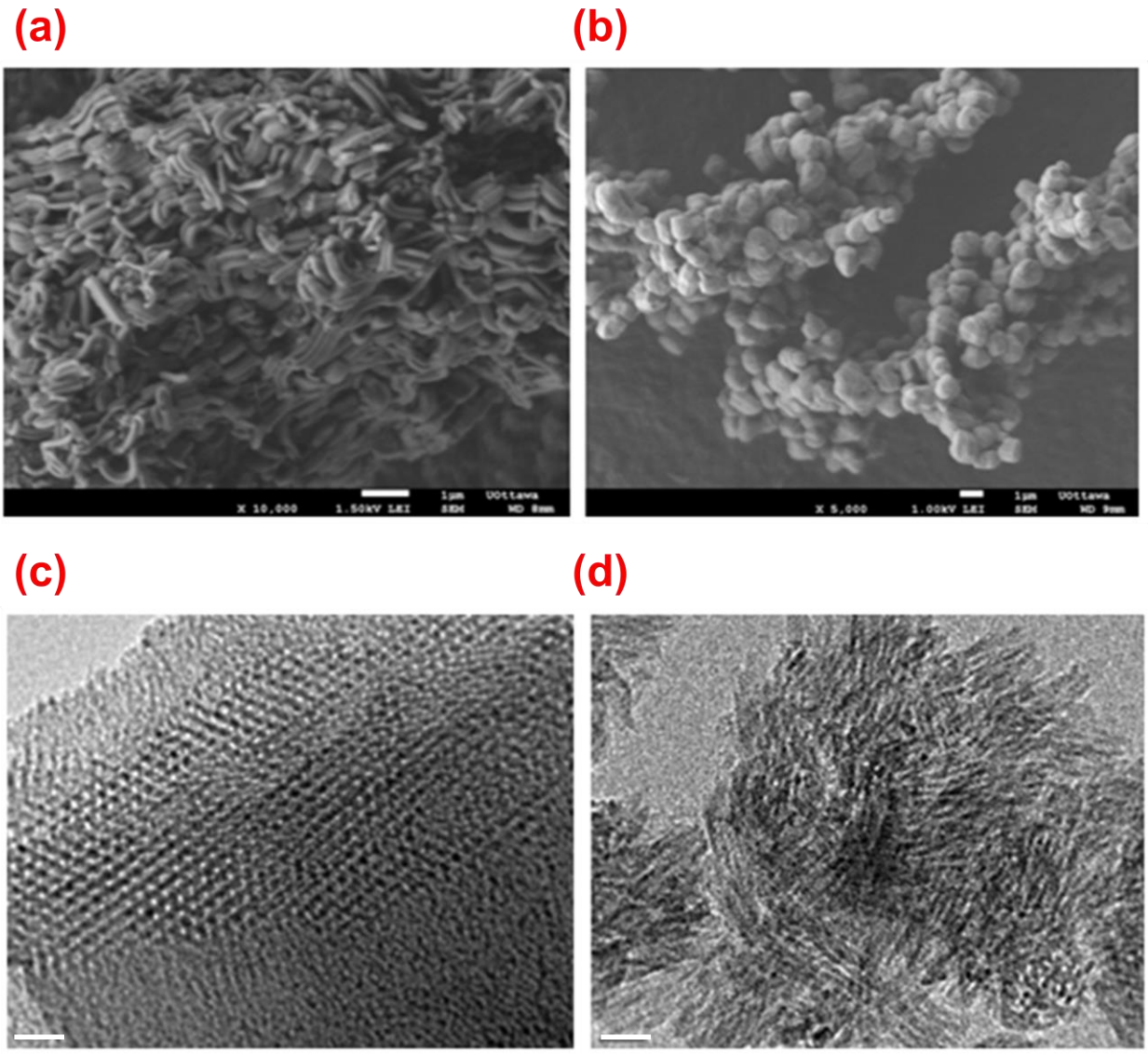

Figure 5.19: SEM (a, b) and TEM images (c, d) of phenylene and biphenylene bridged PMO.

Solid state ^{13}C and ^{29}Si NMR measurements of the mesoporous organosilicas were carried out to confirm the incorporation of the organic spacers within the pore walls of PMOs. The ^{13}C CP MAS NMR spectra of biphenylene-bridged PMO exhibited four distinct peaks with chemical shifts of 126.1, 131.1, 135.6, and 141.5 ppm (Figure 5.20), attributable to the four different carbons in the biphenylene ring [115]. The two small signals a *ca.* 17.2 ppm and 59 ppm are assigned to non hydrolyzed ethoxy groups [110]. The occurrence of covalent Si-C bond in the framework of the phenylene-bridged PMO was also confirmed by ^{13}C CP MAS NMR where the spectra, as shown in Figure 5.20, was dominated by a single resonance at 133.8 ppm assigned to the four identical carbon atoms in the benzene ring [92]. The phenyl-bridged PMO spectrum also includes signals at 17, 70, 73 and 75 ppm, assigned to residual Pluronic P123 [116]. The remaining peaks are spinning sidebands [93].

The ^{29}Si MAS NMR spectra of Ph-PMO and Biph-PMO featured three signals at -62.2, -70.9 and -79.5 ppm, attributable to Si species covalently bonded to carbon atoms of T_1 [C*Si*$(OSi)(OH)_2$)], T_2 [C*Si*$(OSi)_2OH$] and T_3 [*Si*$C(OSi)_3$] respectively [92-93]. No Q_n [*Si*$(OSi)_n(OH)_{4-n}$] species were detected in the PMOs spectrum range - 90 to -110 ppm indicating that no separate silica phase occurred, and all the Si-C bonds were preserved during the material synthesis and surfactant removal (Figure 5.21). In comparison to the phenylene PMO prepared under acidic conditions, biphenylene PMO synthesized in basic conditions showed T_3 to be the dominant silicon species indicating a higher degree of condensation, which is typical when comparing ^{29}Si NMR spectra of PMOs made under these two conditions [114].

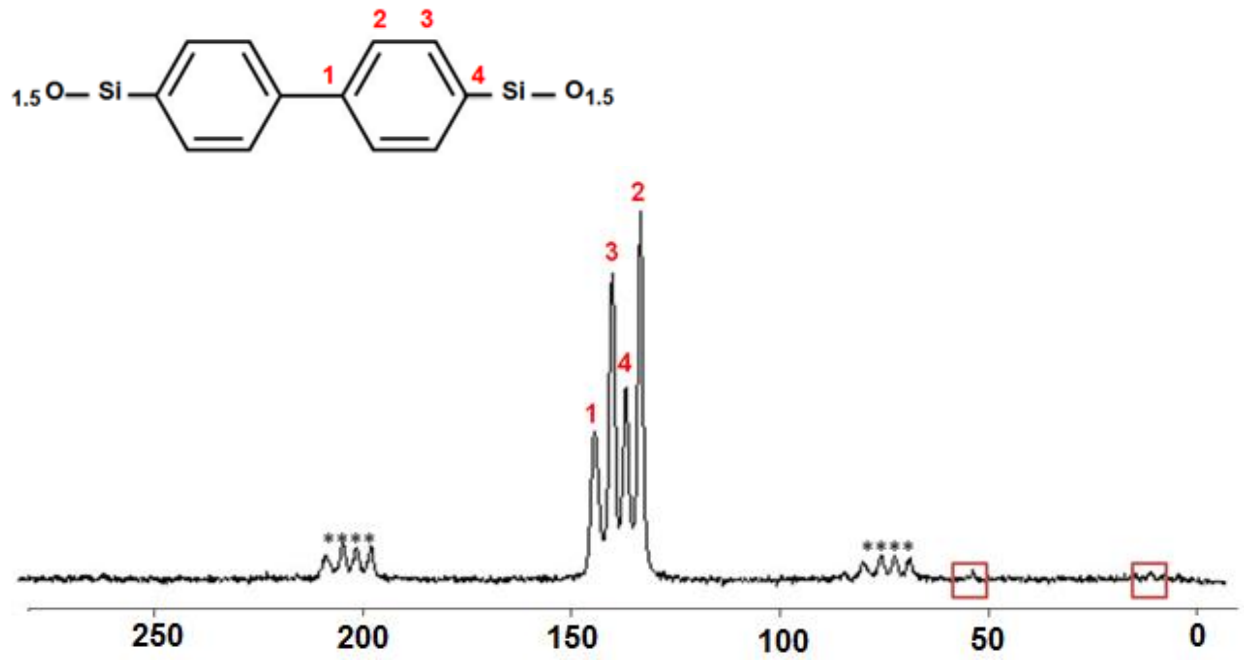

a) Biphenylene-bridged PMO

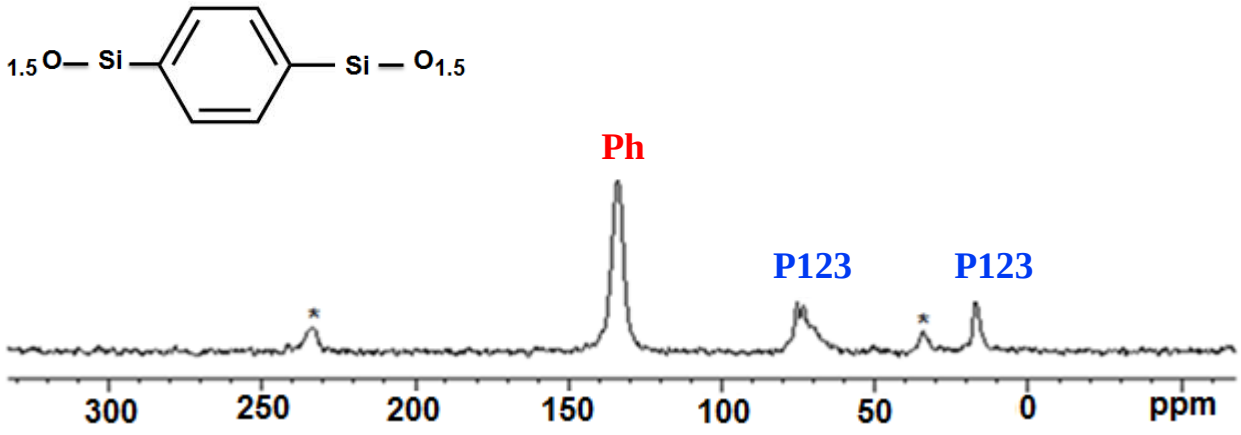

b) Phenylene-bridged PMO

Figure 5.20: ^{13}C CP MAS spectra of biphenylene and phenylene-bridged PMOs.

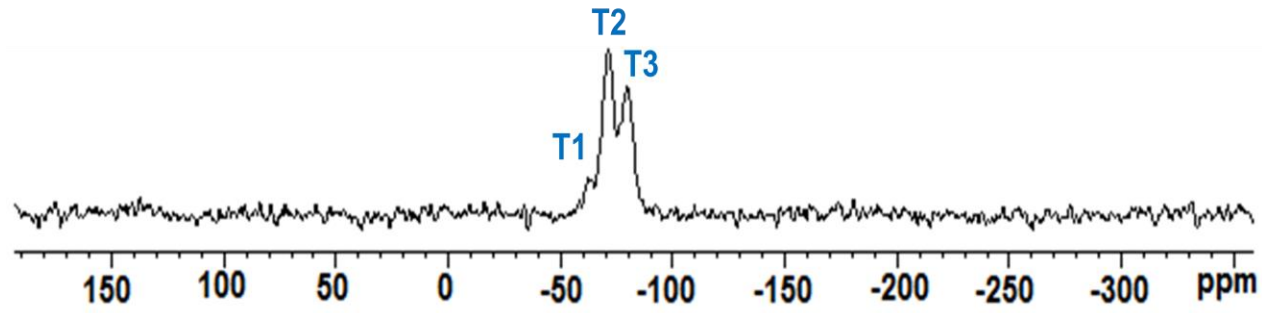

(a) Phenylene PMO

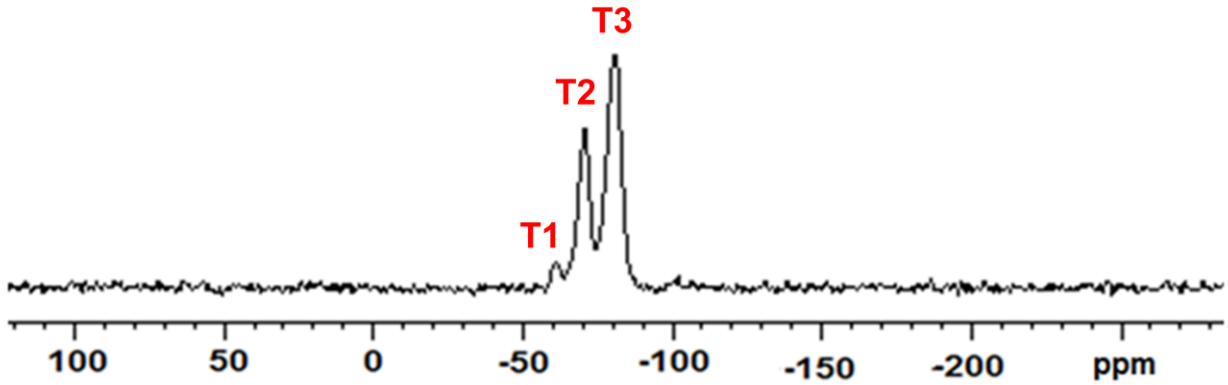

(b) Biphenylene PMO

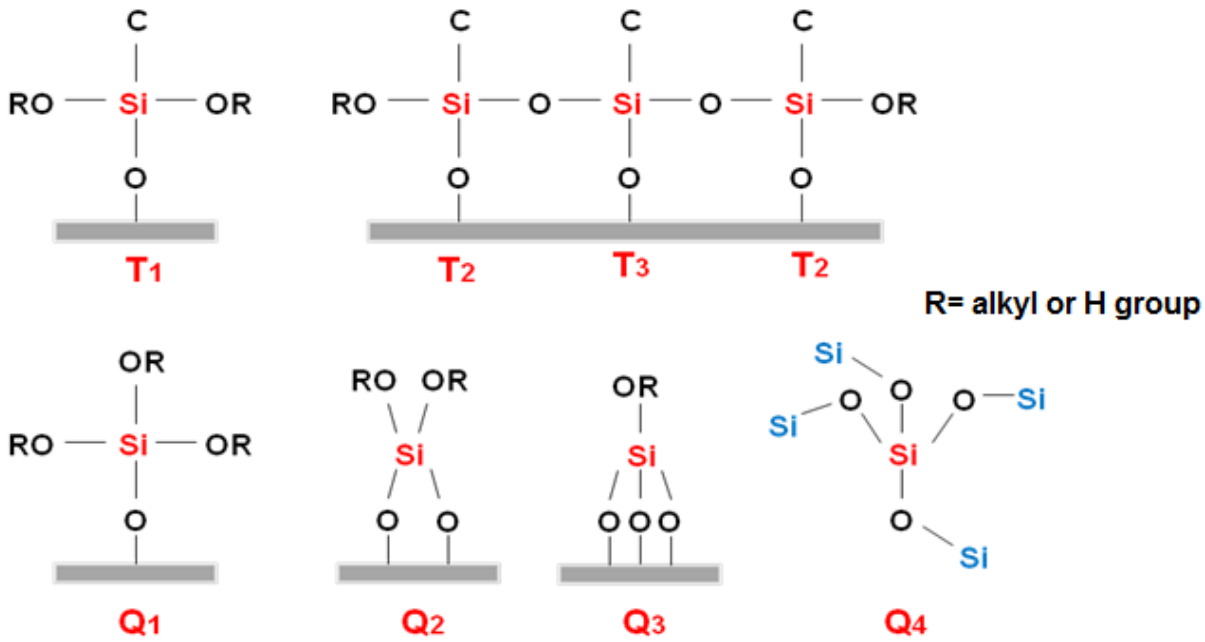

Figure 5.21: ^{29}Si MAS NMR spectra of phenylene and biphenylene-bridged PMOs.

The PMO samples were then characterized by means of thermogravimetric analysis to determine the thermal stability and the results are presented in Appendix II. The TGA profiles for the PMO materials where similar to each other's; the decomposition of the mesoporous organosilicas started around 550-590 °C and reached a maximum between 630 and 690 °C depending on the material, thus the results obtained confirmed that phenylene and biphenylene bridged PMO exhibit high thermal stability.

The resulting PMO materials were reacted with chlorosulfonic acid, giving sulfonic acid functionalized phenylene and biphenylene-bridged PMO, which were used as acid catalysts for the conversion of sucrose to HMF. Chlorosulfonic acid was chosen as the sulfonating agent because both concentrated and fuming sulfuric acids lead to structural degradation of the organosilica framework that was verified by IR. As illustrated in Appendix III, biphenylene PMO show the characteristic bands around 1060 and 804 cm^{-1} assigned to the Si-O-Si stretching and bending vibrations of the condensed silica network and the peak around 960 cm^{-1} corresponds to non-condensed Si-OH groups [105-106]. The broad band around 3370 cm^{-1} and the peak at 1630 cm^{-1} are due to the stretching and bending vibrations of adsorbed water.

The structural and physicochemical properties for the sulfonic acid functionalized PMOs are summarized in Table 5.4. The resulting specific surface area and pore size decrease after the sulfonic acid groups (-SO_3H) were introduced. The results obtained are in good agreement with previously reported data and indicates the occurrence of sulfonic acid groups within the pore channels [108]. The amount of incorporated sulfonic groups was calculated through the sulfur content determined by elemental analysis since all the sulfur atoms are expected to be in the form –SO_3H in both PMO materials. Sulfonated phenylene PMO (denoted as Ph-PMO-S) presented a sulfur loading of 1.48 % corresponding to an acid loading of 0.46 mmol/g while the sulfur

loading in sulfonated biphenylene PMO (denoted as Biph-PMO-S) was equal to 0.56 % with an acid loading of 0.21 mmol/g. The higher acid loading in Ph-PMO-S is attributed to its higher surface area in comparison with Biph-PMO-S (1040 vs. 271 m^2/g respectively).

Table 5.4: *Physicochemical properties of sulfonated mesoporous organosilicas*

Sample	**Surface area (m^2/g)**	**Pore volume (cm^3/g)**	**Pore size (nm)**	**Elemental analysis**		**Acid loading (mmol/g)**
				%C	**%S**	
Ph-PMO-S	1040	1.03	7.5	30.5	1.48	0.46
Biph-PMO-S	271	0.46	2.9	50.7	0.56	0.21

5.4 - Characterization of Carbon Materials

5.4.1 Sulfonated Mesoporous Carbon CMK-3-SO_3H

Mesoporous carbon CMK-3 was synthesized using the hexagonally ordered SBA-15 material as hard template. Basically, the nano-casting method involves three steps. After the synthesis of the template, SBA-15 was impregnated with a carbon precursor by infiltrating sucrose into its mesopores scaffolds twice and the resultant mixture was subject to thermal treatment to carbonize sucrose in two carbonization steps, at 160 °C to allow a partial carbonization and at 550 °C to achieve a deep carbonization. The CMK-3 carbon material, obtained after removing the silica template using hydrofluoric acid (5 wt%), is catalytically inactive owing to its neutral framework. Xing et al. [95] demonstrated that the carbonization at temperature higher than 550 °C was benefit to increase the mesostructure order. However, the CMK-3 obtained presents a negligible content of polycyclic aromatic carbon available for functionalization. An optimum carbonization temperature of 550 °C allowed to obtain a well-ordered mesoporous carbon and simultaneously contained a considerable amount of polycyclic aromatic carbon. For the carbonization other than the optimum temperature, the balance crumbled between the structural order and the content of polycyclic aromatic carbon available for functionalization. The sulfonic acid modified carbon (CMK-3-SO_3H) was prepared through vapour transfer which consists of contacting the sample powders with the vapor from sulfuric acid in a sealed autoclave. Vapour transfer was chosen as the sulfonation method because it was reported to be more effective than dipping the carbon into concentrated or fuming sulfuric acids [95]. The acid functionalized mesoporous carbon was characterized by means of XRD, SEM, TEM, N_2 adsorption-desorption, ^{13}C NMR, FTIR and elemental analysis.

The XRD patterns of CMK-3-SO_3H and SBA-15 are shown in Figure 5.23. The ordered arrangement of the mesoporous channels in SBA-15 was represented by three well-resolved peaks associated with *p6mm* symmetry; a single intense peak corresponding to $d_{(100)}$ and two low intensity signals assigned to $d_{(110)}$ and $d_{(200)}$ spacing. Thus, The pore structure of the carbon material examined by TEM presented in Figure 5.22a revealed the formation of an ordered mesostructure with a hexagonal arrangement of mesoporous channels. SEM image (Figure 5.22b) showed that CMK-3-SO_3H consisted of rod-like particles. The obtained images indicated that hard-templating method give rise to a carbon that was an exact inverse replica to SBA-15.

Figures 5.22 and 5.23 confirmed that SBA-15 exhibited a well ordered hexagonal structure. Notice that the $d_{(100)}$ peak was not well resolved because of limitation of the XRD instrument at very low diffraction angles. The XRD pattern of CMK-3-SO_3H indicated that the mesoporous carbon with a well-ordered mesostructure was truly an inverse replica of SBA-15.

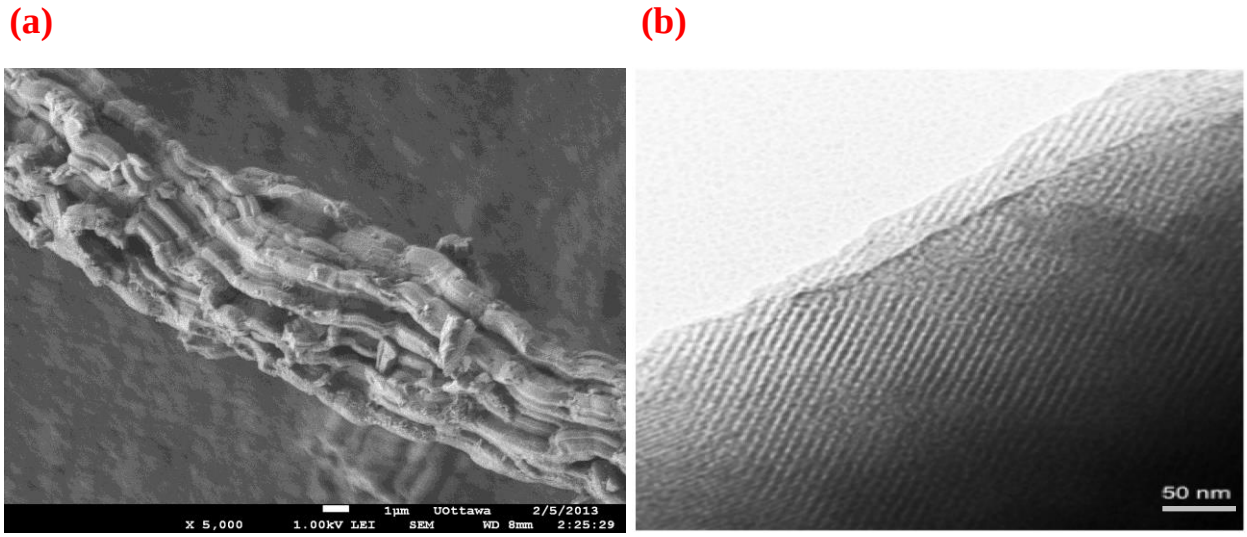

Figure 5.22: SEM (a) and TEM (b) images of CMK-3-SO_3H.

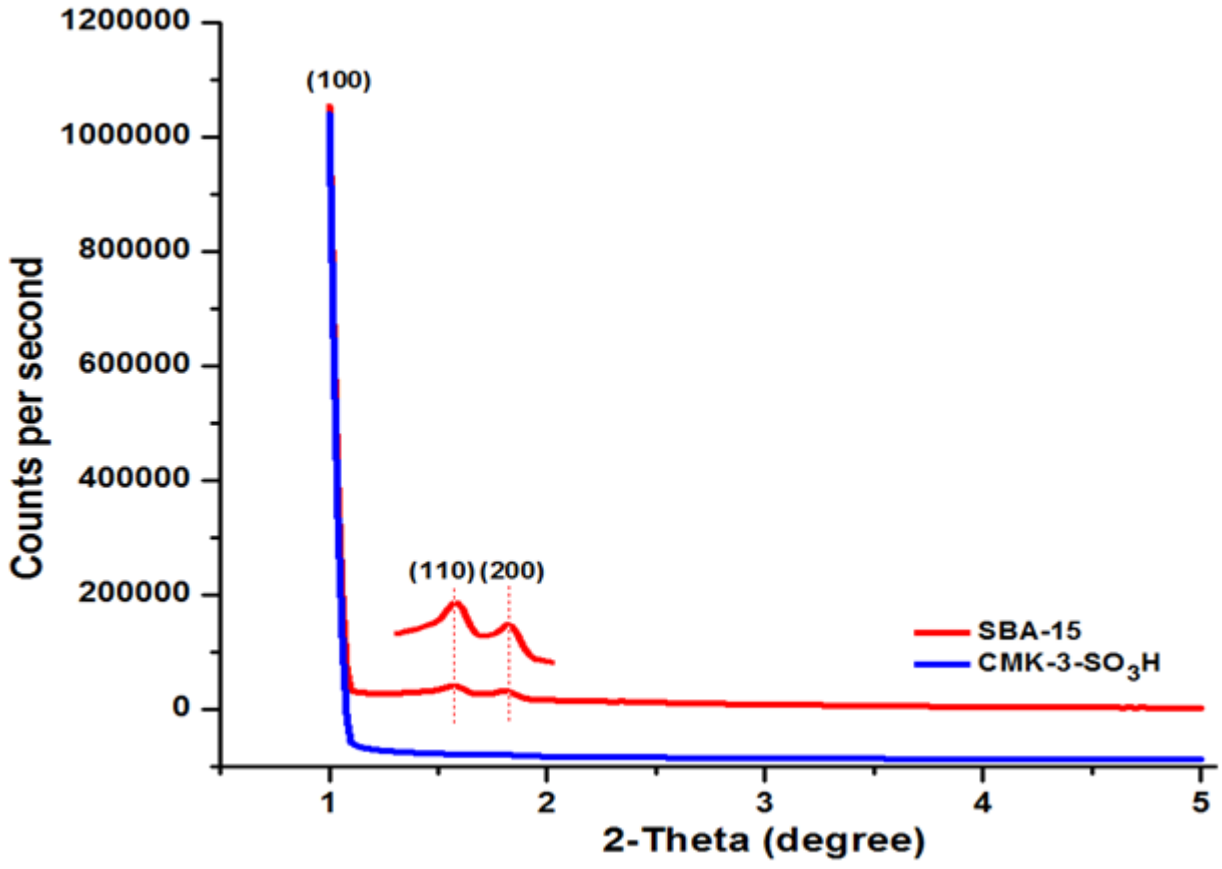

Figure 5.23: Powder XRD patterns of SBA-15 and CMK-3-SO_3H.

The nitrogen adsorption-desorption isotherm at -196 °C for the CMK-3-SO_3H displayed a hysteresis loop in the relative pressure range of 0.45-0.9 associated with capillary condensation and evaporation of nitrogen into the mesopores (Figure 5.24). The structural and physicochemical properties for the synthesized sulfonic acid functionalized mesoporous carbon are summarized in Table 5.5. The resulting specific surface area was 441 m^2/g along with a pore size of 3.3 nm.

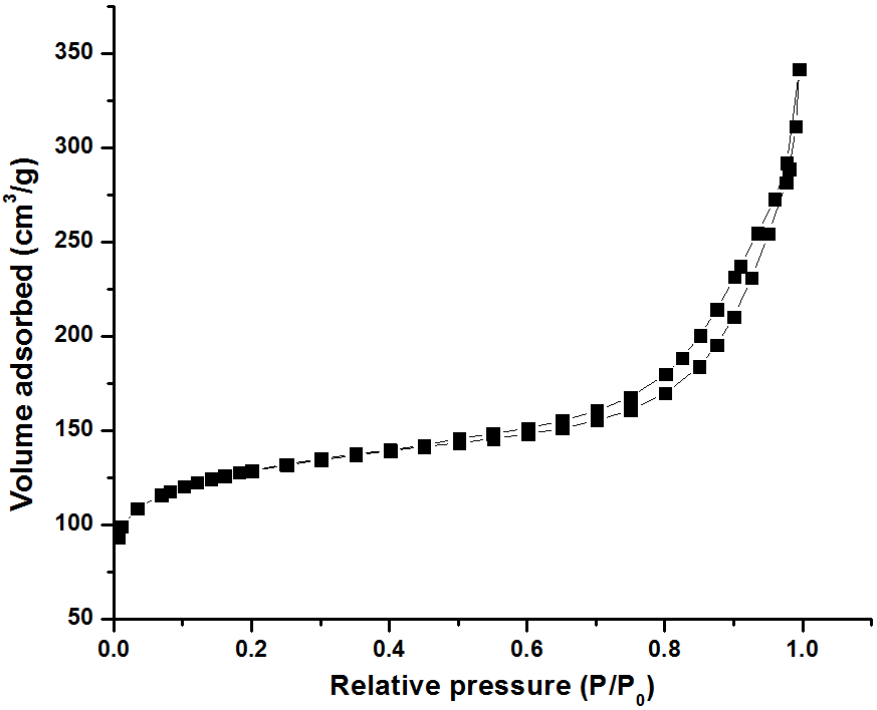

Figure 5.24: N_2 adsorption-desorption isotherm of CMK-3-SO_3H.

Table 5.5: *Physicochemical properties of CMK-3-SO_3H*

Sample	Surface area (m^2/g)	Pore volume (cm^3/g)	Pore size (nm)	Elemental analysis			Acid loading (mmol/g)
				%C	%H	%S	
CMK-3-SO_3H	441	0.43	3.3	59.5	0.6	0.3	0.10

The effective incorporation of SO_3H groups on the polycyclic aromatic carbon framework as a result of carbonization and sulfonation was proved by FTIR, ^{13}C NMR and elemental analysis. The resulting FTIR spectrum shown in Figure 5.25 revealed two bands at 1250 and 1300 cm^{-1} attributed to Ar-OH stretching and two bands at 1466 and 1650 cm^{-1} assigned to the C=C stretching in aromatic rings [118]. The absorbance at 3030 cm^{-1} is attributed to C-H stretching; the band at 1755 cm^{-1} is due to C=O stretching vibration in –COOH groups; the band at 3600 cm^{-1} corresponds to O-H stretching vibration in –COOH and phenolic C–OH groups generated in the process of carbonization and sulfonation [119]. The sulfonation is associated with a band at 940 cm^{-1} attributed to S-O symmetric stretch and a band at 1032 cm^{-1} corresponding to the symmetric stretching of S=O bond as a result of the covalently attached SO_3H groups to the polycyclic aromatic carbon framework.

The solid state ^{13}C MAS NMR spectrum of CMK-3-SO_3H (Figure 5.26) showed two peaks appearing at 130 and 155 ppm attributable to aromatic carbon atoms and to the resonance of carbon in Ar-OH, respectively. This indicates that the polycyclic carbon framework remained stable after sulfonation [95]. The effective introduction of SO_3H groups on the polycyclic aromatic carbon framework would develop a band at 140 ppm due to Ar-SO_3H [120]. However, this peak cannot be clearly resolved due to its overlap with the strong and broad 130 ppm band. The amount of incorporated sulfonic groups was calculated through the sulfur content determined by elemental analysis and the results are presented in Table 5.5.

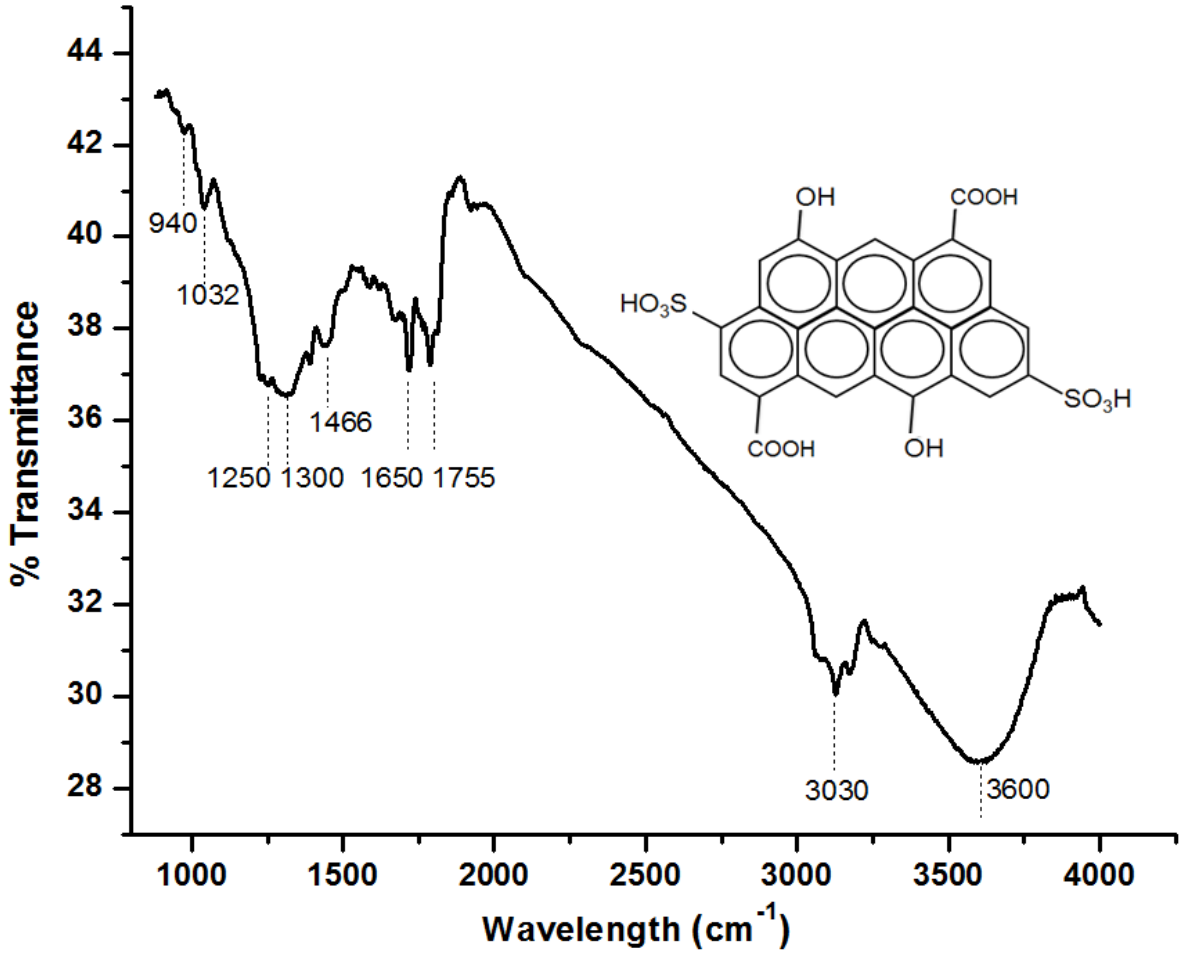

Figure 5.25: FTIR spectrum of CMK-3-SO_3H.

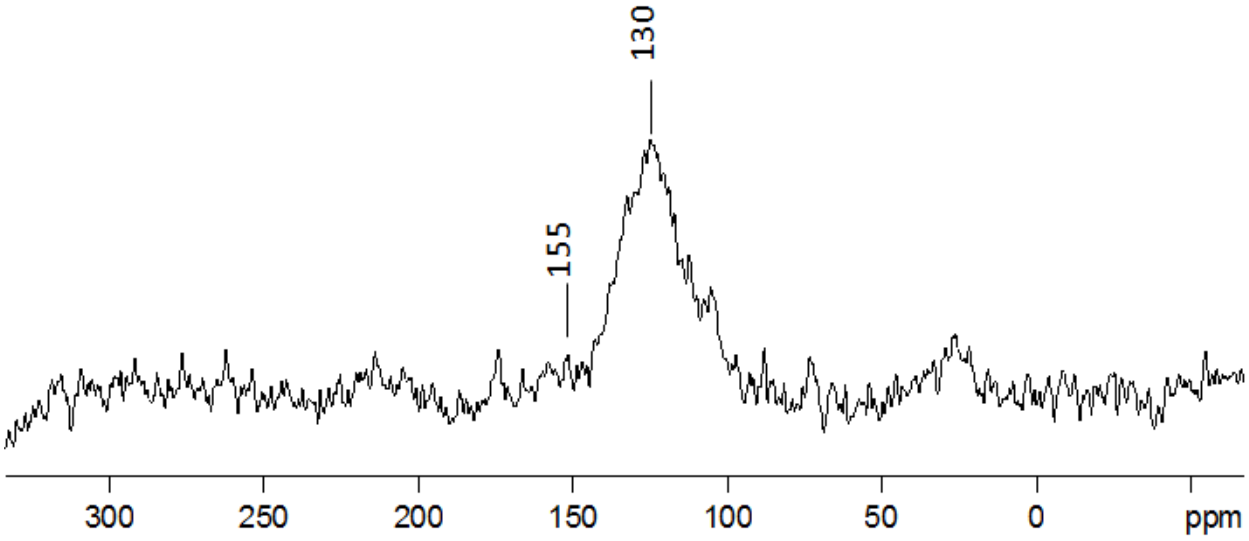

Figure 5.26: ^{13}C NMR spectrum of CMK-3-SO_3H.

5.4.2 Sulfonated Amorphous Carbon AC-SO_3H

Amorphous carbon AC-SO_3H was synthesized via a one-step hydrothermal carbonization process involving the decomposition of glucose in aqueous solution in the presence of vinylsulfonic acid sodium salt at low temperature (190 °C). The method of synthesis has the advantages of being mild and ‘‘green’’ as it involves no organic solvents or surfactants [119]. The nitrogen adsorption-desorption isotherm for AC-SO_3H displayed a type I isotherm, according to the IUPAC classification, which is common for amorphous carbon (Figure 5.27). The structural and physicochemical properties for the synthesized sulfonated amorphous carbon AC-SO_3H are summarized in Table 5.6. The carbon material has low BET surface area (12 m^2/g) and small pore volume (0.01 cm^3/g), which is common for hydrothermally prepared carbons [119].

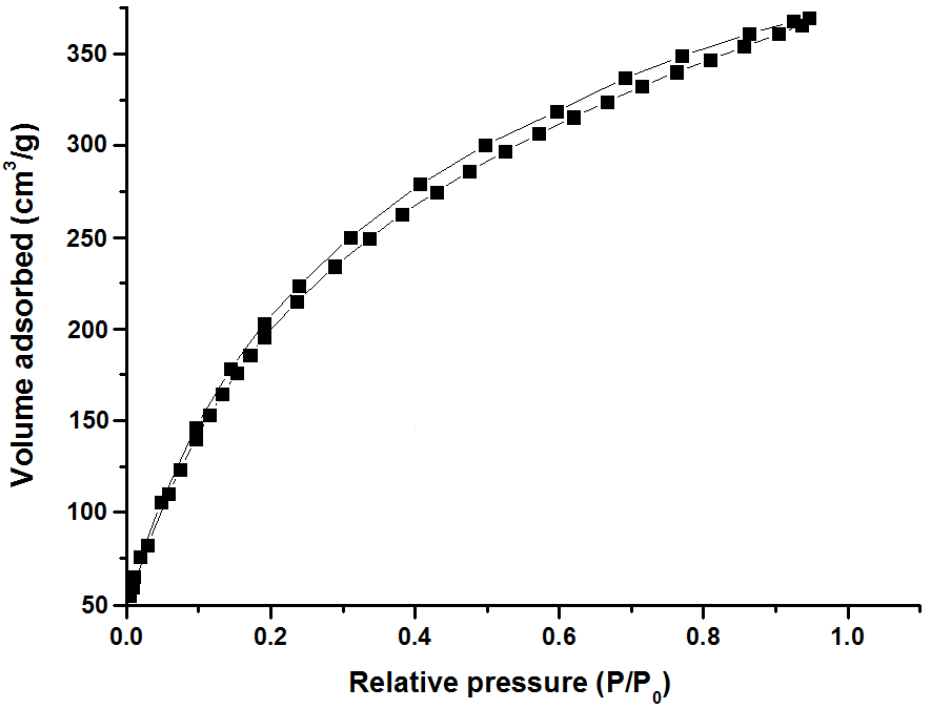

Figure 5.27: N_2 adsorption-desorption isotherm of AC-SO_3H.

The XRD pattern presented in Figure 5.28 exhibited a broad diffraction peak at 10-30° 2θ, attributable to amorphous carbon composed of aromatic carbon sheets oriented in a considerably random fashion [134,137].

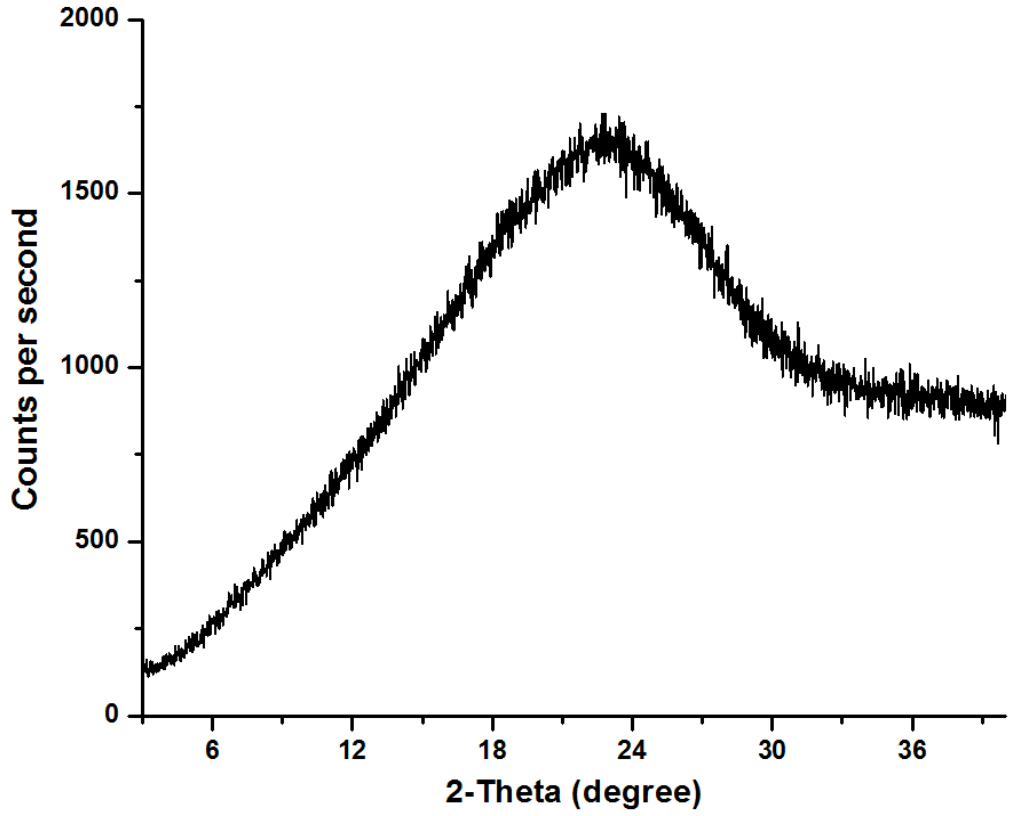

Figure 5.28: Powder XRD pattern of AC-SO_3H.

Table 5.6: *Physicochemical properties of AC-SO_3H*

Sample	Surface area (m^2/g)	Pore volume (cm^3/g)	Pore size (nm)	Elemental analysis			Acid loading (mmol/g)
				%C	%H	%S	
AC-SO_3H	12	0.01	1.9	57.5	4.1	0.57	0.18

The scanning electron microscopy image of the carbonaceous material displayed strawberry-like microporous carbon spheres where many micro-particles were attached to the surface of the big carbon spheres (Figure 5.29).

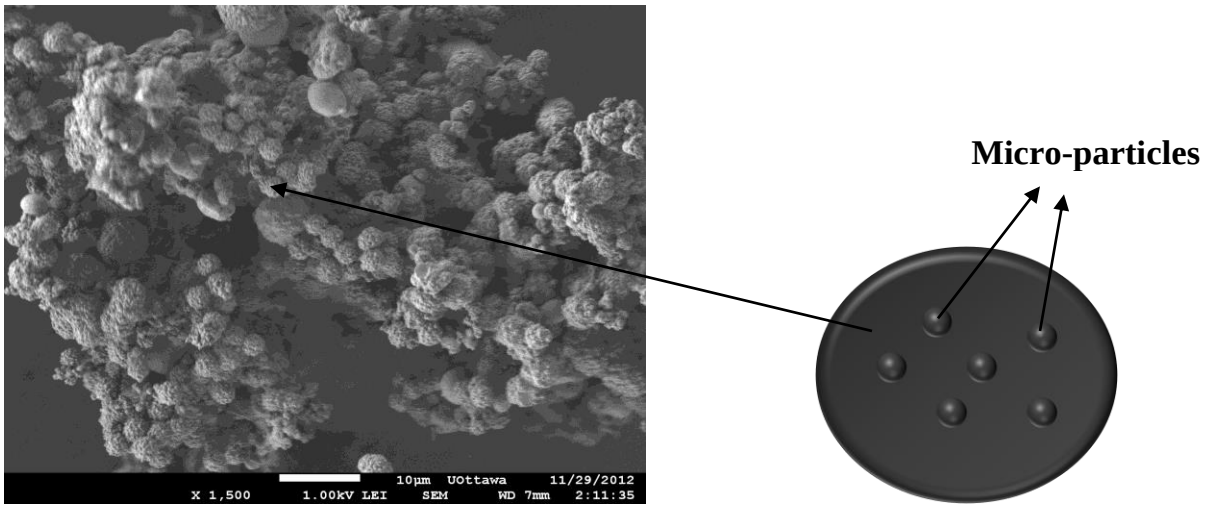

Figure 5.29: SEM image of AC-SO_3H.

The presence of organic groups on the surface was proved by FTIR spectroscopy. The resulting FTIR spectrum in Figure 5.30 revealed two absorption bands at 1466 and 1604 cm^{-1} assigned to the C=C stretching in aromatic carbons and the absorbance at 2916 cm^{-1} is attributed to the Ar-H stretching. The two bands at 1209 and 1300 cm^{-1} corresponds to Ar-OH stretching, the absorbance at 1704 cm^{-1} is assigned to C=O stretching vibration in carboxylic acid group and the band at 3402 cm^{-1} is attributed to O-H stretching vibrations in -COOH and phenolic C–OH groups generated in the process of carbonization and sulfonation [121]. The sulfonation generated a distinct absorption band at 1032 cm^{-1}, corresponding to the symmetric stretching of S=O bond, indicating that $–SO_3H$ groups have been successfully incorporated into amorphous carbon structure.

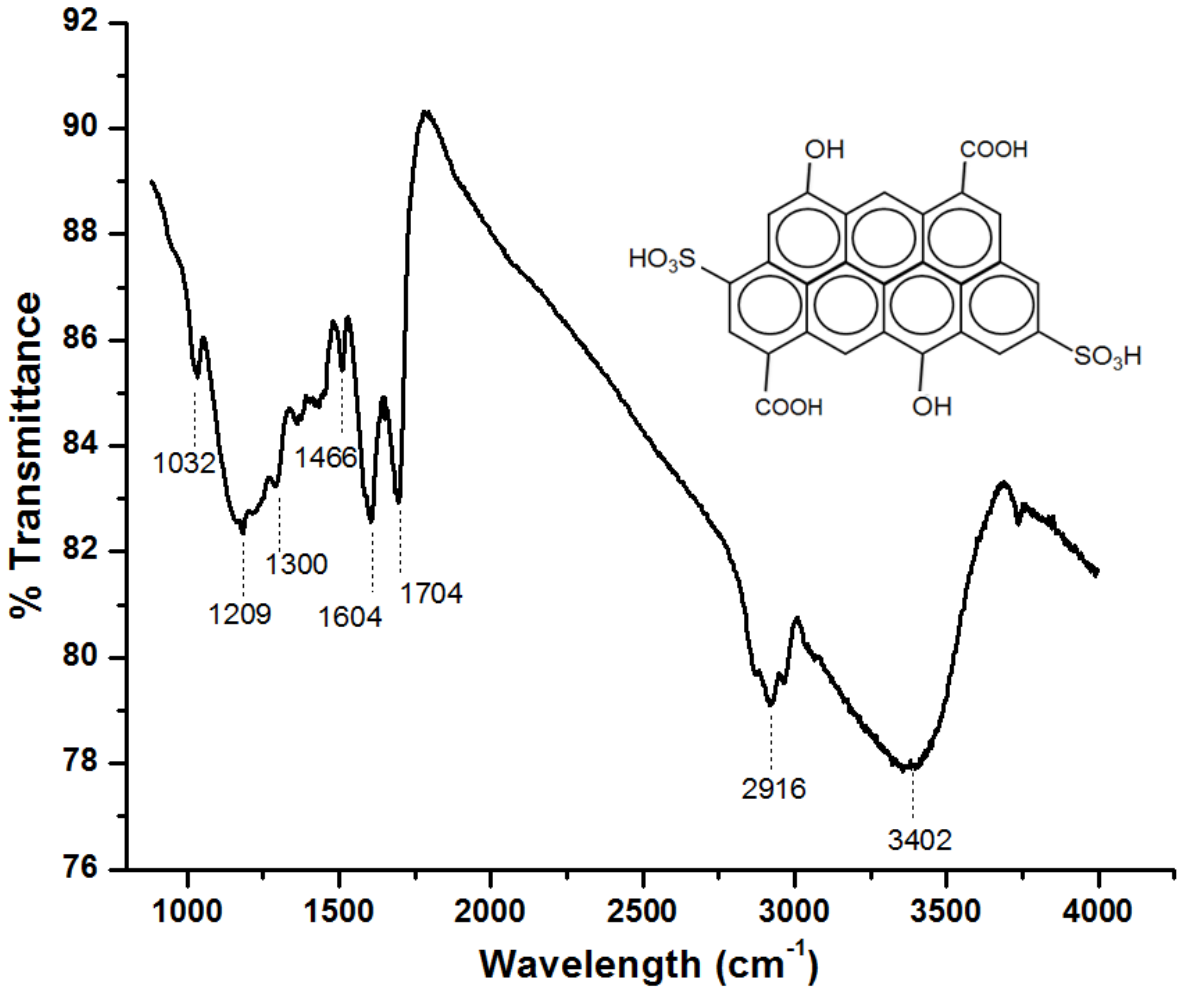

Figure 5.30: FTIR spectrum of AC-SO_3H.

The solid state ^{13}C MAS NMR spectrum of AC-SO_3H (Figure 5.31) shows two peaks: one at 130 ppm assigned to sp^2 hybridized carbon atoms and the other at 150 ppm attributable to the resonance of the carbon in Ar-OH [95]. The resonance appearing at 140 ppm is attributed to AC-SO_3H, thus confirming the effective incorporation of the SO_3H groups on the polycyclic aromatic carbon framework. However, this peak is not clearly resolved due to its overlap with the broad peak at 130 and 150 ppm [133]. In addition, the large peak between 14 and 60 ppm

indicates the presence of aliphatic and ether carbons, the peak at 175 ppm is assigned to carboxylic acid groups while in the 200 ppm region ketones and a small population of aldehydes resonate [119]. Since all S atoms in AC-SO_3H were in -SO_3H form, acid loading was calculated from the elemental content of sulfur. Sulfonated amorphous carbon presented a sulfur loading of 0.57 % corresponding to an acid loading of 0.18 mmol/g.

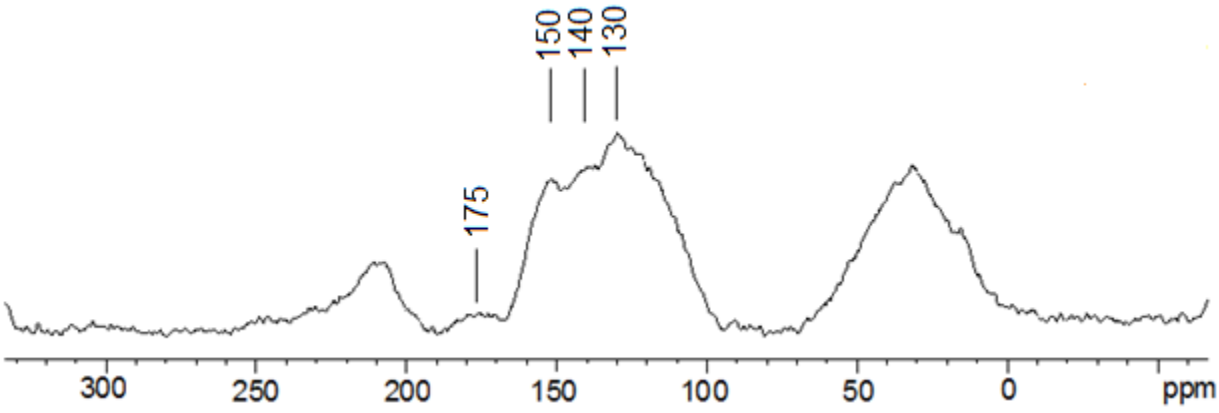

Figure 5.31: ^{13}C NMR spectrum of AC-SO_3H.

Table 5.7: *FTIR absorptions bands for carbon materials*

Absorption bands (cm^{-1})	Assignment
~ 940	S-O symmetric stretch
~1030	S=O symmetric stretch
~1200-1300	C-O stretching
~1466-1650	C=C stretching in aromatic ring
~1700	C=O stretching in COOH
~3030	C-H stretching
~3400-3600	O-H stretching

To sum up, XRD and TEM analysis provided direct evidence that mesoporous silica materials (propyl-SBA-15, phenyl-SBA-15, phenylene and biphenylene PMO) exhibited a well ordered hexagonal structure. Concerning the two carbon-based materials bearing sulfonic acid groups, SEM images showed that CMK-3-SO_3H and AC-SO_3H exhibited different morphologies. Mesoporous carbon CMK-3-SO_3H was an exact inverse replica of SBA-15 and consisted of rod-like particles while AC-SO_3H was an amorphous activated carbon with a strawberry-like morphology. The ^{13}C NMR confirmed the incorporation of the organic group within the mesoporous materials while the existence of sulfonic groups was proved by IR spectroscopy and then quantified by elemental analysis.

5.5 - Optimization of Reaction Conditions

Once the catalysts were synthesized and characterized, the next step in a comparative study is to optimize the reaction conditions of a model reaction to maximize the yield of HMF. Hence, the effect of various reaction parameters on the conversion of sucrose to HMF were examined, namely the selection of the reaction medium, time and temperature using a benchmark catalyst. In this work, the catalytic activity of the sulfonic acid containing catalysts will be expressed in terms of HMF yield. In general, the performance of a catalyst is established based on the ability of a particular catalyst to favour the desirable reactions rather than the undesirable reactions (selectivity), the disappearance of the starting material in the reaction (conversion) and the yield of product obtained. However, due to instrumental limitation, the catalytic activity of the porous catalysts will be represented by the HMF yield.

Firstly, to better understand the effects of reaction time and temperature on the microwave-assisted conversion of sucrose, a commercially available solid acid containing sulfonic acid groups (Amberlyst-15) was selected to optimize the reaction conditions of a model reaction. Amberlyst-15, a sulfonic acid functionalized polymeric resin, is an excellent candidate to be used as a reference catalyst due to its strongly acidic character (Figure 5.32). In addition, Amberlyst-15 presents a similar structure to the acidic nanoporous materials where the sulfonic acid group is attached to a phenyl ring [130].

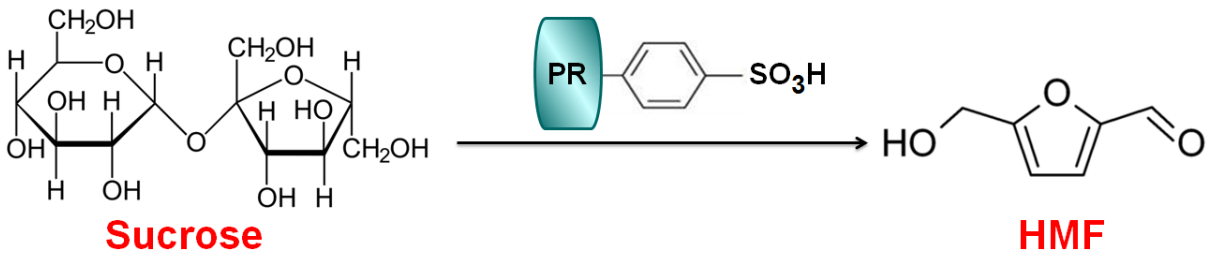

Figure 5.32: Schematic representation of the conversion of sucrose to HMF using Amberlyst-15 as catalyst.

Secondly, one of the fundamental factors influencing the efficiency of sugar conversion into HMF is the solvent in which the carbohydrates are dissolved and the catalytic reaction takes place. In this regard, the choice of solvent in our reaction has a very pronounced effect on the efficiency of the conversion of sucrose. The primary task of the solvent is to induce fluidity and enable contact of reactant and catalyst [19]. Water, as reaction medium, is very convenient from an economical and ecological point of view. However, fructose dehydration is non-selective in water leading to many by-products besides HMF [26]. The low catalytic performance in water is attributed to the following two reasons. On the one hand, the solvent water would inhibit the dehydration process, as HMF is produced by extensive dehydration of fructose by the loss of three molecules of water. On the other hand, it is well known that HMF is readily rehydrated into levulinic acid and formic acid in the presence of water [42]. Among the non-aqueous solvent, reports on the use of DMSO are the most common in literature, and DMSO was found to be one of the best solvents for the conversion of carbohydrates to HMF [123]. The yield of HMF formation is also affected by the tautomeric forms of fructose (furanose and pyranose form, Figure 5.33), among which the fructofuranose exhibits the highest selectivity for the formation of HMF [123]. Therefore, enhancing the ratio of the furanose form of fructose is an option to

increase the yield of HMF in the reaction. However, isotope labelling experiments identified that furanose form is the dominant existing form in the acid-catalyzed conversion of fructose into HMF in DMSO [123]. In addition, DMSO associates with the water released during the reaction, thereby suppressing further degradation of HMF and inhibiting the formation of side-products such as humins [26,28,51]. Therefore, these positive characteristics of DMSO promoted its use as a solvent for our catalytic reaction.

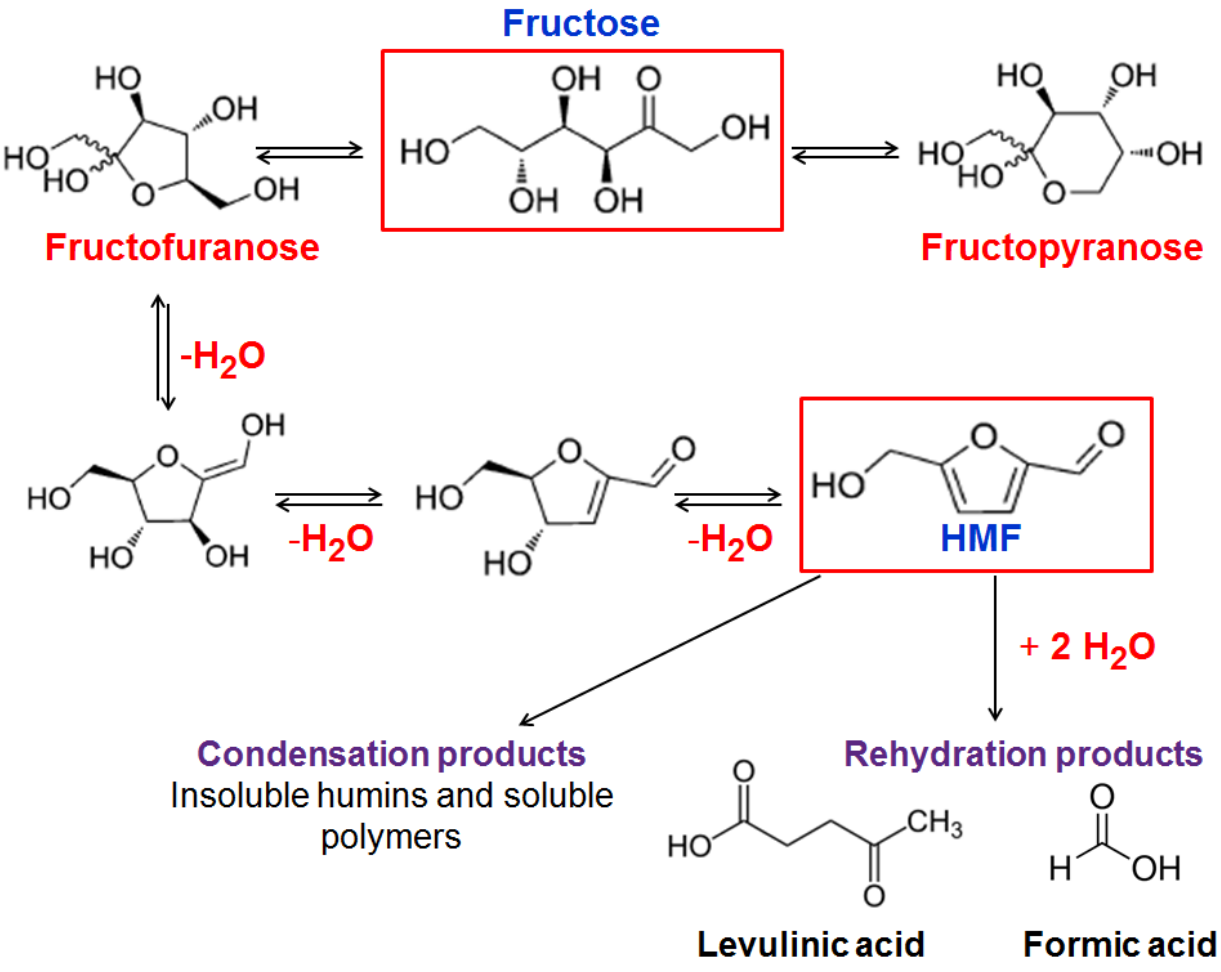

Figure 5.33: Catalytic dehydration of fructose and possible by-products.

Thirdly, microwave synthesis has gained significant attention in recent years and has proven to be very efficient in promoting the conversion of carbohydrates into HMF [28]. Recent literature reports on biomass conversion evidenced that microwave irradiation (MI) not only reduce the reaction time but also dramatically improve the yield of HMF and provides a more homogenous heat distribution [44,47]. Hence, to further optimize the yield of HMF, the reaction was carried out under microwave irradiation.

Consequently, several experiments were conducted in a range of different temperatures and time to adequately select the reaction parameters for our comparative investigation of different acidic nanoporous materials as catalysts in the carbohydrates conversion.

The results of the effect of temperature on the yield of HMF are presented in Figure 5.34. Experiments were carried out at 140, 160, 180, 200 and 220 °C. An increase in temperature from 140 to 180 °C led to a remarkable increase in HMF yield from 37 to 85 %. However, when reaction temperature was further increased to 220 °C, the HMF yield of 32% was lower than that at 180 °C, which is ascribed to the fact that higher temperature gave rise to side reactions that formed undesired by-products [124]. It is important to note that the color of the reaction mixture gradually turned from pale yellow to deep brown suspension with increasing reaction temperature. The color change of the reaction mixture is associated with the decomposition of the product HMF into side-products and this brown insoluble material in the solution is believed to be humins as mentioned in the literature [121,125,132]. Humins results from the oligomerization of either fructose molecules or fructose and HMF [123].

Our results were consistent with previously reported data regarding the effect of reaction temperature on HMF synthesis [127-129]. These results showed that 180 °C was the most appropriate reaction temperature for the conversion of sucrose into HMF in our catalytic system (Figure 5.34).

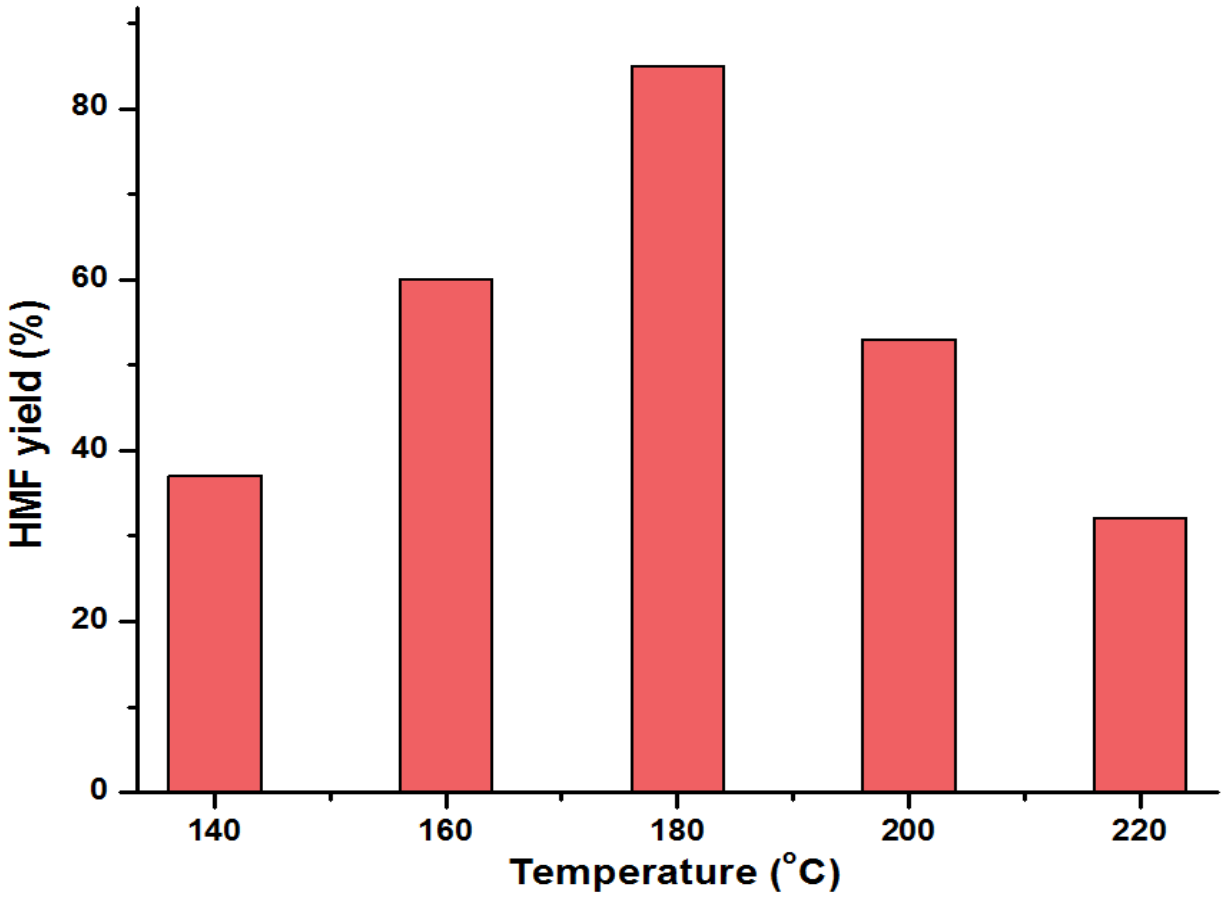

Figure 5.34: Effect of the reaction temperature on HMF yield.

Reaction conditions: 100 mg of sucrose, 50 mg of Amberlyst-15, 2 mL of DMSO, 10 min, MI.

The effect of reaction time on the yield of HMF at 180 °C catalyzed by Amberlyst-15 is shown in Figure 5.35. It was found that the yield of HMF increased gradually during the reaction from 1 to 10 min. When HMF yield reached a maximum value, further increase in reaction time beyond 10 min, resulted in lower yield of HMF, which indicates that starting at ca. 10 min of reaction time, the conversion of HMF to by-products such as humins and levulinic acid started to take place at a higher rate than the generation of HMF [128-129]. Overall, the results obtained are in good agreement with previously reported data [42,47,49,129]. Hence, a reaction temperature of 180 °C and a reaction time of 10 min were chosen as the optimal condition for the catalytic conversion of sucrose into HMF in DMSO.

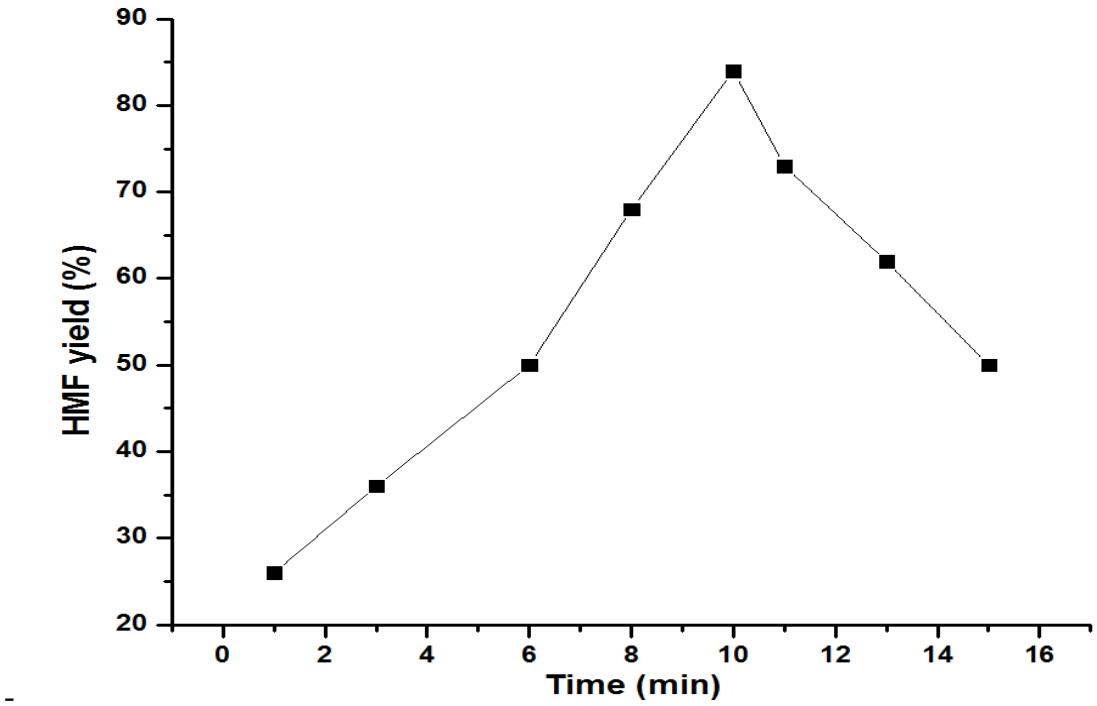

Figure 5.35: Effect of the reaction time on HMF yield.

Reaction conditions: 100 mg of sucrose, 50 mg of Amberlyst-15, 2 mL of DMSO, 180 °C, MI.

As a control experiment, the conversion of sucrose into HMF was carried out at 180 °C in the absence of catalyst and also in the presence of non-functionalized silica material for 10 min under microwave irradiation. The two blank experiments led to low yields of HMF (< 7%). Pure SBA-15 has no acid sites and the results clearly indicate that acidic conditions are crucial for the hydrolysis of sucrose, and the subsequent conversion of fructose to HMF [131]. Altogether, we can conclude than the only source of catalytic activity in the production of HMF from sucrose is the acidic sites, indicating that DMSO had no direct catalytic effect and acted only as a solvent in the conversion of sucrose into HMF.

After determining the reaction conditions, the next step is to test the performance of the sulfonic acid-containing catalysts in HMF production from sucrose applying the following optimized conditions for each acidic nanoporous catalysts: 100 mg of sucrose, 50 mg of catalyst, 2 mL of DMSO, 180 °C for 10 min under microwave irradiation.

5.5 - Conversion of Sucrose over Sulfonated Carbons

AC-SO_3H, which was prepared by a facile and eco-friendly approach from glucose and vinylsulfonic acid sodium salt, was tested in the conversion of sucrose into HMF and the results showed that this catalyst exhibited good catalytic performance. The resultant amorphous carbonaceous material, with an acid density of ~0.2 mmol/g, achieved a HMF yield of 53% in DMSO in 10 min at 180 °C under microwave irradiation. Under identical conditions, the performance of CMK-3-SO_3H, a porous carbon catalyst, is shown in Table 5.8. In comparison with AC-SO_3H, a lower HMF yield of 43 % was achieved with CMK-3-SO_3H as catalyst, and this can be due to the difference in surface properties of both materials. The higher HMF yield of

53 % achieved in the presence of AC-SO_3H is likely to be attributed to the higher sulfonic acid strength (0.2 vs. 0.1 mmol/g) compared to CMK-3-SO_3H. However, it is noteworthy to mention that other surface functional groups on carbon materials certainly play an important role deduced from the fact that AC-SO_3H exhibits higher catalytic performance than CMK-3-SO_3H. Hence, the carbonization temperature also affects the catalytic activity of the sulfonated carbon catalysts [134]. Sulfonated carbonaceous materials usually contain carboxylic and phenolic groups besides –SO_3H, which is in consistence with the results obtained by FTIR and ^{13}C NMR. Obviously, sulfonic acid groups are the active sites in both catalysts. The amorphous carbon AC-SO_3H presents a lower content of polycyclic aromatic carbon, hence, a higher content of hydrophilic functional groups, such as OH and COOH, which was proved by both IR and ^{13}C MAS NMR, as a result of the partial carbonization. From the CMK-3-SO_3H ^{13}C NMR spectrum presented in page 102, we can notice that the feature corresponding to hydrophilic functional groups, namely the carbon attached to a phenolic OH, is negligible in comparison with the peak in AC-SO_3H, as a result of a higher carbonization temperature. As mentioned in the literature [121,132], –COOH and phenolic –OH groups were found to have a strong affinity to glucose through the formation of hydrogen bonds between them and –OH groups of glucose, which further promoted the conversion of glucose into HMF catalyzed by –SO_3H groups. Moreover, AC-SO_3H is expected to accommodate a large amount of hydrophilic molecules such as sucrose, fructose and glucose which allow to better access the acid sites of the catalyst [134]. In the case of mesoporous carbon CMK-3-SO_3H, the high carbonization temperature converted the phenolic OH groups into hydrophobic polycyclic aromatic carbon, which explains the lower yield obtained compared to amorphous carbon.

To sum up, it has been shown that the catalytic activity of the carbon materials was not related to textural properties such as surface area or pore structure because the amorphous carbon AC-SO_3H exhibited a much lower surface area compared to the mesoporous carbon CMK-3-SO_3H (12 vs. 441 m^2/g). The remarkable catalytic activity of AC-SO_3H depends on the acid content and surface composition where the sample carbonized at lower temperature may contain larger amounts of hydrophilic functional groups resulting in higher catalytic performance.

Table 5.8: *Catalytic activity of the sulfonated carbon materials*

Carbon materials	**Surface area (m^2/g)**	**Acid content (mmol/g)**	**HMF Yield (%)**
AC-SO_3H	12	0.18	53
CMK-3-SO_3H	441	0.10	43

5.6 - Conversion of Sucrose over Sulfonated Mesoporous Silica

Within the modified periodic mesoporous silica family, propyl-SBA-15 has been shown to be exceptional solid catalyst for the conversion of sucrose into HMF. The two sulfonic-acid modified SBA-15 present comparable textural properties in terms of pore size and surface area. The higher activity of propyl-SBA-15 (HMF yield of 74%) compared to phenyl-SBA-15 (HMF yield of 58%) is likely to be attributed to the higher content of sulfonic acid active sites occurring in this material. The results presented in Table 5.9 show that mesoporous SBA-15 silica

functionalized with sulfonic acid groups were efficient catalysts for the production of HMF from sucrose.

Table 5.9: *Catalytic activity of the sulfonated periodic mesoporous materials*

Periodic mesoporous materials	**Surface area (m^2/g)**	**Pore size (nm)**	**Acid content (mmol/g)**	**HMF yield (%)**
Propyl-SBA-15	653	7.2	1.17	74
Phenyl-SBA-15	774	8.6	0.30	58
Biph-PMO-S	237	2.9	0.21	52
Ph-PMO-S	1040	7.5	0.46	82

Another family of mesoporous organic-inorganic hybrid materials, known as PMOs, were synthesized by utilizing surfactants as structure-directing agent as in the synthesis of PMS, but organic bridged alkoxysilane precursors instead of inorganic precursors. Data from Table 5.9 evidenced the high activity of the sulfonic-acid modified PMOs in the conversion of sucrose. As expected, the results also indicated that a higher concentration of acid sites can translate into higher catalytic performance for HMF production (Table 5.9). The two organosilica materials (phenylene and biphenylene PMOs) present main differences related to their surface area (1040 vs. 271 m^2/g), pore size (7.5 vs. 2.9 nm) as well as in acid content (0.46 vs. 0.21 mmol/g). Thus, the observed results between sulfonated biphenylene and phenylene PMOs could be rationalized by the fact that the larger surface areas in the mesoporous catalysts can promote the HMF yield and sufficient acidic sites easily accessible for the reactants were responsible for the

stabilization of the cationic intermediate formed during the reaction [131,135]. It is worth noting that non-sulfonated periodic mesoporous materials were not able to catalyze the reaction.

5.7 - HMF Production over Acidic Nanoporous Materials

A vast number of pioneering researchers have reported the synthesis of HMF from sucrose using various metallic chlorides and mineral acids with relatively high HMF yield. However, homogenous catalysts present several disadvantages regarding their separation and recyclability. This research was focused on using heterogeneous solid acid catalysts and compared them in the conversion of sucrose into HMF in an efficient media. The three classes of nanoporous materials presented different catalytic performance depending on the acid content, pore structure and surface composition. In a comparative study, the selection of a model reaction is primordial. Hence, the first step to achieve our goal after synthesizing and characterizing the nanoporous materials was to optimize the reaction parameters using Amberlyst-15 as a reference catalyst. The three main porous materials were tested under similar conditions; sucrose was dissolved in DMSO and its conversion into HMF was performed under microwave irradiation at 180 °C for 10 min.

Among all acidic nanoporous materials, the highest HMF yield obtained were in the presence of sulfonated phenylene bridged PMO with a HMF yield of 82% (Figure 5.36). Definitely, its large pore size and high surface area prompted its performance revolving around several aspects such as (i) enhancing the organic loading, thus, the content of sulfonic acid groups achieved through the functionalization of the aromatic ring increases, (ii) enhanced accessibility of the acid sites.

This acidity enhancement afforded solid acid catalysts with several favorable attributes: (i) greater activity in the conversion of sucrose into HMF as compared to literature data obtained with homogeneous and metallic chlorides catalysts, (ii) good thermal stability, (iii) and good chemical robustness with no acid leaching where the sulfonated catalyst could be recycled without any significant in HMF yield over four reaction cycles (the catalyst reusability is presented in section 5.8).

The HMF yield obtained using AC-SO_3H as catalyst was similar to the yield obtained with sulfonated bridged biphenylene PMO. Since these catalysts had the same acid loading (0.2 mmol/g) but different pore size (AC-SO_3H ~2 nm, biph-PMO-S ~3 nm), the similar HMF yield indicated that the activity was not affected by diffusion limitation and the pore diameter in biphenylene PMO was eventually large enough to allow the carbohydrates and the HMF to diffuse rapidly through the framework [13]. Moreover, the remarkable catalytic activity of AC-SO_3H was also comparable to the mesoporous silica materials such as phenyl-SBA-15 and biph-PMO-S due to its surface composition with hydrophilic functional groups. Thus, AC-SO_3H may accommodate a larger amount of hydrophilic molecules which allow a better access to the sulfonic acid groups leading to a good HMF yield of 53%.

The lower catalytic of the mesoporous carbon CMK-3-SO_3H in comparison with phenyl modified mesoporous silica (PMO and SBA-15) and the amorphous carbon was due its synthesis procedure. The high carbonization temperature of CMK-3-SO_3H results in a very low density of hydrophilic functional groups, namely phenolic OH, and leads to a low acid content.

Overall, the enhancement of the catalyst activity is observed with an increase of –SO_3H loading, thus the catalytic activity is highly dependent on the acid loading of the catalysts. Regardless of

the acid loading, all functionalized materials presented good catalytic activity and reusability attributable to the favorable environment surrounding the sulfonic acid groups. The hydrophobic environment created by the presence of phenyl rings bearing sulfonic acid groups partly prevent the solvation of sulfonic acid sites by water [138]. Moreover, the pore diameter was large enough to avoid the steric constraints imposed by pore size allowing the diffusion of carbohydrates into the pores.

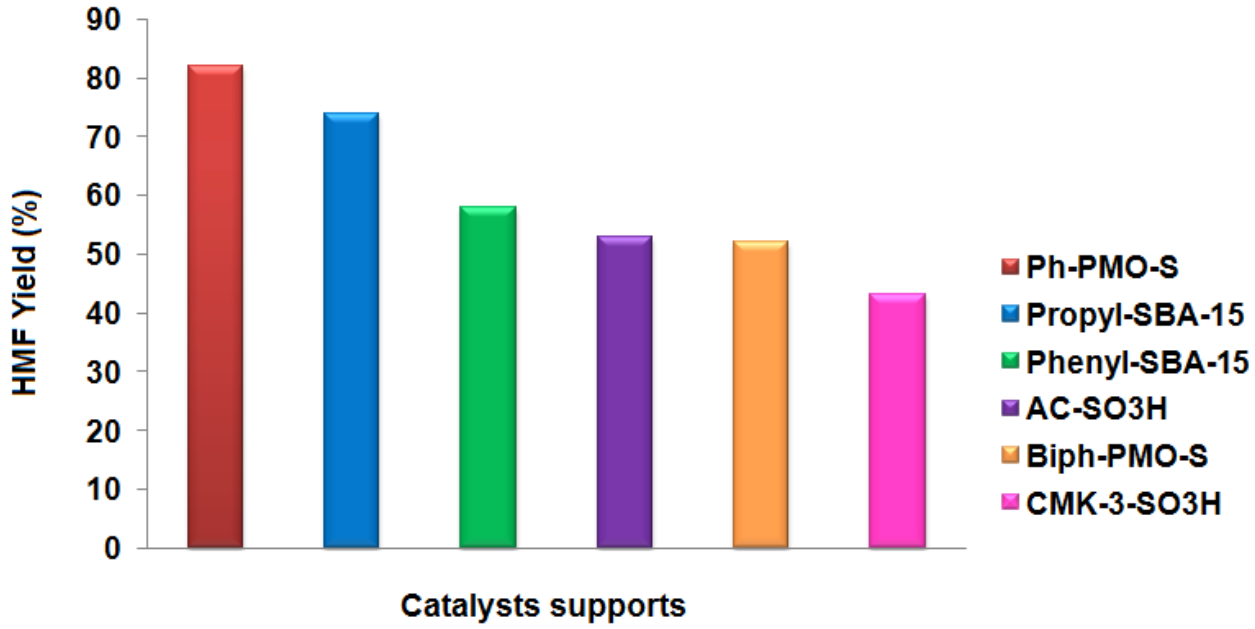

Figure 5.36: HMF synthesis from sucrose with different acidic nanoporous catalysts.

5.8 - Recyclability of Sulfonated Porous catalysts

Catalyst recycling is an important goal in terms of green and sustainable chemistry. Thus, the reusability of the acidic nanoporous catalysts was tested to study their stability and activity. After the first run, the catalyst was filtered, washed with water and dried in air. Subsequently, the recovered catalyst was used in the next run by adding fresh sucrose and DMSO under the same reaction conditions. It is worth mentioning that the hydrothermal stability of mesoporous catalysts depends on both the solvent and the temperature, and the loss of activity may be caused by cleavage of the active sites from the support or the deposition of insoluble reaction products in the pores [136]. The reusability of the catalysts is illustrated in Figure 5.37, in which the catalytic activity in terms of HMF yield is shown for the same catalyst. It was found that the catalytic system could be recycled successively for four times under the same reaction conditions. Slight decreases in activity in the fourth run are attributable to small losses of catalyst after separation and wash cycle and, within experimental error, we conclude that no significant activity is lost through re-use.

The previously reported solid acids suffered from leaching of the acid sites by water [126,136]. For example, Dumesic et al. reported the synthesis of HMF continuously from fructose using silica (SBA-15) and PMO based acid catalysts in a packed-bed tubular reactor [136]. The HMF selectivity of the catalysts ranged from 60 to 75%. Although good yield of HMF were obtained, all catalysts could not be recycled due to the hydrolytic cleavage of the acid sites. However, the innovation in our research is the use of heterogeneous solid acid catalysts where the catalyst can be reused for several reaction cycles, which makes their application highly economical. The choice of the solvent is crucial and governs the yield of HMF. In our catalytic system, the water

generated by the dehydration of fructose is suppressed by DMSO, thus further avoiding the critical decomposition of the acid sites. Altogether, the results showed that acidic nanoporous materials are promising catalysts for the conversion of sucrose into HMF due to their distinctive features such as large pore size to minimize diffusional problems; high concentration of acid sites; high stability against leaching and reutilization capability as well as the possibility to tune the hydrophobicity of the surface to promote the preferential adsorption of substrates.

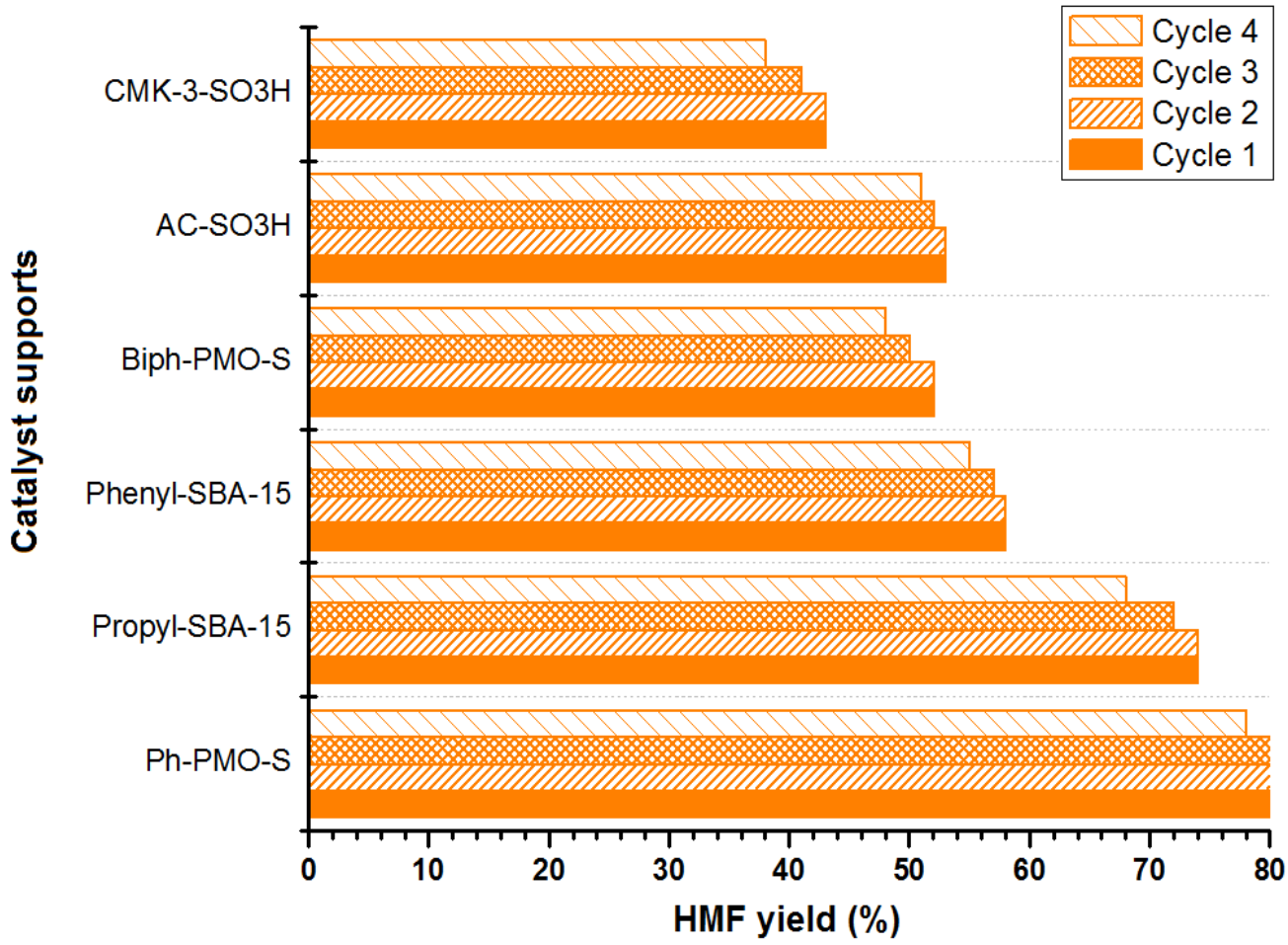

Figure 5.37: Catalysts recyclability for the conversion of sucrose with acidic nanoporous catalysts in DMSO in four successive reactions.

Conclusion and Future Work

HMF is one of the most important intermediates derived from biomass and was identified as a versatile chemical platform to generate a number of useful compounds for the production of various chemicals and liquid fuels. Microwave-assisted direct conversion of sucrose into HMF in DMSO catalyzed by acidic nanoporous materials have been investigated in search of an efficient and environmentally-friendly process. The synthesis of HMF directly from sucrose affords remarkably unique advantages for large-scale production of HMF such as avoidance of isolation and purification of intermediate compounds, which saves time, energy and solvent. To date, few investigations on HMF production from sucrose have been reported using metallic chlorides and mineral acids as catalysts. Although encouraging results were achieved, these types of catalysts present serious drawbacks including hazards in handling, corrosiveness, production of toxic waste and difficulties in separation. Therefore, solid acid catalysts have distinct advantages in recycling, separation, and environmental friendliness which make their application highly economical. Fundamentally, HMF is obtained from sucrose by the hydrolytic cleavage of the glycosidic bond followed by the loss of three molecules of water from a hexose in an acid-catalyzed reaction. Despite the apparent simplicity of the procedure, the occurrence of a number of side-reactions including the rehydration of HMF to levulinic acid and formic acid, and cross-polymerisation to soluble polymers and insoluble humins makes the HMF production very complicated. The first step in our comparative study was to synthesize various sulfonated heterogeneous catalysts such as sulfonated bridged periodic mesoporous organosilicas, carbon materials and ordered mesoporous silicas such as SBA-15. Propyl-SBA-15 and phenyl-SBA-15

were synthesized through a one-pot synthesis involving the co-condensation of a silica source, TEOS, and organosiloxane precursors MPTMS and PTES respectively, in the presence of Pluronic P123 as template. Phenylene and biphenylene-bridged PMOs with crystal-like pore walls was accomplished using BTEB and BTEBP as structural components, and were further reacted with chlorosulfonic acid to introduce Brønsted acid site (-SO_3H). Carbon-based solid acids consisting of polycyclic aromatic carbon and functional groups such as sulfonic acid groups were obtained by carbonization of precursors followed by sulfonation. The textural and structural characterization as well as the physiochemical properties of the synthesized sulfonic acid-modified catalysts were carried out through XRD, SEM, TEM, N_2 adsorption-desorption isotherms, TGA, FTIR, ^{13}C and ^{29}Si NMR. Once the solid acid catalysts were synthesized and characterized, the effects of various reaction parameters such as reaction time and temperature on HMF yield using Amberlyst-15 as a benchmark catalyst were investigated, and it was demonstrated that that a reaction temperature of 180 °C and a reaction time of 10 min are the optimal reaction conditions for the catalytic conversion of sucrose into HMF in DMSO. AC-SO_3H, carbonized at lower temperature, was found to be more active in the conversion of sucrose into HMF in comparison with CMK-3-SO_3H. The amorphous carbon exhibited better catalytic performance than the mesoporous carbon due to the higher acid content. In addition, the sample at lower carbonization contains high densities of hydrophilic functional groups such as OH and COOH, resulting in higher HMF yield despite the low specific surface area. Mesoporous silica and organosilica materials presented large pore diameters as well as large surface areas. The pore diameters were large enough to allow the quick access of carbohydrates which is beneficial for the interaction between the sucrose and the acidic sites of the catalyst materials. The large surface area provides more active sites for the conversion of sucrose which enhance

the catalytic activity. Phenylene bridged PMO resulted in the highest HMF yield and this material is characterized by a large specific surface area, an alternation of hydrophilic-hydrophobic parts and a homogeneous distribution of acid functional groups, possibility associated with the molecular scale periodicity within the pore walls.

Besides the specific surface area, pore size, pore volume, active site density and good affinity for the reactant substrates, solid acid catalysts should be stable in the presence of water. The latter is generated from the dehydration of fructose. The solvent and temperature play an important role in the effectiveness of the conversion of sugar and the hydrothermal stability of catalysts [128,136]. It was found that acidic nanoporous materials can be reused without losing their catalytic activity, being favorable to the potential application for large-scale synthesis and from the industrial point of view. This could be attributed to the presence of phenyl rings in the acidic nanoporous materials that creates a hydrophobic environment capable of partly preventing the leaching of sulfonic sites by solvation with water.

Among the chemicals that may be derived from HMF, DFF is obtained by the selective oxidation of the hydroxyl group of HMF and has attracted much attention due to its versatility in use as an intermediate for pharmaceuticals, funcigides, macrocylic ligands as well as a cross-linking agent for poly(vinylalcohol) [9,10]. So far, the reported routes to synthesize DFF are mostly based on using pure HMF as starting material. Despite the fact that fairly high yield were obtained, the energy-intensive production and the unstable character of HMF during the separation/purification step limit the application of pure HMF as a potential raw material for the large-scale production of DFF [140-141]. As a result, DFF is commercially highly priced and available only in milligram quantities. To overcome the difficulties in HMF separation, attempts

were made to directly synthesize DFF from carbohydrates by using the same solvent for both conversion of carbohydrates into HMF and the subsequent oxidation of HMF (Figure 5.38). This one-pot two-step reaction is characterized by the abundance and low cost of the starting materials and by the elimination of the separation and purification of HMF and offers a great potential for applications in the future production of DFF on a large-scale after further advancements and optimizations. The next piece of work that needs to be completed would be the synthesis of silica and carbon supported metal/metal oxide catalysts. After obtaining HMF from sucrose in the presence of acidic nanoporous materials, the solid acid will be filtered and a subsequent oxidation of HMF to DFF will be carried out by adding the metal supported catalyst to the reaction mixture. The second air-oxidation step could be performed at 150 °C and 1 atm, as reported in the literature [142]. The latter could then be effortlessly isolated from the reaction mixture due to its insolubility in water and good solubility in many organic solvents and purified via extraction-filtration through silica gel-crystallization in a single Soxhlet setup [142]. Finally, the reusability of the catalysts could be evaluated over 4 cycles.

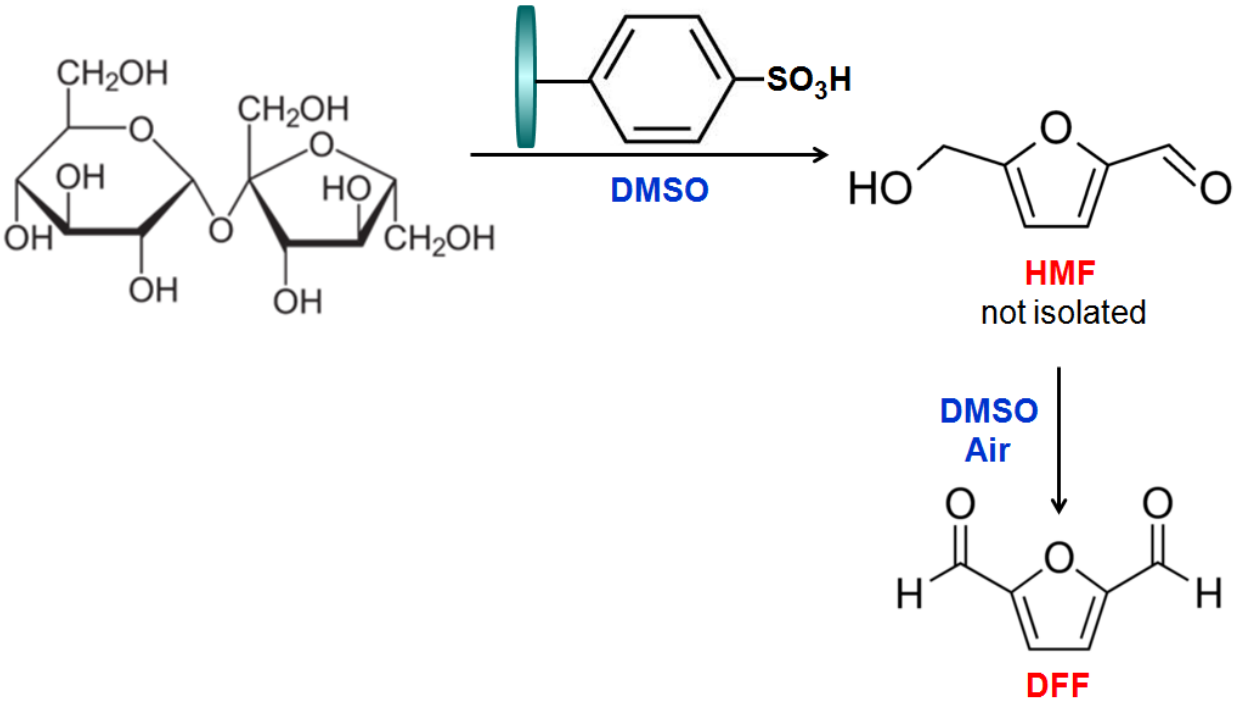

Figure 5.38: One-pot synthesis of DFF from sucrose via conversion to HMF over acidic nanoporous catalysts, followed by in situ catalytic air-oxidation.

References

[1] G.W. Huber, S. Iborra, A. Corma, Synthesis of transportation fuels from biomass: chemistry, catalysts, and engineering, *Chem. Rev*. 106, 2006, 4044.

[2] S. Shafiee, E. Topal, When will fossil fuel reserves be diminished? *Energy Policy* 37, 2009, 181.

[3] P. McKendry, Energy production from biomass: overview of biomass, *Bioresour. Technol*. 83, 2002, 37.

[4] K. Tekin, S. Karagöz, S. Bektaş, A review of hydrothermal biomass processing, *Renew. Sust. Energ. Rev.* 40, 2014, 673.

[5] R. Rinaldi, F. Schüth, Design of solid catalysts for the conversion of biomass, *Energy Environ. Sci*. 2, 2009, 610.

[6] X. Tong, Y. Ma, T. Li, Biomass into chemicals: conversion of sugars to furan derivatives by catalytic processes, *Appl. Catal. A- Gen.* 385, 2010, 1.

[7] A.A. Rosatella, S.P. Simeonov, R.F.M. Frade, C.A.M. Afonso, 5-Hydroxymethylfurfural (HMF) as a building block platform: Biological properties, synthesis and synthetic applications, *Green Chem.* 13, 2011, 754.

[8] M. Antal, W. Mok, G. Richards, Mechanism of formation of 5- (hydroxymethyl)furaldehyde from D-fructose and sucrose, *Carbohydr. Res.* 199, 1990, 91.

[9] K.T. Hopkins, W.D. Wilson, B.C. Bender, D.R. McCurdy, J.E. Hall, R.R. Tidwell, A. Kumar, M. Bajic, D.W. Boykin, Extended aromatic furan amidino derivatives as anti-pneumocystis carinii agents, *J. Med. Chem.* 41, 1998, 3872.

[10] S.M. Nelson, F.S. Esho, M.G.B. Drew, Complexation of alkali and alkaline earth-metal cations by a conjugated tetraimine macrocyclic ligand: synthesis, sodium-23 nuclear magnetic resonance spectra, and the X-Ray structure of a twelve-co-ordinate barium (II) sandwich complex, *J. Chem. Soc. Dalton Trans.* 1983, 1857.

[11] D.M. Alonso, J.Q. Bond, J.A. Dumesic, Catalytic conversion of biomass to biofuels, *Green Chem.* 12, 2010, 1493.

[12] B. Girisuta, L.P.B.M. Janssen, H.J. Heeres, A kinetic study on the decomposition of 5-hydroxymethylfurfural into levulinc acid, *Green Chem.* 8, 2006, 701.

[13] E. Gürbüz, J.Q. Bond, J.A. Dumesic, K. Román-Leshkov, The role of catalysis for the sustainable production of bio-fuels and bio-chemicals, Edited by : K. Triantafyllidis, A. Lappas. M. Stocker, Chapter 8, page 261, Elsevier, USA.

[14] P.E. Savage, R.B. Levine, C.M. Huelsman, Hydrothermal processing of biomass: thermochemical conversion of biomass to liquid, *Royal Society of Chemistry*, 2010, USA.

[15] C. Crestini, M. Crucianelli, M. Orlandi, R. Saladino, Oxidative strategies in lignin chemistry: a new environmental friendly approach for the functionalisation of lignin and lignocellulosic fibers, *Catal. Today* 156, 2010, 8.

[16] A.S. Amarasekara, L.D. Williams, C.C. Ebede, Mechanism of the dehydration of D-fructose to 5-hydroxymethylfurfural in dimethyl sulfoxide at 150 ºC: An NMR study, *Carbohydr. Res.* 343, 2008, 3021.

[17] C. Li, Z. Zhao, Efficient acid-catalyzed hydrolysis of cellulose in ionic liquid, *Adv. Synth. Catal.* 349, 2007, 1847.

[18] M.L. Mednick, The acid-base-catalyzed conversion of aldohexose into 5-(hydroxymethyl)-2-furfural, *J. Org. Chem.* 27, 1962, 398.

[19] B.F.M. Kuster, 5-Hydroxymethylfurfural (HMF): a review focussing on its manufacture, *Starch-Starke* 42, 1990, 314.

[20] S.H. Bhosale, M.B. Rao, V.V. Deshpande, Molecular and industrial aspects of glucose isomerase, *Microbiol. Rev.* 60, 1996, 280.

[21] J.B. Van Beilen, Transgenic plant factories for the production of biopolymers and platform chemicals, *Biofuels Bioprod. Bioref.* 2, 2008, 215.

[22] B.A. Averill, P. Eldredge, Chemistry: Principles, Patterns, and Applications, 1st edition, Pearson Benjamin Cummings, 2007, San Fransisco.

[23] M. Lancaster, Green Chemistry: An Introductory Text, *Royal Society of Chemistry*, 2002, Cambridge.

[24] J.H. Clark, Catalysis for green chemistry, *Pure Appl. Chem.* 73, 2001, 103.

[25] M. Bicker, J. Hirth, H. Vogel, Dehydration of fructose to 5-hydroxymethylfurfural in sub- and supercritical acetone, *Green Chem*. 5, 2003, 280.

[26] Y. Román-Leshkov, J.N. Chheda, J.A. Dumesic, Phase modifiers promote efficient production of hydroxymethylfurfural from fructose, *Science* 312, 2006, 1933.

[27] F.S. Asghari, H. Yoshida, Acid-catalyzed production of 5-hydroxymethyl furfural from D-fructose in subcritical water, *Ind. Eng. Chem. Res*. 45, 2006, 2163.

[28] T.S. Hansen, J.M. Woodley, A. Riisager, Efficient microwave assisted synthesis of 5-hydroxymethylfurfural from concentrated aqueous fructose, *Carbohydr. Res.* 344, 2009, 2568.

[29] J.N. Chheda, Y. Román-Leshkov, J.A. Dumesic, Production of 5-hydroxymethylfurfural and furfural by dehydration of biomass-derived mono- and poly-saccharides, *Green Chem*. 9, 2007, 342.

[30] C. Moreau, R. Durand, S. Razigade, J. Duhamet, P. Faugeras, P. Rivalier, P. Ros, G. Avignon, Dehydration of fructose to 5-hydroxymethylfurfural over H-mordenites, *Appl. Catal. A- Gen.* 45, 1996, 211.

[31] C. Moreau, R. Durand, C. Pourcheron, and S. Razigade, Preparation of 5-hydroxymethylfurfural from fructose and precursors over H-form zeolites, *Indus. Crops Prod.* 3, 1994, 85.

[32] X. Qi, M. Watanabe, T.M. Aida, R.L. Smith, Selective conversion of D-fructose to 5-hydroxymethylfurfural by ion-exchange resin in acetone/dimethyl sulfoxide solvent mixtures, *Ind. Eng. Chem. Res.* 47, 2008, 9234.

[33] C. Lansalot-Matras, C. Moreau, Dehydration of fructose into 5-hydroxymethylfurfural in the presence of ionic liquids, *Catal. Commun.* 4, 2003, 517.

[34] M. Watanabe, Y. Aizawa, T. Lida, R. Nishimura, H. Inomata, Catalytic glucose and fructose conversions with TiO_2 and ZrO_2 in water at 473 K: Relationship between reactivity and acid-base property determined by TPD measurement, *Appl. Catal. A- Gen.* 295, 2005, 150.

[35] X. Qi, M. Watanabe, T.M. Aida, R.L. Smith, Catalytical conversion of fructose and glucose into 5-hydroxymethylfurfural in hot compressed water by microwave heating, *Catal. Comm*. 9, 2008, 2244.

[36] S. De, S. Dutta, B. Saha Microwave assisted conversion of carbohydrates and biopolymers to 5-hydroxymethylfurfural with aluminium chloride catalyst in water, *Green Chem.* 13, 2011, 2859.

[37] A. Mukherjee, M. Dumont, V. Raghavan, Sustainable production of hydroxymethylfurfural and levulinic acid: challenges and opportunities, *Biomass and Bioenergy* 72, 2015, 143.

[38] F. Ilgen, D. Ott, D. Kralisch, C. Reil, A. Palmberger, B. Konig, Conversion of carbohydrates into 5-hydroxymethylfurfural in highly concentrated low melting mixtures, *Green Chem.* 11, 2009, 1948.

[39] X.H. Qi, M. Watanabe, T.M. Aida, R.L. Smith, Fast transformation of glucose and di-/polysaccharides into 5-hydroxymethylfurfural by microwave heating in an ionic liquid/catalyst system, *ChemSusChem*. 3, 2010, 1071.

[40] Z.H. Zhang, Q. Wang, H.B. Xie, W.J. Liu, Z.B. Zhao, Catalytic conversion of carbohydrates into 5-hydroxymethylfurfural by germanium(IV) chloride in ionic liquids, *ChemSusChem*. 4, 2011, 131.

[41] S.Q. Hu, Z.F. Zhang, J.L. Song, Y.X. Zhou, B.X. Han, Efficient conversion of glucose into 5-hydroxymethylfurfural catalyzed by a common Lewis acid $SnCl_4$ in an ionic liquid, *Green Chem*. 11, 2009, 1746.

[42] X. Zhou, Z. Zhang, B. Liu, Z. Xu, K. Deng, Microwave-assisted rapid conversion of carbohydrates into 5-hydroxymethylfurfural by $ScCl_3$ in ionic liquids, *Carbohydr. Res.* 375, 2013, 68.

[43] H. Zhao, J.E. Holladay, H. Brown, Z.C. Zhang, Metal chlorides in ionic liquid solvents convert sugars to 5-hydroxymethylfurfural, *Science* 316, 2007, 1597.

[44] Z. Li, Z.H. Zhang, Z.K. Zhao, Direct conversion of glucose and cellulose to 5-hydroxymethylfurfural in ionic liquid under microwave irradiation, *Tetrahedron Lett.* 50, 2009, 5403.

[45] Z.H. Zhang, Z.K. Zhao, Microwave-assisted conversion of lignocellulosic biomass into furans in ionic liquid, *Bioresour. Technol*. 101, 2010, 1111.

[46] J.B. Binder, R.T. Raines, Simple chemical transformation of lignocellulosic biomass into furans for fuels and chemicals, *J. Am. Chem. Soc.* 131, 2009, 1979.

[47] B. Liu, Z.H. Zhang, Z.K. Zhao, Microwave-assisted catalytic conversion of cellulose into 5-hydroxymethylfurfural in ionic liquids, *Chem. Eng. J.* 215, 2013, 517.

[48] H. Li, Q.Y. Zhang, X.F. Liu, F. Chang, D.Y. Hu, Y.P. Zhang, W. Xue, S. Yang, $InCl_3$-ionic liquid catalytic system for efficient and selective conversion of cellulose into 5-hydroxymethylfurfural, *RSC Advances* 3, 2013, 3648.

[49] S. Xiao, B. Liu , Y. Wang, Z. Fang, Z. Zhang, Efficient conversion of cellulose into biofuel precursor 5-hydroxymethylfurfural in dimethyl sulfoxide-ionic liquid mixtures, *Bioresour. Technol.* 151, 2014, 361.

[50] X. Qi, M. Watanabe, T.M. Aida, R.L. Smith, Catalytic dehydration of fructose into 5-hydroxymethylfurfural by ion-exchange resin in mixed-aqueous system by microwave heating, *Green Chem.* 10, 2008, 799.

[51] P. Bhaumik, P.L. Dhepe, Influence of properties of SAPO's on the one-pot conversion of mono-, di- and poly-saccharides into 5-hydroxymethylfurfural, *RSC Advances* 3, 2013, 17156.

[52] Q. Cao, X. Guo, S. Yao, J. Guan, X. Wang, X. Mu, D. Zhang, Conversion of hexose into 5-hydroxymethylfurfural in imidazolium ionic liquids with and without a catalyst, *Carbohydr. Res.* 346, 2011, 956.

[53] V.V. Ordomsky, J. Van der Schaaf, J.C. Schouten, T.A. Nijhuis, The effect of solvent addition on fructose dehydration to 5- hydroxymethylfurfural in biphasic system over zeolites, *J. Catal.* 287, 2012, 68.

[54] Y. Qu, C. Huang, J. Zhang, B. Chen, Efficient dehydration of fructose to 5-hydroxymethylfurfural catalyzed by a recyclable sulfonated organic heteropolyacid salt, *Bioresour. Technol*. 106, 2012, 70.

[55] P. Daorattanachai, P. Khemthong, N. Viriya-Empikul, N. Laosiripojana, K. Faungnawakij, Conversion of fructose, glucose, and cellulose to 5-hydroxymethylfurfural by alkaline earth phosphate catalysts in hot compressed water, *Carbohydr. Res.* 363, 2012, 58.

[56] J.M.R. Gallo, D.M.Alonso, M.A. Mellmer, J.A. Dumesic, Production and upgrading of 5-hydroxymethylfurfural using heterogeneous catalysts and biomass-derived solvents, *Green Chem.* 15, 2013, 85.

[57] A. Takagaki, M. Ohara, S. Nishimura, K. Ebitani, A one-pot reaction for biorefinery: combination of solid acid and base catalysts for direct production of 5-hydroxymethylfurfural from saccharides, *Chem. Commun*. 2009, 6276.

[58] A. Sayari, Catalysis by Crystalline mesoporous molecular sieves, *Chem. Mater*. 8, 1996, 1840.

[59] B.J. Melde, B.J. Johnson, P.T. Charles, Mesoporous silicate materials in sensing, *Sensors* 8, 2008, 5202.

[60] I.I. Slowing, J.L. Vivero-Escoto, C.W. Wu, V.Y. Lin, Mesoporous silica nanoparticles as controlled release drug delivery and gene transfection carriers, *Adv. Drug Delivery Rev*. 60, 2008, 1278.

[61] K.S.W. Sing, D.H. Everett, R.A.W. Haul, L. Moscou, R.A. Pierotti, J. Rouquérol, T. Siemieniewska, Reporting physisorption data for gas/solid systems with special reference to the determination of surface area and porosity, *Pure Appl. Chem.* 57, 1985, 603.

[62] H.V. Bekkum, E.M. Flanigen, J.C. Jansen, Introduction to zeolite science and practice, *Stud. Surf. Sci. Catal*. 58, 1991.

[63] J. Weitkamp, Zeolites and catalysis, *Solid State Ionics* 131, 2000, 175.

[64] W. Wang, S. Xie, W. Zhou, A. Sayari, Synthesis of periodic mesoporous ethylene silica under acidic conditions, *Chem. Mater*. 16, 2004, 1756.

[65] C.T. Kresge, M.E. Leonowicz, W.J. Roth, J.C. Vartuli, J.S. Beck. Ordered mesoporous molecular sieves synthesized by a liquid crystal template mechanism, *Nature* 359, 1992, 710.

[66] D. Zhao, Q. Huo, J. Feng, B.F. Chmelka, G.D. Stucky, Nonionic triblock and star diblock copolymer and oligomeric surfactant syntheses of highly ordered, hydrothermally stable, mesoporous silica structures, *J. Am. Chem. Soc.* 120, 1998, 6024.

[67] A. Sayari, B.H. Han, Y. Yang, Simple synthesis route to monodispersed SBA-15 silica rods, *J. Am. Chem. Soc.* 126, 2004, 14348.

[68] T. Yanagisawa, T. Shimizu, K. Kuroda, C. Kato, The preparation of alkyltrimethylammonium-kanemite complexes and their conversion to microporous materials, *Bull. Chem. Soc. Jpn.* 63, 1990, 988.

[69] S. Inagaki,Y. Fukushima, K. Kuroda, Synthesis of highly ordered mesoporous materials from a layered polysilicate, *J. Chem. Soc., Chem. Commun.* 1993, 680.

[70] Y. Tozuka, A. Wongmekiat, K. Kimura, K. Moribe, S. Yamamura, K. Yamamoto, Effect of pore size of FSM-16 on the entrapment of flurbiprofen in mesoporous structures, *Chem. Pharm. Bull.* 53, 2005, 974.

[71] Q. Huo, D.I. Margolese, U. Ciesla, D.G. Demuth, P. Feng, T.E. Gier, P. Sieger, A. Firouzi, B.F. Chmelka, F. Schüth, G.D. Stucky, Organization of organic molecules with inorganic molecular species into nanocomposite biphase arrays, *Chem. Mater*. 6, 1994, 1176.

[72] Q. Huo, D.I. Margolese, G.D. Stucky, Surfactant control of phases in the synthesis of mesoporous silica-based materials, *Chem. Mater*. 8, 1996, 1147.

[73] F. Hoffmann, M. Froeba, The supramolecular chemistry of organic–onorganic hybrid materials, Edited by: K. Rurack, R. Martinez-Manez, Chapter 3, page 39, *John Wiley & Sons* 2010, London.

[74] J.N. Israelachvili, D.J. Mitchell, B.W.*J.* Ninham, Theory of self-assembly of hydrocarbon amphiphiles into micelles and bilayers, *Chem. Soc. Faraday Trans.* 72, 1976, 1525.

[75] K. Holmberg, B. Jönsson, B. Kronberg, B. Lindman, Surfactants and Polymers in Aqueous Solution, *John Wiley and Sons* 2003, USA.

[76] S. Inagaki, S. Guan, Y. Fukushima, T. Ohsuna, O. Terasaki, Novel mesoporous materials with a uniform distribution of organic groups and inorganic oxide in their frameworks, *J. Am. Chem. Soc.* 121, 1999, 9611.

[77] T. Asefa, M.J. MacLachlan, N. Coombs, G.A. Ozin, Periodic mesoporous organosilicas with organic groups inside the channel walls, *Nature* 402, 1999, 867.

[78] B.J. Melde, B.T. Holland, C.F. Blanford, Andreas Stein, Mesoporous sieves with unified hybrid inorganic/organic frameworks, *Chem. Mater.* 11, 1999, 3302.

[79] S. Inagaki, S. Guan, T. Ohsuna, O. Terasaki, An ordered mesoporous organosilica hybrid material with a crystal-like wall structure, *Nature* 416, 2002, 304.

[80] N. Mizoshita, T. Tani, S. Inagaki, Syntheses, properties and applications of periodic mesoporous organosilicas prepared from bridged organosilane precursors, *Chem. Soc. Rev.* 40, 2011, 789.

[81] A. Stein, B.J. Melde, R.C. Schroden, Hybrid inorganic-organic mesoporous silicates-nanoscopic reactors coming of age, *Adv. Mater*. 12, 2000, 1403.

[82] S. Fujita, S. Inagaki, Self-organization of organosilica solids with molecular scale and mesoscale periodicities, *Chem. Mater.* 20, 2008, 891.

[83] V. Rebbin, R. Schmidt, M. Froba, Spherical particles of phenylene bridged periodic mesoporous organosilica for high performance liquid chromatography, *Angew. Chem. Int. Ed*. 45, 2006, 5210.

[84] T. Tani, N. Mizoshita, S. Inagaki, Luminescent periodic mesoporous organosilicas, *J. Mater. Chem*. 19, 2009, 4451.

[85] R. Ryoo, S.H. Joo, S. Jun, Synthesis of highly ordered carbon molecular sieves via template-mediated structural transformation, *J. Phys. Chem. B* 103, 1999, 7743.

[86] R. Ryoo, S.H. Joo, M. Kruk, M. Jaroniec, Ordered mesoporous carbons, *Adv. Mater.* 13, 2001, 677.

[87] A.H. Lu, W. Schmidt, B. Spliethoff, F. Schuth, Synthesis of ordered mesoporous carbon with bimodal pore system and high pore volume, *Adv. Mater.* 15, 2003, 1602

[88] R. Ryoo, S.H. Joo, Nanostructured carbon materials synthesized from mesoporous silica crystals by replication, *Stud. Surf. Sci. Catal*. 148, 2004, 241.

[89] F. Kleitz, S.H. Choi, R. Ryoo, Cubic Ia3d large mesoporous silica: synthesis and replication to platinum nanowires, carbon nanorods and carbon nanotubes, *Chem. Commun*. 2003, 2136.

[90] C. Liang, Z. Li, S. Dai, Mesoporous carbon materials: synthesis and modification, *Angew. Chem. Int. Ed*. 47, 2008, 3696.

[91] F. Schuth, Non-siliceous mesostructured and mesoporous materials, *Chem. Mater*. 13, 2001, 3184.

[92] Y. Yang, A. Sayari, Mesoporous organosilicates from multiple precursors: co-condensation or phase segregation/separation, *Chem. Mater.* 20, 2008, 2980.

[93] Y. Goto, S. Inagaki, Synthesis of large-pore phenylene-bridged mesoporous organosilica using triblock copolymer surfactant, *Chem. Commun.* 2002, 2410.

[94] B. Saha, M. Abu-Omar, Advances in 5-hydroxymethylfurfural production from biomass in biphasic solvents, *Green Chem.* 16, 2014, 24.

[95] R. Xing, Y. Liu, Y. Wang, L. Chen, H. Wu, Y. Jiang, M. He, P. Wu, Active solid acid catalysts prepared by sulfonation of carbonization controlled mesoporous carbon materials, *Microporous Mesoporous Mater*. 105, 2007, 41.

[96] I.K. Mbaraka, D.R. Radu, V.S.Y. Lin, B.H. Shanks, Organosulfonic acid-functionalized mesoporous silicas for the esterification of fatty acid, *J. Catal.* 219, 2003, 329.

[97] S. Shylesh, P.P. Samuel, C. Srilakshmi, R. Parischa, A.P. Singh, Sulfonic acid functionalized mesoporous silicas and organosilicas: synthesis, characterization and catalytic applications, *J. Mol. Catal. A- Chem*. 274, 2007, 153.

[98] D. Zuo, J. Lane, D. Culy, M. Schultz, A. Pullar, M. Waxman, Sulfonic acid functionalized mesoporous SBA-15 catalysts for biodiesel production, *Appl. Catal. B- Environ*. 129, 2013, 342.

[99] J.A. Melero, G.D. Stucky, R. Van-Grieken, G. Morales, Direct syntheses of ordered SBA-15 mesoporous materials containing arenesulfonic acid groups, *J. Mater. Chem.* 12, 2002, 1664.

[100] J.A. Melero, R. Van-Grieken, G. Morales, Advances in the synthesis and catalytic applications of organosulfonic-functionalized mesostructured materials, *Chem. Rev.* 106, 2006, 3790.

[101] K.S.W. Sing, D.H. Everett, R.A.W. Haul, L. Moscou, R.A. Pierotti, J. Rouquérol, T. Siemieniewska, Reporting physisorption data for gas/solid systems with special reference to the determination of surface area and porosity, *Pure Appl. Chem.* 57, 1985, 603.

[102] F. Rouquerol, J. Rouquerol, K. Sing, Adsorption by powders and porous solids, *Academic Press* 1999, San Diego.

[103] S. Lowell, J.E. Shields, M. Thomas, M. Thommes, Characterization of porous solids and powders: surface area, pore size and density, *Springer*, 2004, USA.

[104] M. Kruk, M. Jaroniec, A. Sayari, Application of large pore MCM-41 molecular sieves to improve pore size analysis using nitrogen adsorption measurements, *Langmuir* 13, 1997, 6267.

[105] X. Wang, S. Cheng, J.C.C. Chan, J.C.H. Chao, Template-free synthesis of mesoporous phenylsulfonic acid functionalized silica, *Microporous Mesoporous Mater*. 96, 2006, 321.

[106] P.J. Launer, Infrared analysis of organosilicon compounds: spectra-structure compilation, Edited by: B. Arkles, Laboratory for materials, New York, 1987.

[107] R. Tailor, A. Ahmadalinezhad, A. Sayari, Selective removal of SO_2 over tertiary amine-containing materials, *Chem. Eng. J.* 240, 201, 462.

[108] B. Rac, P. Hegyes, P. Forgo, A. Molnar, Sulfonic acid-functionalized phenylene-bridged periodic mesoporous organosilicas as catalyst materials, *Appl. Catal. A- Gen.* 299, 2006, 193.

[109] Q. Yang, M.P. Kapoor, S. Inagaki, N. Shirokura, J.N. Kondo, Ka. Domen, Catalytic application of sulfonic acid functionalized mesoporous benzene–silica with crystal-like pore wall structure in esterification, *J. Mol. Catal. A Chem*. 230, 2005, 85.

[110] A. Sayari, Y. Yang, Nonionic oligomeric polymer directed synthesis of highly ordered large pore periodic mesoporous organosilica, *Chem. Commun.* 2002, 2582.

[111] P.J.E. Harlick, A. Sayari, Applications of Mesoporous silica pore-expanded. 5. triamine grafted material with exceptional CO_2 adsorption equilibrium and dynamic performance, *Ind. Eng . Chem. Res.* 46, 2007, 446.

[112] J.A. Melero, L.F. Bautista, J. Iglesias, R. Sanchez-Vasquez, Biodiesel production from crude oil using sulfonic acid modified mesostructured catalysts, *Chem. Eng. J.* 161, 2010, 323.

[113] E.M. Usai, M.F. Sini, D. Meloni, V. Solinaz, A. Salis, Sulfonic acid-functionalized mesoporous silica: microcalorimetric characterization and catalytic performance toward biodiesel synthesis, *Microporous Mesoporous Mater*. 179, 2013, 54.

[114] Y. Yong, A. Sayari, Molecularly ordered biphenyl-bridged mesoporous organosilica prepared under acidic conditions, *Chem. Mater.* 19, 2007, 4117.

[115] M.P. Kapoor, Q. Yong, S. Inagaki, Self-assembly of biphenylene bridged hybrid mesoporous solid with molecular scale periodicity in the pore walls, *J. Am. Chem. Soc.* 124, 2002, 15176.

[116] O.H. Han, Y.K. Bae, Solid-state NMR study on the structure and dynamics of triblock copolymer P123 remaining in SBA-15 after solvent washing, *Bull. Korean Chem. Soc*. 29, 2008, 911.

[117] A. Sayari, S. Hamoudi, Y. Yang, I.L. Moudrakovski, J.R. Ripmeester, New insights into the synthesis, morphology, and growth of periodic mesoporous organosilicas, *Chem. Mater*. 12, 2000, 3857.

[118] W. Zhou, M. Yoshino, H. Kita, K. Okamoto, Carbon molecular sieve membranes derived from phenolic resin with a pendant sulfonic acid group, *Ind. Eng. Chem. Res.* 40, 2001, 4801.

[119] R. Demir-Cakan, N. Baccile, M. Antonietti, M.M. Titirici, Carboxylate rich carbonaceous materials via one-step hydrothermal carbonization of glucose in the presence of acrylic acid, *Chem. Mater*. 21, 2009, 484.

[120] K. Nakajima, I. Tomita, M. Hara, S. Hayashi, K. Domen, J. N. Kondo, A Stable and Highly Active Hybrid Mesoporous Solid Acid Catalyst, *Adv. Mater*. 17, 2005, 1839.

[121] L. Hu, G. Zhao, X. Tang, Z. Wu, J. Xu, L. Lin, S. Liu, Catalytic conversion of carbohydrates into 5-hydroxymethylfurfural over cellulose-derived carbonaceous catalyst in ionic liquid, *Bioresour. Technol*. 148, 2013, 501.

[122] H.I. Ryoo, L.Y. Hong, S.H. Jung, D.P. Kim, Direct syntheses of sulfonated mesoporous SiO_2-TiO_2-SO_3H materials as solid acid catalysts, *J. Mater. Chem*. 20, 2010, 6419.

[123] G. R. Akien, L. Qi, I.T. Horvath, Molecular mapping of the acid catalysed dehydration of fructose, *Chem. Commun*. 48, 2012, 5850.

[124] L. Hua, Y. Suna, L. Lina, S. Liu, Catalytic conversion of glucose into 5-hydroxymethylfurfural using double catalysts in ionic liquid, *J. Taiwan Inst. Chem. Eng.* 43, 2012, 718.

[125] S. De, S. Dutta, B. Saha, Microwave-assisted conversion of carbohydrates and biopolymers to 5-hydroxymethylfurfural with aluminium chloride catalyst in water, *Green Chem.* 13, 2011, 2859.

[126] M. Karaki, A. Karout, J. Toufaily, F. Rataboul, N. Essayem, Synthesis and characterization of acidic ordered mesoporous organosilica SBA-15: application to the hydrolysis of cellobiose and insight into the stability of the acidic functions, *J. Catal.* 305, 2013, 204.

[127] K. Su, X. Liu, M. Ding, Q. Yuana, Z. Li, B. Cheng, Effective conversion sucrose into 5-hydroxymethylfurfural by tyrosine in [Emim]Br, *J. Mol. Catal. A- Chem*. 379, 2013, 350.

[128] F. Guo, Z. Fang, T. Zhou, Conversion of fructose and glucose to 5-hydroxymethylfurfural with lignin-derived carbonaceous catalyst under microwave irradiation in dimethyl sulfoxide-ionic liquid mixtures, *Bioresour. Technol*. 112, 2012, 313.

[129] C. Wang, L. Fu, X. Tong, Q. Yang, W. Zhang, Efficient and selective conversion of sucrose to 5-hydroxymethylfurfural promoted by ammonium halides under mild conditions, *Carbohydr. Res.* 347, 2012, 182.

[130] A.J. Crisci, M.H. Tucker, J.A. Dumesic, S.L. Scott, Bifunctional solid catalysts for the selective conversion of fructose to 5-hydroxymethylfurfural, *Top Catal.* 53, 2010, 1185.

[131] X. Guo, Q. Cao, Y. Jiang, X. Wang, X. Mu, Selective dehydration of fructose to 5-hydroxymethylfurfural catalyzed by mesoporous SBA-15-SO_3H in ionic liquid BMIMCl, *Carbohydr. Res.* 351, 2012, 35.

[132] J. Wang, W. Xu, J. Ren, X. Liu, G. Lu, Y. Wang, Efficient catalytic conversion of fructose into 5-hydroxymethylfurfural by a novel carbon-based solid acid, *Green Chem.* 13, 2011, 2678.

[133] M. Hara, T. Yoshida, A. Takagaki, T. Takata, J.N. Kondo, S. Hayashi, K. Domen, A carbon material as a strong protonic acid, *Angew. Chem. Int. Ed*. 43, 2004, 2955.

[134] M. Kitano, K. Arai, A. Kodama, T. Kousaka, Ki. Nakajima, S. Hayashi, M. Hara, Preparation of a sulfonated porous carbon catalyst with high specific surface area, *Catal. Lett.* 131, 2009, 242.

[135] P. Gupta, S. Paul, Solid acids: Green alternatives for acid catalysis, *Catal. Today* 236, 2014, 153.

[136] M.H. Tucker, A.J. Crisci, B.N. Wigington, N. Phadke, R. Alamillo, J. Zhang, S.L. Scott, J.A. Dumesic, Acid-functionalized SBA-15 type periodic mesoporous organosilicas and their use in continuous production of 5-hydroxymethylfurfural, *ACS Catal.* 2, 2012, 1865.

[137] M. Hara, Biomass conversion by a solid acid catalyst, *Energy Environ. Sci*. 3, 2010, 601.

[138] C. Bispo, K. De Oliveira Vigier, M. Sardo, N. Bion, L. Mafra, P. Ferreira, F. Jerome, Catalytic dehydration of fructose to HMF over sulfonic acid functionalized periodic mesoporous organosilicas : role of the acid density, *Catal. Sci. Technol.* 4, 2014, 2235.

[139] A. Sayari, Recent advances and new horizons in zeolite science and technology, Edited by: Chon, S.I. Woo, S.E. Park, Volume 102, Chapter 1, page 1, Elsevier.

[140] C.A. Antonyraj, B. Kim, Y. Kim, S. Shin, K.Y. Lee, I. Kim, J.K. Cho, Heterogeneous selective oxidation of 5-hydroxymethyl-2-furfural(HMF) into 2,5-diformylfuran catalyzed by vanadium supported activated carbon in MIBK, extracting solvent for HMF, *Catal. Commun.* 57, 2014, 64.

[141] Y. Liu, L. Zhu, J. Tang, M. Liu, R. Cheng, C. Hu, One-pot, One-step synthesis of 2,5-diformylfuran from carbohydrates over Mo-containing keggin heteropolyacids, *ChemSusChem* 7, 2014, 3541.

[142] G. A. Halliday, R. J. Young, V.V. Grushin, One-Pot, two-Step, practical Catalytic synthesis of 2,5-diformylfuran from fructose, *Org. Lett.* 5, 2003, 2003.

[143] A.J. Crisci, M.H. Tucker, M.Y. Lee, S.G. Jang, J.A. Dumesic, S.L. Scott, Acid-functionalized SBA-15-type silica catalysts for carbohydrate dehydration, *ACS Catal.* 1, 2011, 719.

[144] C. Fan, H. Guan, H. Zhang, J. Wang, S. Wang, X. Wang, Conversion of fructose and glucose into 5-hydroxymethylfurfural catalyzed by a solid heteropolyacid salt, *Biomass and Bioenergy* 35, 2011, 2659.

Appendix I: HMF Calibration Curve

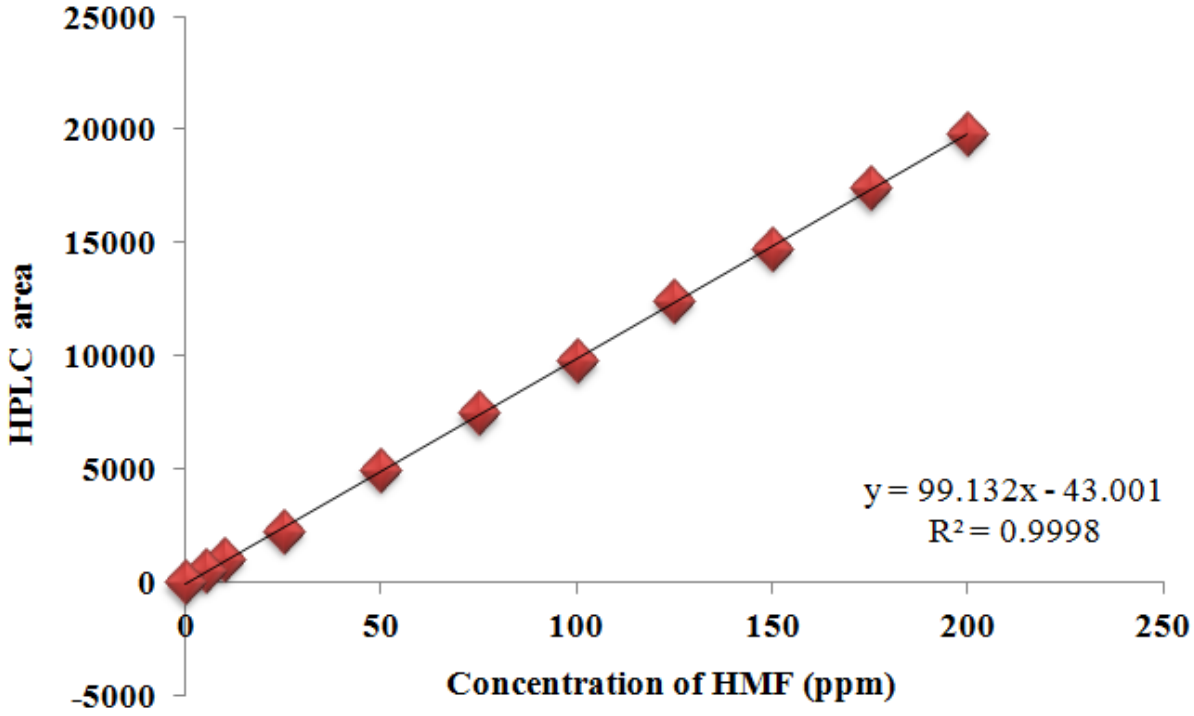

Figure A$_I$: Calibration curve for authentic HMF in water.

Appendix II: TGA Profiles of PMO

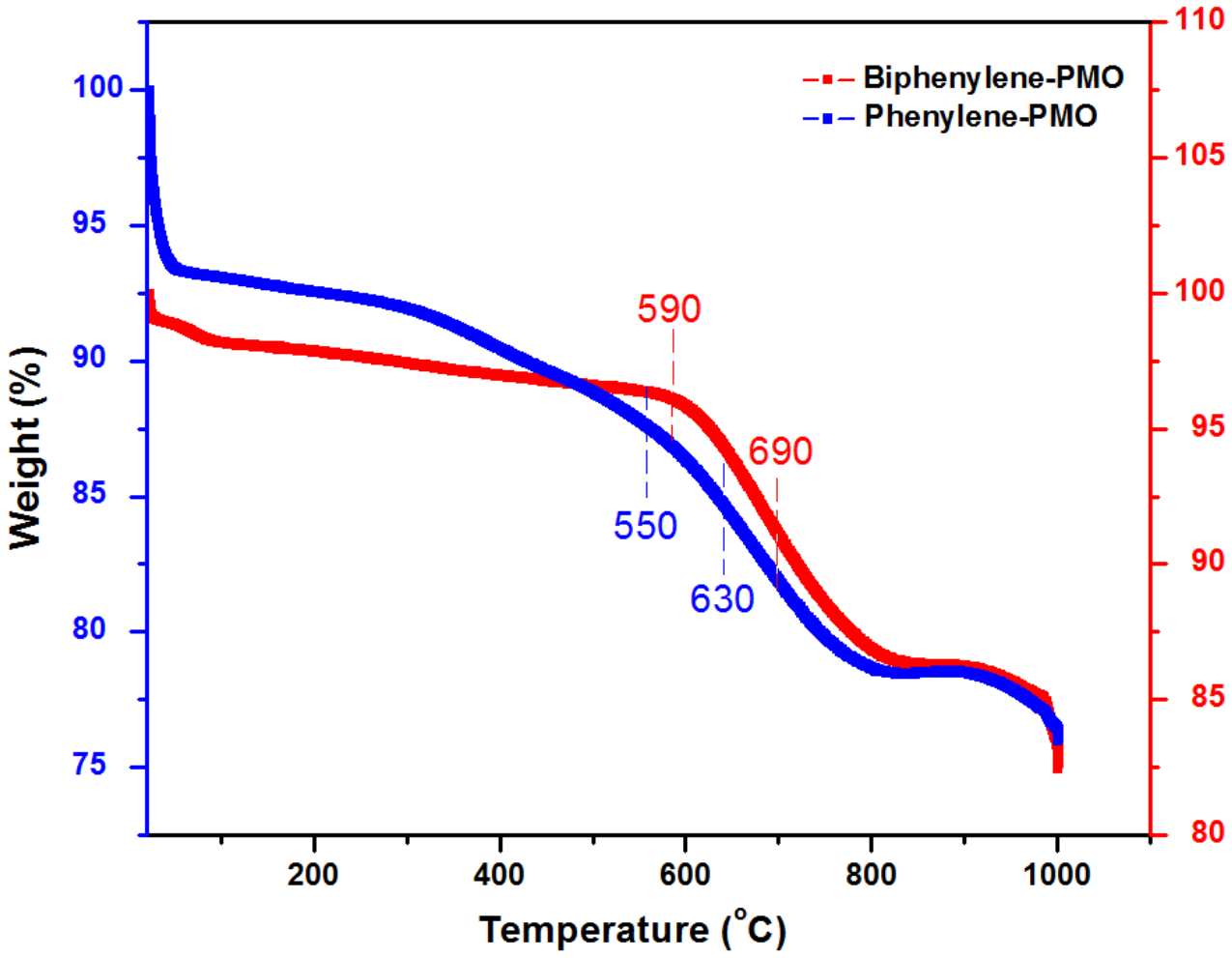

Figure A$_{II}$: TGA profiles of phenylene and biphenylene-bridged PMO.

Appendix III: Sulfonation of PMO

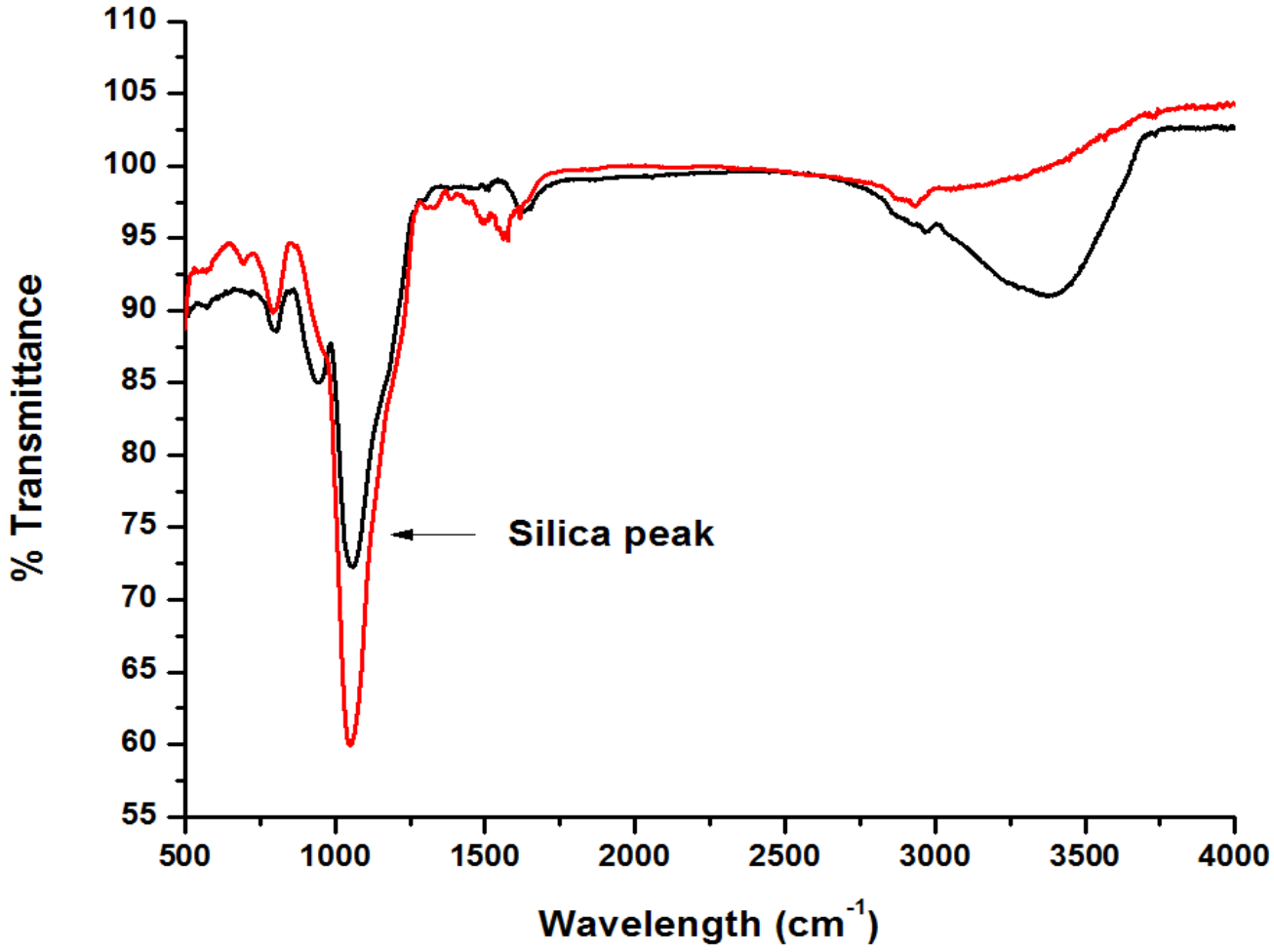

Figure A_{III}: Sulfonation of PMO using concentrated (black) and fuming sulfuric acids (red) as sulfonating agent.